

**SETTING UP METHODS FOR THE STUDY OF
INTRACELLULAR MECHANOTRANSDUCTION**

M.Sc. Thesis
Henrik Hammarén
Institute of Biomedical Technology
University of Tampere
January 2012

PRO GRADU -TUTKIELMA

Paikka: TAMPEREEN YLIOPISTO
Biolääketieteellisen teknologian instituutti (IBT)
Tekijä: HAMMARÉN, HENRIK MAXIMILIAN
Otsikko: Solunsisäisen mekanotransduktion tutkimiseen tarvittavien metodien pystytys
Sivumäärä: 74 sivua, 15 hakemisto- ja liitesivua
Ohjaajat: Dosentti Vesa Hytönen ja Jenita Pärssinen, FT
Tarkastajat: Prof. Markku Kulomaa ja Dosentti Vesa Hytönen
Aika: Tammikuu 2012

Tiivistelmä

Fokaaliadheesiöt (FA) ovat suuria proteiinikomplekseja, joiden avulla solut tarttuvat ympäristönsä solunulkoiseen matriksiin liittämällä sen mekaanisesti solunsisäiseen tukirankaansa. FA:t ovat mekanosensorisia rakenteita, joilla solut aistivat ympäristönsä mekaanisia ominaisuuksia. Vaikka suurin osa tärkeimmistä FA-proteiineista on tunnettu jo pitkään, niiden toimintaa ja vuorovaikutuksia on alettu ymmärtää vasta hiljattain. Yksi ehdotetuista mekanosensorisista kokonaisuuksista FA:issa on taliini-vinkuliini-vuorovaikutus. Taliini on suurehko proteiini, joka muodostaa linkin solukalvossa sijaitsevien integriinien ja solutukirangan aktiinisäikeiden välille. Taliinin mekanosensoristen ominaisuuksien on ehdotettu johtuvan proteiinin rakenteen osittaisesta epälakostumisesta, joka voiman vaikutuksen alaisena voisi johtaa aiemmin suljettujen (nk. kryptisten) vinkuliininsitomispaikkojen aukeamiseen. Tämä Pro Gradu -tutkielma kuvaa mekanotransduktion tutkimiseen hiiren alkion fibroblastisoluissa tarvittavan metodologian pystytyksen. Tutkimuksissa soluihin transfektoidaan vihreän fluoresoivan proteiinin (EGFP) ja Strep-Tag-puhdistuskahvan (ST) kanssa yhteen liitetty vinkuliinirakenne (EGFP-Vinkuliini-ST), joka mahdollistaa adheesioiden visualisoinnin fluoresenssimikroskopiolla sekä FA-proteiinikompleksien affiniteettipuhdistuksen. Transfektion optimointi kuvataan ja kationisen polymeeripohjaisen transfektioareagenssin, TurboFect:n, osoitetaan olevan paras vaihtoehto tulevia kokeita ajatellen. Solujen ympäristön mekaanisten ominaisuuksien muuttamiseksi käytetään polyakryyliamidigeelikasvatusalustoja, joiden valmistus ja käyttö esitellään. Erijäykkyyden alustojen vaikutuksia tutkitaan puoliautomatisoidulla kuva-analyysillä, jota käyttäen solujen sekä adheesioiden pinta-alan näytetään kasvavan odotetulla tavalla pinnan jäykkyyden kasvaessa. Solujen pinta-ala-analyysissä nähdään myös, että vinkuliinia sisältämättömien MEF^{Vin-/-}-solujen fenotyyppi ei ole täysin pelastettavissa transfektoimalla EGFP-Vinkuliini-ST:a soluihin. Tämän odottamattoman tuloksen syitä pohditaan aiemmin julkaistun kirjallisuuden valossa. Lisäksi esitellään FA-proteiinikompleksien puhdistukseen käytettäviä menetelmiä pitäen painopisteenä kemiallisia ristositoja hyödyntävät fysikaaliset ja affiniteettipuhdistuspohjaiset menetelmät, joista ainakin jälkimmäisellä saadaan onnistuneesti puhdistettua EGFP-Vinkuliini-ST:a sekä pieniä määriä solun omaa vinkuliinia ja taliinia. Nämä kokeet luovat pohjan tuleville mekanotransduktiotutkimuksille biologisesti relevanteissa ympäristöissä ja ne ovat siten tärkeä askel kohti fokaaliadheesioiden mekanosensoristen ominaisuuksien molekyyli-tason ymmärtämistä.

Avainsanat: mekanoaistiminen, mekanotransduktio, fokaaliadheesiöt, taliini, vinkuliini, hiiren alkion fibroblastit, polyakryyliamidigeeli solujen kasvatusalustana

MASTER'S THESIS

Place: UNIVERSITY OF TAMPERE
Institute of Biomedical Technology (IBT)
Author: HAMMARÉN, HENRIK MAXIMILIAN
Title: Setting up methods for the study of intracellular mechanotransduction
Pages: 74 pages, 15 index and appendix pages
Supervisors: Docent Vesa Hytönen and Dr. Jenita Pärssinen
Reviewers: Prof. Markku Kulomaa and Docent Vesa Hytönen
Date: January 2012

Abstract

Cells feel and respond to the mechanical properties of their environment mainly through large protein complexes called focal adhesions (FA), which are mechanosensory entities that link the extracellular matrix (ECM) to the cytoskeleton. Despite the fact that the most important FA proteins have been long known, knowledge about the function and interplay of cytoplasmic FA proteins is just emerging. One of the proposed mechanosensory systems in adhesions is the talin–vinculin interaction. Talin is a large protein that functions as a linker between integrins and actin fibres, and its mechanosensory properties have been suggested to rely on partial force-induced unfolding of domains in talin, which could lead to the opening of previously cryptic vinculin binding sites. This thesis covers setting up the required methodology to utilise a mammalian cell culture model to study mechanosensing in adhesions of mouse embryonic fibroblasts (MEF) transiently transfected with enhanced green fluorescent protein (EGFP) and Strep-Tag (ST) associated vinculin fusion constructs. Optimisation of transient transfection in MEF cells is presented and the cationic polymer-based transfection reagent TurboFect is shown to be the best choice for future experiments. Manufacture of biofunctionalised polyacrylamide substrates of different rigidity is demonstrated, and these substrates are successfully used to alter mechanical properties of the cell environment. The effects of different substrate rigidities on cell and adhesion area are assessed using semiautomated image analysis, and increasing substrate rigidity is shown to increase cell and adhesion area, as expected. Transient transfection with the EGFP-Vinculin-ST fusion constructs is shown not to be able to completely rescue the vinculin-null phenotype in MEF^{Vin^{-/-}} cells when measured as cell area only. Possible reasons for this unexpected result are discussed. Additionally, methods for the extraction of FA protein complexes are assessed with a focus on using chemical cross-linkers and Strep-Tag-based affinity chromatography, with which small amounts of endogenous vinculin and talin are shown to be extracted alongside EGFP-Vinculin-ST from cell lysates. The important knowledge gained from these experiments paves the way for future studies and is thus an important step towards the elucidation of mechanosensing in focal adhesions on a molecular level.

Key words: mechanosensing, mechanotransduction, focal adhesions, talin, vinculin, mouse embryonic fibroblasts, polyacrylamide gel cell culture substrates

Acknowledgements

This thesis covers the most important insights and results gained from around 6 months of intense lab work in Vesa Hytönen's Protein Dynamics lab at the Institute of Biomedical Technology at the University of Tampere. Like practically any product of modern experimental scientific work, this thesis is not the creation of the author alone, but rather represents the combined effort of a larger group of people, without which this thesis would not have seen daylight.

As this work embodies the first ever attempt at experimental science in the field of intracellular mechanobiology in the Protein Dynamics group, everyday lab-work was characterised by the need for solving practical problems. Thus, I'd like to first of all thank our absolutely exceptional laboratory technician Ulla Kiiskinen for showing utmost patience and resourcefulness even when faced with my most complicated and/or ridiculous requests in the lab.

Secondly, I'd like to thank our summer student Ville Hynninen for lending his much-needed pair of hard-working hands and an outstandingly meticulous character to our project for ten weeks during the summer of 2011. Without him many of the laborious experiments could not have been done in a practical time-scale. Additionally, I have to give Ville a special hat's off for fearlessly joining me even in the most daring endeavours while seeking to find creative ways to solve everyday problems in the lab.

I'd also like to give special thanks to my second instructor Jenita Pärssinen who joined the project during spring 2011 and enabled us to get a fresh start after many failed experiments in summer 2010. Her know-how of mammalian cell culture and her can-do attitude along with all the preparatory work she did was vital for the efficient progress of this project during the most productive months of experimental lab work. A big 'thank you' goes to her also for indispensable assistance in planning many of the experiments and for having an ever watchful eye on the literature during hectic lab days, thus keeping us all up-to-date in an extremely rapidly evolving field.

Other thanks go to the numerous people helping me out in many specific and technical aspects of the work. These people include Kristiina Salonoja, Jani Sarin, Vilppu Tuominen, and Daniela Ungureanu.

Finally, this project would not have been possible without our group leader and my primary instructor, Vesa Hytönen. I thank him very much for giving me the opportunity to test myself at this challenging project, and for all the faith he has put into me. He has always encouraged me in my studies and endeavours, and he has been a significant contributor to what I think are a pair of good steps on the start of a scientific career.

Lastly, but most importantly, I'd like to thank my soon-to-be wife Milka for relentlessly spurring me on during this project and for the exceptional support and patience that she has shown while putting up with me during the making of this thesis.

Abbreviations

Actn	α -actinin
AFM	Atomic force microscopy
APTES	Aminopropyltriethoxysilane
BSA	Bovine serum albumin
DAPI	4',6-diamidino-2-phenylindole, a fluorescent dye binding strongly to A-T rich regions of DNA
DMEM	Dulbecco's modified Eagle medium
DTBP	Dimethyl 3,3'-dithiobispropionimide, a homobifunctional, amine-reactive, cleavable cross-linker
DTT	Dithiothreitol
ECM	Extracellular matrix
EGFP	Enhanced green fluorescent protein
FA	Focal adhesion
FAK	Focal adhesion kinase
FB	Fibrillar adhesion
FBS	Fetal bovine serum
FERM	A protein domain often found in proteins near the plasma membrane. Named after 4.1 protein, ezrin, radixin, and moesin. ¹
FITC	Fluorescein isothiocyanate, a green fluorescent dye (emission / excitation λ : 495 nm / 521 nm)
Fln	Filamin
FN	Fibronectin
FX	Focal complex
GFP	Green fluorescent protein
HRP	Horseradish peroxidase
iPALM	Interferometric photoactivated localisation microscopy
LIM	A zinc finger-like protein domain found, among other things, in many actin-associated proteins. First named after the three proteins LIN-11, Isl-1, and MEC-3. ²
MEF	Mouse embryonic fibroblasts
MLC	Myosin light chain
PAA	Polyacrylamide
Pax	Paxillin
PBS	Phosphate buffered saline
Plec	Plectin
PT	Post-transfection
RGD	Arginine-glycine-aspartate
RIPA	Radioimmunoprecipitation assay (also name of a lysis buffer)
SDS-PAGE	Sodium dodecyl sulphate polyacrylamide gel electrophoresis
TIRF	Total internal reflection microscopy
Tln	Talin
Tns	Tensin
VASP	Vasodilator-stimulated phosphoprotein
VBS	Vinculin binding site
Vcl, Vin, Vinc	Vinculin
Vd1–4	α -helical domains found in the vinculin head

¹ <http://www.ebi.ac.uk/interpro/IEntry?ac=IPR000299>, accessed on 11.10.2011

² <http://www.ebi.ac.uk/interpro/IEntry?ac=IPR001781>, accessed on 12.11.2011

Vh	Vinculin head (residues 1–835) ³
Vt	Vinculin tail (residues ~836–1066)
WB	Western blotting
WT	Wild type
Zyx	Zyxin

³ <http://www.uniprot.org/uniprot/P18206>, accessed on 16.1.2012

Contents

Abstract	ii
Acknowledgements	iii
Abbreviations	iv
1 Review of the literature	1
1.1 Introduction	1
1.2 Focal adhesions	2
1.2.1 Formation and maturation of FAs	2
1.2.2 The adhesome	4
1.2.3 The nanoarchitecture of focal adhesions shows layers with distinct functionalities	6
1.2.4 FA functions are controlled by local signalling proteins	7
1.2.5 FAs and force	8
1.2.6 What causes the tight force–assembly relationship in FAs?	11
1.3 The focal adhesion proteins talin and vinculin	13
1.3.1 Talin	13
1.3.2 Vinculin	15
1.3.3 The talin–vinculin interaction	16
1.4 Introduction to methods used in this study	21
1.4.1 Using compliant cell culture substrates for studying mechanotransduction	21
1.4.2 Purifying FA proteins	23
2 Main goals of the thesis	24
3 Materials and methods	25
3.1 Mammalian cell culture	25
3.1.1 Cell strains	25
3.1.2 Maintenance of cells	25
3.1.3 PAA cell culture substrates	25
3.2 Expression constructs	27
3.2.1 Transfection	27
3.3 Antibodies	29
3.4 Immunofluorescence staining of cells	30
3.5 Purification of FA proteins	31
3.5.1 Unspecific FA protein purification	31
3.5.2 Affinity chromatography purification of vinculin-associated complexes using the Strep-Tag®/Strep-Tactin® system	34
3.5.3 Acetone precipitation of protein samples	36
3.5.4 SDS-PAGE and Western blotting	36

3.6	Image processing and analysis	37
3.6.1	Estimation of transfection efficiency	37
3.6.2	Estimation of cell area	38
3.6.3	Measuring focal adhesion size and number	39
4	Results.....	40
4.1	Optimisation of transfection.....	40
4.2	Purification of the talin–vinculin complex from cytoplasmic parts of FAs..	41
4.2.1	Physical FA protein purification	41
4.2.2	None of the other previously published methods tested proved to be useful in purifying FAs from untransfected MEFwt cells	44
4.2.3	Strep-Tag-based affinity chromatography enables purification of ST-tagged vinculin.....	46
4.3	EGFP-Vinculin-ST fusion proteins localise correctly into focal adhesions along with talin.....	48
4.4	Effects of substrate stiffness on MEF cells	49
4.4.1	Both transfected MEF ^{Vin-/-} and untransfected MEFwt cells show increased spreading on substrates of increasing stiffness	49
4.4.2	Expression of the EGFP-Vinculin-Strep-Tag-constructs cannot entirely rescue the MEF ^{Vin-/-} phenotype	50
4.5	The HTI-deficient T12 vinculin mutant in EGFP-Vinculin-ST causes an increase in adhesion site density, but no difference in adhesion size compared to EGFP-VinWT-ST.....	50
5	Discussion.....	54
6	Conclusions.....	69
	References.....	70
	Appendix 1.....	75
	ImageJ macros used in image analysis	75

1 Review of the literature

1.1 Introduction

Cells and tissues are influenced not only by biochemical signals, but also by mechanical cues. In fact, mechanical stimulation is, much like biochemical input, vital to almost all known cell types (Eyckmans et al. 2011). While the idea of meaningful connections between mechanical stimuli and biological systems arose already through tissue-level observations in the late 19th century, the field of *mechanobiology* has gathered new interest in the scientific community only relatively recently (Eyckmans et al. 2011). New insights in the fields of cell biology quickly established mechanical stimuli as essential for a multitude of basic biological processes like proliferation, migration, and differentiation of cells (Eyckmans et al. 2011, Critchley 2009, Geiger, Yamada 2011). Even though many of these processes are often thought to be mainly intrinsic to embryogenesis and tissue formation, they also play a role in many diseases like atherosclerosis and cancer (reviewed in Ingber 2003).

One of the most important aspects in the field has long been the question of *mechanotransduction* – i.e. the mechanics of converting mechanical information and stimuli into biochemical signals (Kamm, Mofrad 2010). Entities capable of mechanotransduction have thus far been implied in numerous biological systems. The best-known and most thoroughly characterised mechanotransducers are probably mechanosensitive ion-channels, which change their permeability to ions when subjected to lateral stretching forces. Beyond these, other, more hypothetical, membrane-associated mechanotransducers are the glycocalyx and the primary cilia in endothelial cell membranes, both of which have been implicated to be able to respond to shear-stress induced deformations of the membrane (Davies, Helmke 2010). Another system hypothesised to take part in membrane-mediated mechanotransduction is mechanically induced change in membrane lipid composition potentially causing activation of G-protein coupled receptors (Zhang, Frangos & Chachisvilis 2010). Furthermore, mechanotransduction may occur following changes in autocrine signalling caused by cell deformation in epithelial cell sheets (Kojic, Tschumperlin 2010). In the context of an adherent cell lying on a substrate of extracellular matrix (ECM), however, one of the most important mechanosensory entities is undoubtedly the focal adhesion (FA) and, through it, the whole cell–ECM-module (Zaidel-Bar, Geiger 2010).

1.2 Focal adhesions

Focal adhesions are dynamic protein complexes that provide a mechanical linker point between cells and their ECM environment. They form onto and around clustered integrins, which are the actual transmembrane mechanoreceptors linking the cytoskeleton to the ECM. Functional integrins are heterodimers consisting of an α - and a β -subunit, of which human FAs contain 18 and 8 different forms, respectively (Zaidel-Bar, Geiger 2010, Doyle, Yamada 2010). These different α - and β -integrins can together form at least 24 different heterodimer structures, which have slightly different ligand binding properties. Although there are numerous different integrin ligand sequences identified for different integrin heterodimers, the best known ligand is the RGD-peptide found in many extracellular adhesion molecules like fibronectin and vitronectin, which bind to most β_1 and β_3 -integrin pairs (Doyle, Yamada 2010).

While the extracellular parts of FAs consist practically only of the ECM-binding extracellular head domains of integrins, there are numerous proteins forming the rather substantial intracellular portions of FA complexes. These proteins contain multiple scaffolding, force-bearing, and signalling proteins which assemble mainly around the small cytoplasmic parts of β -integrins. Some of the most important of these intracellular FA proteins include talin (Tln), vinculin (Vcl, Vin, or Vinc; referred here as Vin), paxillin (Pax), focal adhesion kinase (FAK), Arp2/3, zyxin (Zyx), α -actinin (Actn), tensin (Tns), filamin (Fln), plectin (Plec), and vasodilator-stimulated phosphoprotein (VASP) (Eyckmans et al. 2011, Zaidel-Bar, Geiger 2010, Doyle, Yamada 2010, Bershadsky, Balaban & Geiger 2003, Kanchanawong et al. 2010). Of these, direct linkers of integrin β -subunits to cytoskeletal actin are at least talin, α -actinin, filamin, and tensin (Bershadsky, Balaban & Geiger 2003), while paxillin can provide a direct link to microtubules and plectin can bind to the intermediate filament vimentin (Zaidel-Bar, Geiger 2010).

1.2.1 Formation and maturation of FAs

Focal adhesion protein complexes are dynamic (Zaidel-Bar, Geiger 2010) and they mature and change with time and proceed through many different stages during their formation. Some of these stages are sufficiently distinct to often be regarded and named as separate entities (Geiger, Yamada 2011, Doyle, Yamada 2010, Bershadsky, Balaban & Geiger 2003). One way of classifying the complexes distinguishes three different adhesion plaques: focal complexes (FX), focal adhesions (FA), and fibrillar adhesions (FB) (Geiger, Yamada 2011, Doyle, Yamada 2010).

The formation of all of the adhesion types mentioned above initiates with activation of the integrin mechanoreceptor. This can be brought about by an inside-out mechanism, like the binding of the talin head FERM-domain or kindlin proteins to the cytoplasmic tail of β -integrins. Activation can, on the other hand, also be brought about in an outside-in fashion by extracellular factors, like divalent cations (Doyle, Yamada 2010).

The first adhesion structures to form are typically focal complexes (FX), which are new, freshly formed complexes that arise as initial points of contact between a cell and its surrounding ECM. FXs are sometimes further subdivided into nascent adhesions and 'true FXs' (Eyckmans et al. 2011, Choi et al. 2008). In this division nascent adhesions are considered to be the primary contact points forming in protruding lamellipodia driven largely by Arp2/3-mediated actin-mesh polymerisation (Choi et al. 2008). Both nascent adhesions and FXs are relatively unstable and transient, and they contain mostly $\alpha_v\beta_3$ -integrins (also other combinations depending on the cell and substrate type), talin, α -actinin, paxillin, vinculin, and FAK (Doyle, Yamada 2010). Furthermore, FXs also themselves contain Arp2/3 to nucleate actin filament growth further (Choi et al. 2008). Unlike the later forms of adhesion complexes, FX formation is not dependent on force applied through them, and they do not vanish if force generation is blocked inside cells with inhibitors of the actomyosin machinery (Bershadsky, Balaban & Geiger 2003, Kuo et al. 2011).

If initial FXs find suitable conditions for contact in the ECM, FXs may mature into focal adhesions (FA). FAs are built up onto FXs with the addition of zyxin, and the partial departure of paxillin, which has been proposed to continuously leave nascent FAs and move towards newly forming FXs at the leading edge of the cell (Doyle, Yamada 2010). FAs are furthermore characterised with actin assembling into strong, force-conducting stress fibres. As was previously already alluded to, maturation of FXs to FAs depends on application of mechanical force through the complex (Geiger, Yamada 2011, Bershadsky, Balaban & Geiger 2003).

FAs are sometimes quoted to further mature into a third type of adhesion: the fibrillar adhesion (FB). While FAs are mostly found at the edges of cells, FBs are beneath the cell body, are elongated in appearance, and assemble along actin stress fibres (Doyle, Yamada 2010). FBs are characterised by the presence of the protein tensin, and they are thought to regulate ECM assembly for example through fibronectin fibrillogenesis (Geiger, Yamada 2011, Doyle, Yamada 2010).

Characteristics of the different types of integrin-mediated adhesions along with information about their size, characteristic molecules and presumed functions in cells are summarised in Table 1. Table 1 also includes a further, rather independent type of integrin-mediated adhesion, the podosome-type adhesion (Block et al. 2008), which is included for the sake of completeness, but will not be discussed further in this work.


While there have been some suggestions that the different forms of adhesion complexes described above (with the exception of podosomes) would, in fact, simply represent different stages in a single continuum (Eyckmans et al. 2011), it should be noted that the different stages seem to have distinct molecular composition and, furthermore, different abilities to transmit force (see Table 1 and 1.2.5.3 below), and should therefore probably be considered separate. In this work FXs, FAs, and FBs are together referred to as ‘adhesions’, while the term ‘focal adhesion’ (FA), will be reserved to mechanosensitive adhesions. Since most of the core proteins in the different adhesion types are the same, however, the term ‘FA proteins’ will be used as an umbrella term to refer to these common adhesion proteins.

1.2.2 The adhesome

Although adhesion complexes were previously introduced to contain around ten different core proteins, the total adhesome is significantly larger. According to a recent meta-analysis by Zaidel-Bar and Geiger (2010) the adhesome would consist of around 180 proteins, which have the potential to form at least 742 interactions, some of which are mutually exclusive. It should be noted, however, that these numbers reflect the sum from a large number of individual proteomic and *in vitro* interaction studies, and that they, therefore, should not be considered to represent any single state found in any given cell (Zaidel-Bar, Geiger 2010). Single direct proteomic approaches, for example, usually only identify a subset of these proteins, while at the same time identifying numerous other proteins (Humphries et al. 2009, Schiller et al. 2011). Humphries et al. (2009), for example, found 37 of the aforementioned 180 proteins, while Schiller et al. (2011) identified 87. These differences partly reflect differences in the experimental setup where slight changes in cell type, cell culture substrate, purification protocol, and throughput quality of the hardware and software of mass spectrometrical (MS) analyses all influence the final readout. Even though this sensitivity of the adhesome composition to experimental setups presents a problem for reproducibility of experiments, it also nicely reflects the exquisitely sensitive

dynamics of adhesion complexes towards changes in, for example, the mechanical state of the cell and its surroundings (Zaidel-Bar, Geiger 2010, Schiller et al. 2011).

Table 1: Summary of different forms of integrin-positive adhesion complexes. The shown proteins are characteristic mainly for cells on substrates containing fibronectin as the primary ECM protein. Note that in most cases the distinction between different adhesion types is still open for debate and not clearly definable. (Sources: Geiger, Yamada 2011, Doyle, Yamada 2010, Block et al. 2008, Tan et al. 2003.)

Order of appearance	Name	Size (μm^2)	Characteristic molecules	Presumed function in cells	Notable characteristics
	Nascent adhesion	< 1.0	$\alpha_v\beta_3$ -integrins, Tln, Actn, Pax, Vin, FAK, Arp2/3	<ul style="list-style-type: none"> • Nucleate actin growth 	<ul style="list-style-type: none"> • Unstable • Transient
	Focal complex (FX)	< 1.0		<ul style="list-style-type: none"> • Facilitate membrane protrusion • Probe surface for suitable contact points 	<ul style="list-style-type: none"> • Highly dynamic • Transient • Able to transmit large forces • High levels of Y-phosphorylation
	Focal adhesion (FA)	$\sim 1-3^4$	$\alpha_v\beta_3$ -integrins, Tln, Actn, Zyx, Vin, FAK, Arp2/3, kinectin	<ul style="list-style-type: none"> • Contact points of actin stress-fibres 	<ul style="list-style-type: none"> • Mechanosensitive assembly
	Fibrillar adhesion (FB)	> 1.0	$\alpha_5\beta_1$ -integrins, Tln, Tns	<ul style="list-style-type: none"> • Regulate ECM assembly through FN fibrillogenesis 	<ul style="list-style-type: none"> • Elongated form • Assemble along actin stress-fibres beneath cell body • Colocalise with extracellular FN • No Y-phosphorylation
	3-D matrix adhesion	-	Integrins, Tln, Vin, FAK, Tns	<ul style="list-style-type: none"> • Same as FAs and FBs 	<ul style="list-style-type: none"> • Long and slender form
	Podosome / Invadopodium	~ 1.0	Integrins, Actn, Pax, Vinc, Vasp, Arp2/3, Cortactin, Dynamin	<ul style="list-style-type: none"> • Facilitate matrix-remodelling (e.g. bone resorption in osteoclasts) and matrix-invasion 	<ul style="list-style-type: none"> • Small, ring-like form • Invadopodia linked to cancer-related matrix-invasion

⁴ The size of FAs (and to some extent also of the other adhesion types) varies considerably with the cell type and environment chosen. See discussion for details.

1.2.3 The nanoarchitecture of focal adhesions shows layers with distinct functionalities

While the main protein components of focal adhesion complexes have been known for quite a while, the detailed structure, i.e. the way in which the proteins form the functional complex, has largely been elusive to previously used experimental approaches. Using the cutting-edge super-resolution microscopy technique interferometric photoactivated localisation microscopy (iPALM) Kanchanawong et al. (2010) shed light on the three-dimensional ultrastructure of focal adhesions in mouse embryonic fibroblast (MEF) cells. By tagging various FA proteins with photoactivatable fluorescent proteins (PAFP) they could identify three partially overlapping layers of proteins including proteins that populate the ~40 nm wide gap (or ‘focal adhesion core’) between integrin cytoplasmic tails and the actin cytoskeleton (Kanchanawong et al. 2010). The most important proteins identified by Kanchanawong et al. along with their position along the z-axis relative to the basal the membrane of the cell are compiled in Table 2. Interestingly, assigning the layers formed by the proteins according to their previously known functions creates a logical picture of FA function with an integrin-associated signalling layer directly next to cytoplasmic integrin tails, followed by a force-transduction layer (including the proteins talin and vinculin, among others), an actin-regulatory layer, and finally cytoskeletal actin fibres (Table 2 and Figure 1).

Table 2: The spatial organisation of the main focal adhesion proteins as determined by iPALM microscopy. Values indicated are as reported by Kanchanawong et al. (2010).

Peak centre (relative to plasma membrane) (nm)	Peak width (as estimated from σ of gaussian distribution) (nm)	Example proteins	Name of the region
37	7	Integrin α_v	Cytoplasmic part of integrin
36	10	FAK	Integrin signalling layer
43	9	Paxillin-C	
46	12	Paxillin-N	
43	10	Talin-N	Force- transduction layer
77	16	Talin-C	
54	13	Vinculin	
73	18	Zyxin	Actin regulatory layer
81	23	VASP	
104	23	α -actinin-C	Actin cytoskeleton fibres
106	26	α -actinin-N	
97	31	Actin	

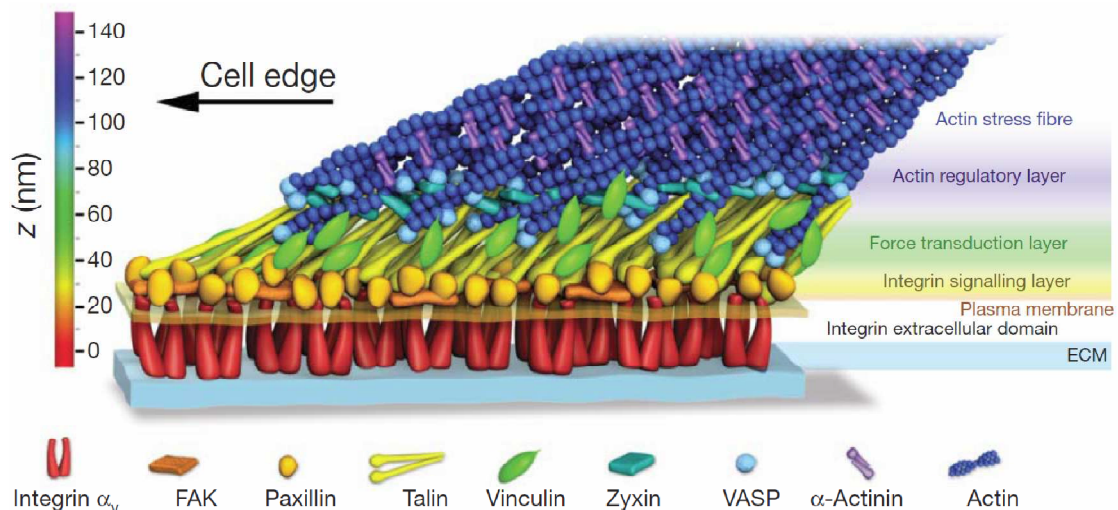


Figure 1: Schematic cartoon depicting the nanoscale architecture of focal adhesions. Proteins are depicted at the correct position along the z-axis according to iPALM-measurements of fluorescently-tagged proteins constructs. Depicted protein numbers do not represent correct stoichiometry. Figure adopted from Kanchanawong et al., (2010).

In addition to being defined by the distinct set of proteins described above, recent experiments looking into the effects of local lipid composition and structure in FAs suggest that membrane composition and fluidity might also partly determine for example integrin clustering and signalling in FAs. Following these results, FAs could thus be seen to not only be intricate cytoplasmic protein complexes, but also to form their own lipid microdomains – not much unlike caveolae or lipid rafts. (Butler, Chien 2010).

1.2.4 FA functions are controlled by local signalling proteins

In addition to the mostly structural proteins mentioned in Table 2, FAs contain multiple signalling proteins like ERK, JNK, Src, MEK, Ras, and Raf, which likely represent a link to signalling cascades directly controlling cell migration, proliferation, and differentiation (Eyckmans et al. 2011). In terms of controlling protein functions, phosphorylation plays a major role in FAs, as around half of the 180 FA proteins mentioned earlier are known to contain one or more serine, threonine, or tyrosine residues that are phosphorylated (Zaidel-Bar, Geiger 2010). There are several tyrosine kinases in FAs (FAK, Src, Fyn, etc.) (Bershadsky, Balaban & Geiger 2003), many of which are essential for proper FA function. As a counterbalancing force, FAs contain also some protein tyrosine phosphatases, some of which (like receptor-like tyrosine phosphatase α (RPTP- α)) are known to be important for mechanotransduction events (Zaidel-Bar, Geiger 2010).

FA functions are also controlled by multiple groups of small GTPases. One of the most often-quoted is the Rho family of GTPases, which contains key players in activating actomyosin contraction in cells. The activation mainly happens through the activation of Rho-kinase (ROCK), which in turn activates myosin light chain (MLC) through phosphorylation. Furthermore, ROCK also phosphorylates myosin phosphatase, thus enhancing the MLC-activating effect. (Davies, Helmke 2010, Chicurel, Chen & Ingber 1998).

In addition to direct protein–protein interactions, phosphorylation, and small effector GTPases, many FA proteins are also subject to regulatory protease activity. Probably the most studied protease here is calpain, which causes turnover and possibly activation of multiple FA components (Bershadsky, Balaban & Geiger 2003), like integrin, vinculin, paxillin, and tensin (Zaidel-Bar, Geiger 2010). In the case of FA turnover needed for cell migration, for example, calpain-II-mediated cleaving of the talin head from its rod domain seems to be essential (Critchley 2009).

1.2.5 FAs and force

As a physical linker of mechanical force FAs serve as an integral part forming the cell–ECM module, in which the structural organisation of both the ECM and the cell cytoskeleton are determined largely by cell adhesion and cell–ECM interaction (Eyckmans et al. 2011). FAs act as structural hot spots along which force is transmitted in both directions – a cell can exert traction forces on its substrate during, for example, cell migration, while simultaneously being anchored firmly to its substrate and experiencing stretching and pushing forces from the ECM (Eyckmans et al. 2011). Actually, FAs are practically continually stressed by forces, of which the actomyosin contractility caused by myosin II actin on the cell's own cytoskeletal actin bundles is probably the most ubiquitous one (Bershadsky, Balaban & Geiger 2003). FAs respond to force transmitted through them in various ways, like increasing in strength or aligning themselves to the direction of the force, for example when the cell is subjected to shear stress caused by flowing fluid (Davies, Helmke 2010).

1.2.5.1 Force transmitted through FAs is influenced by the stiffness of the substrate

As previously mentioned, most cells generate force themselves mainly through their actomyosin system of the cytoskeleton. Because of this force, FAs in adherent cells are practically under constant stress as the cell pulls on its surface, which, according to basic Newtonian laws in a mechanical equilibrium, generates equally large

opposing forces. Interestingly however, the force generated by cells – and thus also experienced by their FAs and substrate – depends on the rigidity of the surface they are on. Using MDCK epithelial cells and microfabricated elastic pillars previously introduced by Tan et al. (2003), Saez et al. (2005) could demonstrate that the force exerted by cells on their substrate through FAs is actually *directly proportional* to the spring constant (i.e. rigidity) of the substrate. Thus the more relevant factor from the point of view of the cell would seem to be the deformation rather than force (Saez et al. 2005). Naturally this is expected to only hold true for deformable substrates, whereas the exerted force would be expected to reach a plateau on totally rigid surfaces like glass. This plateau region is, however, not straightforward to measure, as force-measurement methods based on visually observing substrate deformation become increasingly inaccurate as substrate rigidity increases and the magnitude of deformation decreases (Saez et al. 2005).

1.2.5.2 Focal adhesions strengthen their grip on ligands when mechanically stimulated

In a classic study, Choquet et al. (1997) demonstrated the, now well-known, ability of integrin-mediated FAs to strengthen their grip on a bound bead when force is applied to the bead. They also demonstrated that integrin binding to the cytoskeleton required either the spatial clustering of integrins (achieved in the study using antibody-mediated cross-linking) or the binding of integrins to integrin ligands, like fibronectin. However, while the activation of integrins did not absolutely require integrin–ligand interactions, the strengthening of the grip did, as was shown using beads coated with anti- β_1 -integrin antibodies or fibronectin (Choquet, Felsenfeld & Sheetz 1997). Similarly, they also showed that the strengthening was specific to the linkages that had been mechanically stressed rather than being caused by some form of general reinforcement of the whole cytoskeleton, for example. Interestingly, the reinforcement of FAs has been later shown to be induced by applying external forces even when the generation of intracellular forces is inhibited (Bershadsky, Balaban & Geiger 2003). These findings of the strengthening of binding brought forth the idea of a so-called slip bond or clutch, which requires among other things the structural FA protein, talin1 (Critchley 2009), and the action of tyrosine phosphatases (Zaidel-Bar, Geiger 2010, Choquet, Felsenfeld & Sheetz 1997)(.). The strengthening has later been proposed to be mainly caused by recruitment of the FA proteins talin and vinculin to the adhesion complexes (Ziegler, Liddington & Critchley 2006).

1.2.5.3 Force and FA formation are linked

Further study into the reinforcement and general formation of FAs showed that the growth, and thus also strengthening, of FAs are a result of increased force transmitted through the adhesion, and not an effort of the cell to exert more force on its substrate (Bershadsky, Balaban & Geiger 2003). The dependence of FA formation on force transmitted through it is actually so intimate, that there seems to be a linear correlation between the force transmitted through a growing focal adhesion and its size.

Balaban et al. (2001) considered the relationship between FAs and force in terms of 'FA intensity' measured as the fluorescence intensity of GFP-tagged vinculin. Their results suggested that the relationship between force and adhesion site formation is intricately linked on a time-scale of under a few seconds, which was their experimental resolution. They used the actomyosin inhibitor BDM (2,3-butanedione monoxime) to decrease the force exerted through FAs and measured this decrease by observing the displacement of micropatterns on a compliant substrate. They observed a virtually simultaneous decrease in FA intensity linked to force reduction (Balaban et al. 2001), which suggested a tight link between FA size and the force that could be transmitted through it. The reliance of FAs on force is so strong that FAs actually dissolve entirely in the complete absence of actomyosin generated tension (Bershadsky, Balaban & Geiger 2003).

There has been much debate regarding the correlation between force and FA area after this (see e.g. Doyle, Yamada 2010). Yet, Tan et al. introduced the notion of a linear correlation already in 2003 using a novel approach of elastic microcolumns, which enabled isolation of forces much more readily than the micropatterned substrates used earlier. Analysing smooth muscle cells they concluded that the constant relating force and FA area would be around $4.8 \text{ nN}/\mu\text{m}^2$ (Bershadsky, Balaban & Geiger 2003, Tan et al. 2003), which, in other words, meant that the FAs analysed caused a *size-independent shear stress* of 4.8 kPa on their substrate. Similar results had been previously reported for different cell types for example by Balaban et al. (2001), who measured shear stresses of $5.5 \pm 2 \text{ kPa}$ for human foreskin fibroblast FAs. This linear correlation has later been corrected in a very recent study from Stricker et al. (2011) to only cover assembling FAs in their myosin-dependent growth steps found (mostly) in the leading edge of the cell. Other adhesions, on the other hand, would not seem to show any strict force–area correlation (Stricker et al. 2011).

Furthermore it should be noted, that the linear correlation described by Tan et al. (2003) seemed to hold true only for assembling adhesions roughly larger than $1\ \mu\text{m}^2$. For vinculin-positive adhesion sites smaller than this, Tan et al. (2003) reported disproportionally high forces, which did not correlate with adhesion size. For these small adhesions they reported forces up to 60 nN, which would thus correspond to shear stresses of well over 60 kPa depending on the actual size of the adhesion. These small adhesion sites were primarily found in the leading edges of migrating cells, which led to the suggestion that they could serve as the primary anchor points generating the force necessary for movement (Doyle, Yamada 2010, Bershadsky, Balaban & Geiger 2003), and that they would, in fact, represent the earlier mentioned focal complex (FX) stage in FA maturation (Tan et al. 2003). These small adhesions generating strong forces could, however, also be an experimental artefact caused by the use of micropillar systems, which hardly represent *in vivo* -like environments for cells.

Taken together, the results of studies looking into the force–area relationship in FAs indicate significant structural mechanosensitivity in maturing adhesions, where the recruitment of FA proteins to forming adhesions happens in a strictly force-dependent manner (Tan et al. 2003, Stricker et al. 2011).

1.2.6 What causes the tight force–assembly relationship in FAs?

While the phenomenon of the force-induced catch-bond in assembling FAs is well-known, rigorous portrayal of the molecular mechanisms behind it has thus far remained elusive. On the biochemical signalling side, mechanical stimulation, like pulling on integrin-bound microbeads using magnetic or optical tweezers, for example, is known to elicit a number of intracellular signalling responses. These responses include among other things release of intracellular calcium (Bershadsky, Balaban & Geiger 2003, Chicurel, Chen & Ingber 1998), action of RPTP- α phosphatases resulting in activation of Src kinases, like Fyn (Zaidel-Bar, Geiger 2010, Bershadsky, Balaban & Geiger 2003), general involvement of the FAK pathway (Doyle, Yamada 2010, Bershadsky, Balaban & Geiger 2003), and recruitment of the transcriptional machinery in the form of mRNAs and ribosomes to sites of ECM-binding and force application (Chicurel, Chen & Ingber 1998). Force-induced FA growth additionally needs at least talin1 (Critchley 2009), correct cell morphology, and, in the case that the force for FA growth comes from the cell itself, the activation of the cytoskeletal

contractile apparatus through the small GTPase Rho and its substrates ROCK, which activates myosin II (Bershadsky, Balaban & Geiger 2003, Tan et al. 2003).

1.2.6.1 Possible mechanosensors in FAs

There has been much speculation regarding the primary mechanosensory proteins in FAs (Bershadsky, Balaban & Geiger 2003). Since the strengthening of FAs happens on a spatially highly confined level, stretch-activated ion channels or other sensors causing diffuse responses seem unlikely as the primary mechanosensor (Bershadsky, Balaban & Geiger 2003). Furthermore the strengthening seems to even be independent of the integrity of the cell plasma membrane, which rule out ion channel-mediated changes in electrolyte concentrations and other membrane-associated mechanosensors altogether (Bershadsky, Balaban & Geiger 2003). As previously mentioned, the correlation between FA area and the force transmitted seems to be temporally almost instantaneous, which would seem to imply some mechanism on the conformational level of proteins, like force-induced unfolding of protein structures (Bershadsky, Balaban & Geiger 2003, Balaban et al. 2001).

The most promising proteins for the position of primary mechanosensor are nowadays probably talin, p130Cas (Eyckmans et al. 2011), and so-called LIM-domain proteins, like paxillin, zyxin, and migfilin (Schiller et al. 2011). Many of the LIM-proteins bind to filamentous actin (F-actin), which in itself has also been speculated to be a mechanosensor (Schiller et al. 2011). Beyond these, $\alpha_5\beta_1$ integrin and the transmembrane proteoglycan syndecan-4 have also been mentioned as potential candidates (Doyle, Yamada 2010). In the case of p130Cas, the mechanosensing has been proposed to happen through so-called ‘substrate priming’ (Dubin-Thaler, Sheetz 2010), in which opening of the protein structure under mechanical stress could expose previously shielded, ‘cryptic’ phosphorylation sites thus enabling Src-mediated phosphorylation (Sawada, Sheetz 2002, Sawada et al. 2006). Interestingly, cryptic interaction sites have also been implicated in large extracellular proteins. The ECM protein fibronectin, for example, has been suggested to have mechanosensitive properties through the opening of cryptic engagement sites as a result of mechanical force (Eyckmans et al. 2011).

Probably the most interesting and promising of the mechanosensor candidates to date is, however, talin, which together with one of its most important binding partners, vinculin, seems to be able to form a mechanosensory protein pair.

1.3 The focal adhesion proteins talin and vinculin

1.3.1 Talin

Talin is a rather large (~270 kDa) protein consisting of a ~50 kDa globular head on its N-terminus (residues 1–432) and a larger, more flexible C-terminal rod domain (433–2541) (Critchley 2009). The head contains a putative FERM domain with at least one unique unstructured loop, which is thought to have prevented any successful crystallisation of the whole head domain. The linker region between the head and tail domains is flexible and contains multiple phosphorylation sites, the functions of which are still uninvestigated (Critchley 2009). The talin rod, on the other hand, has been predicted to contain 62 helices organised into multiple sequential bundles of four to seven α -helices. Whereas the structure of several of the helical bundles has been solved (e.g. PDB-entries 2JSW and 2X0C), the tertiary structures of the bundle-connecting linkers have remained elusive. The most C-terminal helix has been implicated to be responsible for observed formation of talin dimers (Critchley 2009).

There are two talin genes in vertebrates: *Tln1* and *Tln2*. The genes share 74% of their sequence, and the more complex *Tln2* with larger introns has been suggested to be the ancestral gene. Despite their differences, the two talin forms share a common domain structure and most of their ligands (Critchley 2009). This similarity also renders making talin knockout cell lines difficult, since one gene can take over the function of its knocked-out sibling.

1.3.1.1 Talin offers binding sites for numerous FA proteins creating a structural hub

As is evident from the values given in Table 2 for the talin C and N-terminal parts, talin has a highly polarised orientation in the focal adhesion core with the C-terminal tail being around 30 nm nearer to the membrane than the N-terminal head (Kanchanawong et al. 2010). Like the focal adhesion protein tensin, talin binds to the cytoplasmic parts of β -integrins with its phosphotyrosine-binding (PTB) -like module in the head domain that interacts with the conserved NPxY (or NPxF) motif of the cytoplasmic integrin tail (Bershadsky, Balaban & Geiger 2003). It should be noted, however, that this interaction is not necessarily dependent on tyrosine phosphorylation of the NPxY motif, but that the phosphorylation might in some cases even inhibit the interaction (Bershadsky, Balaban & Geiger 2003).

In its position as a primary integrin-binder, talin functions as a sort of scaffold to which numerous other proteins can bind. Talin has several protein binding sites all

along the length of its structure. Some of the binding partners of the head domain include cytoplasmic parts of β -integrins, the hyaluronan receptor layilin, and the phosphatidylinositol-4-phosphate kinase PIPK1 γ 90, which has been implicated to have FA-regulating functions (Critchley 2009). The talin head also binds acidic phospholipids and might be able to insert itself into lipid bilayers, which has even been hypothesised to provide a mechanism for talin to topically change the curvature properties of the lipid membrane thus for example facilitating membrane protrusion at the leading edge of migrating cells (Critchley 2009). The talin rod, on the other hand, has also at least one integrin binding site (with an as yet still not fully understood function), a site for binding a muscle-specific intermediate filament protein (α -synemin), and multiple vinculin binding sites (VBS). Additionally, talin has three different regions identified as F-actin binding sites all along its length, and it has been implicated to be able to stimulate actin fibre growth (Critchley 2009).

Although numerous other proteins have also been identified to be interaction partners of talin using, for example, pull-down assays, direct interaction has proven somewhat difficult to show, as talin functions as a hub in a large-scale protein complex with multiple levels. Thus it should be no surprise that many proteins originally identified as interaction partners of talin could (and probably are) in fact simply interacting indirectly with talin – this has for example been the suggested for the focal adhesion kinase FAK (Critchley 2009).

The complete regulatory machinery controlling talin activity is still unknown, but binding of many of the ligands is likely to be regulated to some extent by an autoinhibitory intramolecular interaction in talin. It has been suggested that the usually linear talin could also form a more globular structure (observed thus far mainly in experimental low salt buffers), in which some of its binding sites (especially VBSs) would be shielded and thus inaccessible (Critchley 2009).

The key role of talin in FAs is strikingly displayed in experiments with cells devoid of both Tln1 and Tln2 expression. Although these cells still interact with their substrates in some ways – cell spreading is still initiated, for example – they are unable to fully support integrin activation, maintain spread cell morphology, assemble FAs, and hither exert traction forces on the underlying substrate (Critchley 2009).

1.3.2 Vinculin

One of the most important binding partners of talin is vinculin. Vinculin is one of the ‘typical’ FA proteins, and it is, like for example paxillin, often used as a FA marker (Tan et al. 2003, Diez et al. 2011). Vinculin seems to be a general adapter-like protein in complexes requiring mechanical stability, as it can also be found in adherens junctions, where it serves as a linker between junction proteins and actin filaments (Eyckmans et al. 2011, Ziegler, Liddington & Critchley 2006). In FAs, around half of the vinculin molecules coincide vertically with the actin cytoskeleton, thus putting vinculin in a key position in terms of force transmission from FAs to the cytoskeleton (see Table 2). The other half resides in the ‘focal adhesion core’, and thus serves as an integral part of focal adhesion structure (Kanchanawong et al. 2010). The main role of vinculin has long been thought to be purely structural in a sense that it would be reinforcing the integrin–cytoskeleton-connection by cross-linking talin to actin. Recent evidence using mutant vinculin constructs have, however, suggested that vinculin would have a key regulatory role as well (Cohen et al. 2006, Cohen et al. 2005).

1.3.2.1 The structure of vinculin reveals multiple ligand binding sites reflecting its role as a regulatory linker

The vinculin molecule consists of 1066 amino acids, which are divided into three regions: (i) a globular head domain (Vh) consisting of four α -helical vinculin domains (Vd1 through Vd4), of which Vd1 contains most of vinculin’s known ligand binding sites; (ii) a proline-rich linker region; and (iii) an α -helical tail domain (Vt) (Ziegler, Liddington & Critchley 2006). While the head domain’s binding sites for talin, α -actinin, and α and β -catenin are probably the most well-studied, the proline-rich linker and Vt also have distinct ligand binding activities. Known ligands there are Arp2/3, vinexin, VASP for the linker region, and F-actin, paxillin, and acidic phospholipids like phosphatidylinositol 4,5-bisphosphate (PIP₂) for Vt (Ziegler, Liddington & Critchley 2006). Interestingly, the Vt domain seems to also contain a further site allowing Vt-mediated vinculin dimerisation, which is activated only after binding of Vt to actin suggesting a mechanism for vinculin-mediated actin cross-linking (Ziegler, Liddington & Critchley 2006).

1.3.2.2 Lessons learned from vinculin-null cells

Much of the information currently available about the functions of vinculin stems from studies using cells lacking vinculin derived from knockout model organisms.

Cell strains like these have traditionally been employed in studies regarding the effect of vinculin on cell morphology, motility, and FAs (Kanchanawong et al. 2010, Diez et al. 2011, Xu, Coll & Adamson 1998, Humphries et al. 2007, Saunders et al. 2006). On the level of the whole organism, knocking-out vinculin is lethal due to major defects in brain and heart development in the embryo (Xu, Baribault & Adamson 1998). Vinculin-deficient fibroblasts, however, are readily isolatable from knock-out murine embryos, and after spontaneous immortalisation they present a viable model for the analysis of vinculin functions (Xu, Baribault & Adamson 1998).

Generally $\text{Vin}^{-/-}$ cells are characterised by increased migration rates and decreased cell spreading (Xu, Coll & Adamson 1998, Saunders et al. 2006). Cell morphology in general is also affected with vinculin-null cells being more elongated and spindle-like in shape than wild-type cells. Furthermore, while cells lacking vinculin do generate integrin-mediated, talin-positive focal adhesions, these adhesions have been reported to show increased turnover rates and smaller sizes compared to wild-type cells (Saunders et al. 2006), which would suggest that vinculin could act as a negative regulator of FA turnover. These results also suggest an explanation for the tumour-suppressive activities sometimes ascribed to vinculin (Ziegler, Liddington & Critchley 2006).

1.3.3 The talin–vinculin interaction

Initial experiments suggested that talin had three vinculin binding sites (VBSs 1–3) (Critchley 2009). Further studies have later revealed several other amphipathic α -helices along the talin rod capable of binding to Vd1 with varying affinities (Critchley 2009). Each of these binding sites consist of an amphipathic VBS peptide forming a short α -helix that is in most cases an integral part of a helical bundle domain of the talin rod (Critchley 2009). While the different VBSs have somewhat varying binding affinities towards vinculin, the mode of vinculin binding of all of them is the same. During binding the amphipathic VBS helix inserts itself into the helical bundle of the Vd1 domain replacing one of the helices there (Ziegler, Liddington & Critchley 2006). While the affinity of separate VBS peptides to vinculin is quite high, the binding is significantly weaker when VBS peptides are in their native environment in the talin rod domain bundles (Critchley 2009). In fact, it seems that most of the vinculin binding sites in talin are cryptic in a way that they are shielded in their respective bundle domains and thus inaccessible to vinculin binding in relaxed conditions.

The binding of VBSs to the vinculin head lies under rather severe structural constraints. Since the binding effectively has to open the vinculin fold, talin binding is affected directly by the stability of the Vd1 domain, and stabilising the domain experimentally has been shown to drastically decrease talin binding affinity (Ziegler, Liddington & Critchley 2006). Furthermore, talin as a whole has to be active and not in the autoinhibited globular form described in 1.3.1.1 above. This activation seems to be controlled by biochemical signalling pathways containing, for example, PIP₂ created by a phosphatidyl inositol kinase bound to talin (Bershadsky, Balaban & Geiger 2003).

Since integrin-bound talin in FAs is mostly expected to be in the active conformation, the binding of an individual VBS seems mostly to be reliant on two events: (i) the activation of vinculin from its autoinhibited form, and (ii) the loosening of the helical bundle in the talin rod containing the VBS peptide in question. Both of these events have received quite a lot of attention in the past few years and they shall be analysed in more depth next.

1.3.3.1 An autoinhibitory head–tail interaction (HTI) in vinculin controls the protein’s activity by inhibiting binding of VBS peptides

Vinculin has at least two conformations: an ‘open’ active and a ‘closed’ inactive, the autoinhibited inactive of which is predominant in cellular vinculin (Critchley 2009). The autoinhibition is caused by an intramolecular interaction between vinculin domain 1 (Vd1; residues 1–258) in the globular vinculin head and the vinculin tail (Vt; residues 881–1066) (Critchley 2009, Humphries et al. 2007). Vd1 comprises a total of seven α -helices which form two bundles of four helices linked together by one long, common helix (Critchley 2009). Since the Vt–Vd1 interaction is in essence very similar to the binding of VBS peptides of talin to Vd1, the binding of Vt or VBSs to Vd1 is mutually exclusive (Critchley 2009).

The effects of the autoinhibitory head–tail interaction (HTI) on vinculin’s affinity to talin and on the dynamics of FA complex proteins have been extensively studied using HTI-deficient vinculin mutants (Cohen et al. 2005, Humphries et al. 2007). One of the most promising mutants, named vinculin T12 (VinT12), has multiple charged amino acids (D974, K975, R976, R978) mutated to alanine in the tail region of vinculin (Cohen et al. 2005). These mutations effectively disrupt the autoinhibitory HTI, which has significant consequences for the occurrence of talin–vinculin interactions in cells (Cohen et al. 2006). In their 2006 study, Cohen et al. showed that

vinculin could be colocalised with talin ectopically localised to the outer membranes of mitochondria (and *vice versa*) by introducing the VinT12 mutations to vinculin (Cohen et al. 2006). Furthermore, these ectopic binary talin–vinculin complexes were found to be functional to a degree where they recruited cytoplasmic parts of β_1 -integrin to form a membrane-bound ternary complex (Cohen et al. 2006). Additionally, Cohen et al. showed that the T12 mutant enhances the residency time of vinculin in FAs by up to 3-fold – an enhancement that could be rescued by a talin binding site mutation, suggesting that the observed lag seemed to be caused by overly stable talin–vinculin interactions.

1.3.3.2 Vinculin binding to VBS peptides in talin requires opening of helical bundle domains in the talin rod

As was previously alluded to, most VBS peptides in talin are cryptic. In fact, it could be argued that practically all of the around 11 binding sites are cryptic in a sense that they are not available for vinculin binding without sometimes major conformational change in their respective domain. Thus the activity of each individual VBS in the talin rod is regulated by the structural stability of the individual α -helix bundle domain of the talin rod (Critchley 2009). This stability is naturally affected by the whole microenvironment of the domain. Problematically, studying the individual VBSs of talin with mutational experiments is difficult because of the redundancy in vinculin binding caused by the numerous binding sites on the talin molecule. Single-molecule experiments of tandem repeats of single talin helix-bundle domains have been proposed as an answer to this problem (Lee, Kamm & Mofrad 2010), but thus far none have been presented. Simultaneously, however, talin with its multimodular structure does seem to present a case in which multiple sequential protein structural modules with differing mechanical stabilities and biochemical binding partners could form a structure that elicits different biochemical responses as a function of mechanical force. This hypothesis of multimodularity, as postulated for example in (Hytönen, Smith & Vogel 2010), is an intriguing example of a way to bring forth a complex force–response pattern that is needed for efficient and meaningful mechanotransduction in cells.

1.3.3.3 Activation of talin VBSs through application of mechanical force

While the mode of activation of the cryptic VBSs in talin has not been solved completely, conformational unfolding induced by mechanical stretching seems likely.

The ability of mechanical force to open up individual helical bundle domains in such a way that VBS peptides are exposed was implied, for example, in steered molecular dynamics simulations by Hytönen and Vogel (2008). They used a structural all-atom model of a talin rod fragment (residues 486–889) in constant-force and constant-velocity simulations to show that previously shielded VBS peptides could be exposed to solvent during stretch-induced unfolding of the helical bundle domain (Hytönen, Vogel 2008). Simultaneously, they were also able to show that the sequential unfolding brought about a situation, where individual VBS helices were exposed at different stages in the simulation, possibly suggesting a mechanism for quantitative force-sensing through gradual unfolding.

Further encouraging results were later produced in experimental studies by del Rio et al. (2009), who showed that recruitment of the vinculin head to the talin rod is indeed stimulated by the application of mechanical stress. They used an *in vitro* assay with a recombinant talin rod fragment (near the same residues as used by Hytönen and Vogel (2008) in their study) linked N-terminally to a rigid surface and C-terminally to magnetic beads. Using magnetic tweezers and a vinculin head domain–fluorophore construct they could then observe increased binding of Vh to the talin rod, when force was applied to it (del Rio et al. 2009). Furthermore, an extremely recent study from the Sheetz group (Margadant et al. 2011) could show that intracellular forces were sufficient to cause major stretching of talin molecules in adhesion structures, thus for the first time demonstrating that a stretch-induced mechanism could, in principle, also be activated inside cells. Interestingly, Margadant et al. (2011) could also see that the stretching of talin was oscillating in time and that the dynamics and range of the stretching could be influenced by introducing exogenous vinculin head domain into the cells. These results therefore further implied that talin could not only be stretched *in vivo*, but also that vinculin might bind to stretched talin in cellular conditions.

Considering these results and the long-known fact that vinculin recruitment to focal adhesions is induced by the application of mechanical force (Critchley 2009), it would seem highly likely that the talin–vinculin system does function as a primary mechanosensor in FAs. However, although the hypothesis regarding VBS activation in talin is rather strong, direct evidence of the interaction using full-length proteins in biologically relevant environments has been, and still is, lacking (Eyckmans et al. 2011, Lee, Kamm & Mofrad 2010).

1.3.3.4 The talin–vinculin interaction is likely controlled by both HTI-regulation and unfolding

Given the results highlighting the significance of both means of talin–vinculin regulation, there has been some speculation in the literature over which of the means is predominant in regulation of vinculin recruitment to FAs. The results from vinculin mutation studies presented earlier have led, for example, Cohen et al. (2005 and 2006) to conclude that vinculin conformation, as determined by the autoinhibitory HTI, would directly be the determining factor regulating the lifetime of talin–vinculin complexes in FAs. Their results, however, were based largely on fluorescence recovery after photobleaching (FRAP) experiments done on stiff substrates without modulating the force transmitted through FAs (Cohen et al. 2006). Thus these experimental setups could not assess possible mechanoactivation of VBSs in talin. On stiff substrates most of the VBSs are expected to already be in an open conformation, thus removing the potential for mechanosensitive regulation of VBSs in talin, and creating a situation, where vinculin conformation is, indeed expected to be the only limiting factor. Simultaneously however, the ectopic recruitment assays done by Cohen et al. (2006) show that activated VinT12 could be recruited also to mechanically relaxed talin localised to mitochondria. This clearly does suggest a significant role of vinculin HTI-mediated activation also in the binding to mechanically relaxed talin.

Although the need for vinculin to be in the active conformation for efficient talin binding seems to be widely accepted through detailed molecular dynamics simulations (Golji, Lam & Mofrad 2011) and the experimental assays discussed (Cohen et al. 2006), the mechanisms of vinculin activation *per se* are still somewhat unclear (Critchley 2009, Ziegler, Liddington & Critchley 2006). Revealing/activating the cryptic binding sites in talin has, for example, been suggested to be enough to also cause an opening of the autoinhibitory head–tail interaction in vinculin, thus enabling vinculin–talin interactions (Ziegler, Liddington & Critchley 2006, Bois et al. 2006). In the end, the talin–vinculin interactions seem to be controlled by a reciprocal mechanism, in which activation of vinculin and talin are mutually strengthening phenomena.

1.4 Introduction to methods used in this study

1.4.1 Using compliant cell culture substrates for studying mechanotransduction

The notion that traction forces are modifiable by the stiffness of the substrate (see Saez et al. (2005) and 1.2.5.1 above) enables a convenient way of using the traction forces generated by the cells themselves to modulate the force transmitted through FAs simply by culturing the cells on substrates with different stiffness.

1.4.1.1 Biofunctionalised polyacrylamide presents a convenient substrate material with adjustable rigidity

Polyacrylamide (PAA) gels bonded to glass substrates have been used for over a decade in cell culture (Buxboim et al. 2010). They provide a convenient method of creating pliable substrates using materials available in most laboratories. While a PAA gel is basically a porous matrix of polymers filled with water, the pore size is substantially smaller at around tens of nm, than what is relevant for FAs or other cell adhesion structures (Buxboim et al. 2010). PAA substrates have so far found use in numerous mechanotransduction studies and some improvements have been suggested to the manufacturing protocol since the first publication of the method by Pelham and Wang (1997). In summary, polyacrylamide is first covalently bonded onto a cleaned glass surface (e.g. a coverslip) by chemically activating the glass surface using aminosilane compounds (e.g. aminopropyltriethoxysilane, APTES), and then bonding the PAA gel onto the activated surface's amine groups using the ubiquitous amine-reactive cross-linker glutaraldehyde (Pelham, Wang 1997, Engler et al. 2004c, Yeung et al. 2005). Since solution-based silanisation can create a strongly autofluorescent surface, a vapour-based silanisation treatment should be preferred in cases where fluorescence microscopy will be used for analysis later (Smith M. 2010, *Personal communication*).

In order to create a level and smooth PAA gel surface, a second non-treated glass slip is laid onto the PAA mixture for the duration of polymerisation. After removal of the top glass the PAA surface has to be further made accessible for cell adhesion using, for example, ECM proteins that can be added onto the surface. Since cells exert forces onto the substrates via these proteins, covalent linking is essential (Smith M. 2010, *Personal communication*). One cross-linker used for this is Sulfo-SANPAH (Stricker et al. 2011, Yeung et al. 2005, Engler et al. 2004b), which has an aminoreactive Sulfo-NHS-ester group on one end and a UV-activatable nitrophenyl

azide group on the other end. The aminoreactive group links onto the PAA gel, while the photoactivatable group is used to link any desired proteins, like collagen I (Engler et al. 2004b) or fibronectin onto the surface. The build-up of a biofunctionalised PAA gel is summarised in Figure 2.

1.4.1.2 Altering and measuring stiffness of PAA substrates

One considerable advantage of PAA over, for example, polydimethylsiloxane (PDMS) is that a PAA-gels' stiffness, or Young's modulus (E), changes considerably with only slight changes in the chemical composition (Buxboim et al. 2010). By varying the amount of the main polymer-forming chemical acrylamide and its ratio to the cross-linker bis-acrylamide, PAA gels spanning approximately two orders of magnitude of E can be made (Buxboim et al. 2010, Yeung et al. 2005). Sadly, however, measuring microscale E in general is by no means straightforward. Results vary depending on the method and the size and shape of the probe used (Buxboim et al. 2010). This has been evident especially in measurements of tissue samples with atomic force microscopy (AFM) (e.g. Engler et al. 2004b). In the case of PAA gels, E changes furthermore as a function of the thickness of the gel, and is also not constant inside a gel due to non-uniform swelling of the gel in solution (Buxboim et al. 2010). Due to these and other difficulties, research done with PAA gels often uses a semiquantitative measure of substrate rigidity, simply comparing 'rigid' substrates to a series of 'soft' substrates (Doyle, Yamada 2010).

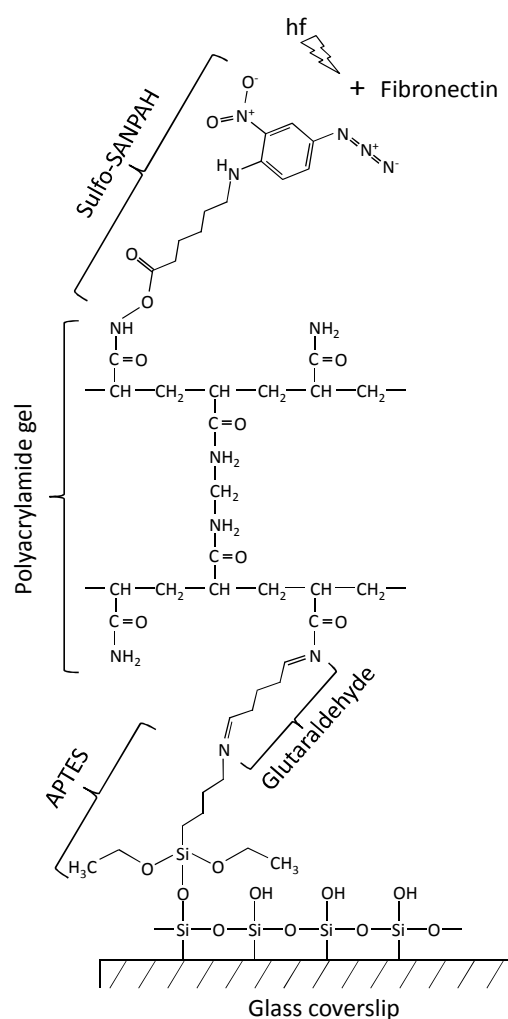


Figure 2: Schematic representation of the chemical build-up of a PAA cell culture substrate. The individual components, the derivatives of which form the end structure, are labeled. The thickness of the PAA gel is not to scale.

1.4.2 Purifying FA proteins

Several studies investigating the composition of focal adhesion protein complexes have been published during the last few years (Kuo et al. 2011, Humphries et al. 2009, Schiller et al. 2011). These, and some earlier studies looking into FA proteins (Plopper, Ingber 1993), have been mostly based around semi-specific protein extraction methods. In these methods the differentiation between FA proteins and other cellular proteins has mainly been the subcellular localisation of FA protein complexes to the basal membrane of cells, and the tight, cross-linkable association of the complexes to integrin ligands via integrin proteins. A significant challenge in these sorts of extraction methods is the inherently unstable build-up of FA complexes. In a case where protein–protein interactions are reliant on, for example, mechanical stretching, disruption of the cell during lysis can be expected to simultaneously disrupt most mechanical integrity of the cell and thus cause the disintegration of many complexes. Thus some sort of chemical cross-linking to fix protein complexes is often necessary.

Although the methodology described above is more or less well-established for the use of mechanobiological studies, each of the methods naturally requires optimisation and validation whenever implemented in a new environment in new conditions. This thesis will focus mainly on this optimisation and testing work related to the use of new methodology.

2 Main goals of the thesis

The primary aim of this thesis was to set up the methodology needed for studying protein–protein interactions in the cytoplasmic parts of FA protein complexes, with a special emphasis on the talin–vinculin interaction. This interaction and its possible mechanosensory characteristics were approached using a simple mammalian cell model and various EGFP-fused vinculin proteins. Mouse embryonic fibroblasts (MEF) will be used as a model, because of the availability of a vinculin-deficient cell line besides wild-type cells.

The work was divided into the following tasks: (i) selection of suitable transfection conditions for the chosen cell line and EGFP-fusion constructs, (ii) assessment of different purification methods for FA protein purification from both transfected and untransfected cells, (iii) use of non-rigid, PAA-made cell culture substrates in modulating the mechanical environment of cells and FA complexes, and (iv) preparing methodology for analysis of cellular responses to changes caused by altered mechanical environments and/or the presence of mutant FA protein constructs. The last mentioned analyses (iv) were to be based mainly on image analysis tools designed for analysing fluorescence microscope images.

The goal of these aims (i–iv) was to provide a set of tools for detailed elucidation of the talin–vinculin interaction on a molecular level thus addressing the question of the potential mechanosensitivity of the talin rod in FAs. Thorough portrayal of the talin–vinculin interaction could be one of the first detailed descriptions of an actual mechanotransduction event caused by opening of cryptic binding sites in a cellular context.

3 Materials and methods

3.1 Mammalian cell culture

3.1.1 Cell strains

Mouse embryonic fibroblasts (MEF) were obtained from Dr. Wolfgang Ziegler (Hannover, Germany). Both wild type and vinculin-null cell lines are spontaneously immortalised strains isolated from mouse embryos produced in heterozygous crosses of $\text{Vin}^{+/-}$ mice. The isolation and characterisation of the cells are described in (Xu, Baribault & Adamson 1998).

3.1.2 Maintenance of cells

MEF cells were routinely cultured in T75 cell culture flasks (Sarstedt) in Dulbecco's modified Eagle medium (DMEM) (Lonza BioWhittaker[®], Cat. No. BE12-614F) with 4.5 g/l glucose. The medium was supplemented with 10% fetal bovine serum (FBS) (Lonza BioWhittaker[®], Cat. No. DE14-801F), 2 mM L-glutamine and 0.1 mM β -mercaptoethanol according to Xu et al. (1998). For routine maintenance culturing, cells were subcultured on average twice a week using standard cell culture methods with a subcultivation ratio of 1:12 or 1:15. Cell culture grade PBS without divalent Ca and Mg ions (Lonza BioWhittaker[®], Cat. No. BE17-516F) and trypsin-EDTA (170,000 U/l and 200 mg/l, respectively) (Lonza BioWhittaker[®], Cat. No. BE17-161E) were used for subcultivation. Care was taken to avoid reaching complete confluency during maintenance culture. No cells of passage number 20 or greater were used for experiments. Care was also taken to handle the two cell lines separately to avoid any issues generated from potential cross-contamination.

3.1.3 PAA cell culture substrates

PAA-derived cell culture substrates were made using a modified form of the protocol published by the Wang lab⁵ (Carnegie Mellon University, Pittsburgh, PA, USA). Glass coverslips were used as a base for the substrates to facilitate sample preparation for immunofluorescence microscopy. The glasses were cleaned by flaming them with a bunsen burner, soaking in 0.1 M NaOH, and then briefly rinsing with dH₂O to avoid excess salt formation, before air drying and aminosilanisation. Aminosilanisation was done in an exicator under vacuum with the silanisation agent, (3-aminopropyl)triethoxysilane (APTES, Sigma Aldrich Cat. No. 440140), present in

⁵ [http://www.ece.cmu.edu/~yuliwang/Methods/Materials/Artificial Materials/PAASubstrates.pdf](http://www.ece.cmu.edu/~yuliwang/Methods/Materials/Artificial%20Materials/PAASubstrates.pdf), accessed on 9.10.2011

the excicator in an open plastic bottle. After 1 h of incubation under vacuum conditions at room temperature, the glasses were covered with 0.5% glutaraldehyde (in PBS) and incubated for 30 min, followed by extensive washing with dH₂O. Acrylamide / bis-acrylamide mixtures were prepared in a Hepes buffered (final c = 50 mM) solution varying the amount of acrylamide and bis-acrylamide from 5% to 8% and 0.025% to 0.1%, respectively, to create substrates of different stiffness. The solution was degassed using a USB ThermoVac (MicroCal LLC, Northampton, MA, USA) degassing station to remove excess oxygen which might inhibit polymerisation, before adding ammonium persulfate (APS) and tetramethylethylenediamine (TEMED, Sigma Aldrich Cat. No. T9281) to final concentrations of 0.06% w/v and 0.4% v/v, respectively, to initiate polymerisation of the acrylamide. 20 µl of this solution was then immediately added onto each silanised and glutaraldehyde treated coverslip. This amount covered with a second coverslip theoretically results in gels of ~300 µm in height, which is well beyond the threshold thickness to negate any effects of an underlying rigid substrate on cell behaviour (Buxboim et al. 2010).

After polymerisation and removal of the top coverslips, the gels were rinsed with 50 mM Hepes buffer (pH 8.5) before adding the cross-linker Sulfo-SANPAH (Thermo Scientific, Cat. No. 22589; 1 mg/ml in 50 mM Hepes; 80 µl per coverslip) onto the gels. The cross-linker was activated by exposing the gels in wells of a 6-well plate to the UV-light of a UV-table with eight 8 W UV lamps for 2×1.5 min, removing excess cross-linker solution in between the two activations. Photoactivation could be verified by observing a colour change in the Sulfo-SANPAH solution from bright red to a reddish brown. The gels were then washed once again quickly with 50 mM Hepes (pH 8.5) before adding a 1 mg/ml fibronectin (YoProteins, Cat. No. 663) solution onto the gels. Care was taken to minimise the time of Sulfo-SANPAH in solution before addition of FN, since the cross-linkers activity decreases quickly in solution⁶. The FN solution was incubated for 1 h at 37 °C, after which the substrates were transferred to sterile conditions in a cell culture laminar hood, rinsed with sterile PBS, sterilised by exposing them to the UV-light of the laminar hood for 30 min, and finally rinsed once again with sterile PBS. Ready-made substrates were stored at +4 °C for up to a week.

⁶ Product instructions, Thermo Scientific (<http://www.piercenet.com/instructions/2160635.pdf>), accessed on 9.10.2011

Functionalisation of glass coverslips with covalently linking FN onto them was done by aminosilanising the glass as described above, washing with 50 mM Hepes, and then linking FN onto the aminosilanised surface with Sulfo-SANPAH exactly as described above for PAA gels.

3.2 Expression constructs

Both EGFP-Vinculin fusion proteins used were based on the plasmids pEGFPC1/V1-1066 wt and pEGFPC1/V1-1066 T12 (kind gifts of Prof. Susan Craig from Johns Hopkins University). Both constructs have EGFP fused to the N-terminus of full-length vinculin under a cytomegalovirus (CMV) promoter. The plasmids have a Kan^r/Neo^r gene (neomycin 3'-phosphotransferase II) enabling kanamycin selection in prokaryotes and G418 (geneticin) selection in eukaryotes. C-terminal Strep-Tag II's (ST, amino acids) were added to both constructs by Dr. Jenita Pärssinen creating the constructs EGFP-VinWT-ST and EGFP-VinT12-ST, respectively. EGFP-VinT12-ST contains the following vinculin HTI-disrupting mutations: D974A, K975A, R976A, R978A (Cohen et al. 2006, Cohen et al. 2005). Plasmids were produced in TOP10 *E. coli* cells using heat-shock transformation and kanamycin selection (50 µg/ml in LB medium). Plasmids were extracted using a Wizard[®] Plus MidiPrep kit (Promega) following the manufacturer's instructions. The sequence of the plasmids was confirmed by sequencing by Dr. Jenita Pärssinen (data not shown). A schematic map of the plasmids is shown in Figure 3.

3.2.1 Transfection

Transfection of MEF cells with EGFP-VinWT-ST and EGFP-VinT12-ST plasmids was done using the following transfection reagents: TransIT[®]-2020 (Mirus, Cat. No. MIR5410s), Lipofectamine[™] 2000 (Invitrogen, Cat. No. 11668-019), TurboFect[™] (Fermentas, Cat. No. R0539), FuGENE[®] 6 (Promega, Cat. No. E2691), and SuperFect (Qiagen, Cat. No. 301305). Transfection via electroporation was done using Ingenio[®] Electroporation Solution (Mirus, Cat. No. MIR50110). Serum-free Opti-MEM[®] I medium (Invitrogen, Cat. No. 11058-021) was used for plasmid dilution and transfection complex formation for all reagents.

3.2.1.1 Determining transfection efficiency for different reagents

Transfection efficiency was tested for MEFwt cells using the EGFP-VinWT-ST plasmid on a 24-well plate format. Six transfection reagents were tested following the manufacturers' instructions for transfection protocols as well as suggestions for initial

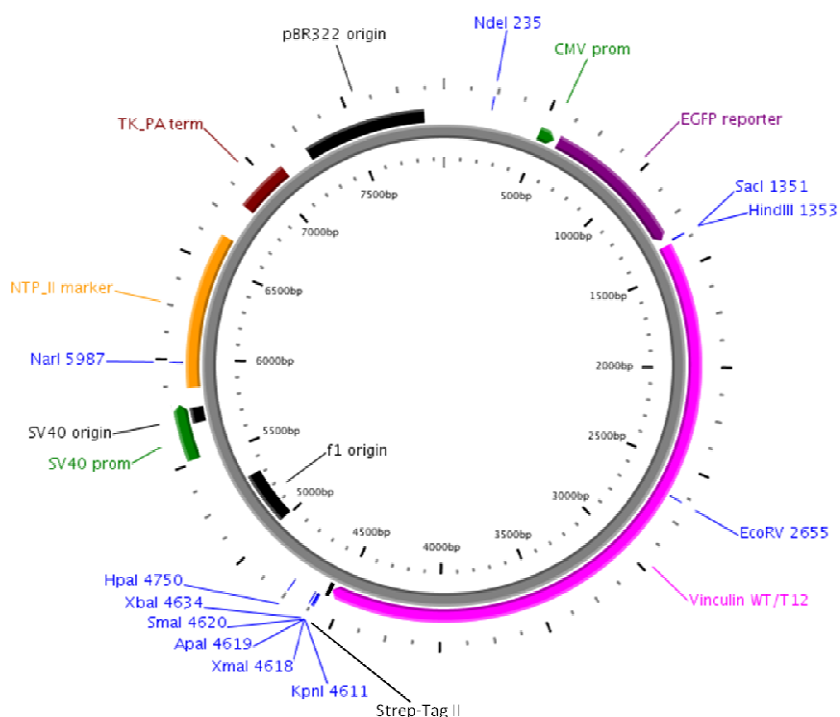


Figure 3: Schematic map of the plasmid used for transfection. The same plasmid was used for delivering both EGFP-VinWT-ST and EGFP-VinT12-ST with only the vinculin sequence changing. Unique restriction sites are shown in blue. NTP_II-marker is neomycin 3'-phosphotransferase II. Image created using PlasMapper v2.0 (<http://wishart.biology.ualberta.ca/PlasMapper/>).

plasmid DNA:transfection reagent ratios. These ratios and the amount of reagent for each well of a 24 well plate were as follows: 0.5 µg:1.5 µl for TransIT[®]-2020, 0.8 µg:2.0 µl for Lipofectamine[™] 2000, 1.0 µg:2.0 µl for TurboFect[™], 0.5 µg:1.5 µl for FuGENE[®] 6, and 1.0 µg:5.0 µl for SuperFect. Cells were seeded with two different seeding densities (4×10^5 and 10^5 cells per well) 24 h prior to transfection. Electroporation was tested on 6×10^6 cells resuspended in 200 µl of Ingenio Electroporation Solution, divided into two 0.2 cm electroporation cuvettes. 2.0 µg of plasmid DNA was used per cuvette. Cells were electroporated at 150 V using a BioRad GenePulser electroporator. Electroporated cells were seeded onto wells of a 24 well plate at densities of 1.5×10^5 and 7.5×10^4 cells per well. All conditions (seeding density and reagent) were tested as duplicates.

Cells were checked for EGFP-expression 24 h and 48 h post-transfection (PT) using an inverted fluorescence microscope (Olympus IX71 equipped with a Qimaging RETIGA 2000R FAST, Cooled Mono 12-bit CCD-camera) using a 10x objective (N.A. = 0.30) with the Surveyor software (Version 5.5.5.26, Objective Imaging Ltd, Cambridge, UK), taking a mosaic image of 9 images (3×3) of a random location from each well. Exposure times were adjusted separately by eye for each imaging set. Image analysis was done using ImageJ (see 3.6.1.1 below).

Expression levels of transfected proteins were furthermore assessed with immunoblotting of whole-cell lysates created by first washing adherent cells twice with PBS, then scraping cells off into a small volume of PBS using a pipette tip, centrifuging cells for 2.5 min at 3000 g (+4 °C), resuspending the resulting cell pellet into SDS-PAGE sample buffer (see 3.5.4 below), and mixing by vortexing. Lysates were stored at -20 °C before analysis with SDS-PAGE and western blotting (WB) (see 3.5.4 below).

The effects of the plasmid DNA:transfection reagent ratio was additionally tested with the TurboFect™ transfection reagent using the EGFP-VinWT-ST plasmid transfected into both MEFwt and MEF^{Vin-/-} cells. Cells were seeded onto wells of a 24-well plate 72 h prior to transfection: 5×10^3 cells per well for MEFwt and 10^3 cells per well for MEF^{Vin-/-} cells, which yielded confluencies of ~60% (as estimated by eye) for both cell types at the time of transfection. The following DNA:transfection reagent ratios were used: 1.0 µg:1.0 µl, 1.0 µg:2.0 µl, and, 1.0 µg:2.8 µl. EGFP-expression was checked 24 h PT as described above.

3.3 Antibodies

The following primary antibodies were used in the study: anti-vinculin mouse monoclonal antibody (clone hVIN-1, Sigma, Cat. No. V9131), anti-talin1 mouse monoclonal antibody (Abcam, Cat. No. ab57758), anti-GFP rabbit polyclonal antibody (Thermo Scientific, Cat. No. PA1-5204), anti-paxillin mouse monoclonal antibody (clone 349/Paxillin, BD Biosciences Cat. No. 610051, expected MW in WB is ~68 kDa⁷), anti-FAK mouse monoclonal antibody (clone 77/FAK, BD Biosciences Cat. No. 610087, expected MW in WB is ~116–125 kDa⁸). All primary antibodies were divided into aliquots of ~25 µl directly upon arrival, and then stored at -70 °C for long-time storage. Once-thawed aliquots were stored at +4 °C to avoid unnecessary freeze–thaw cycles.

Primary antibodies were diluted as follows for WB (in 1% BSA (Sigma, Cat. No. A7906-50G) in TBS-Tween (0.05%)), and immunofluorescence (IF) staining of fixed cells (in 1% BSA, 5% FCS, and 0.05% Triton X-100): anti-vinculin WB: 1/1,000, IF:

⁷ Purified Mouse Anti-Paxillin Technical Data Sheet, BD Transduction Laboratories, http://www.bdbiosciences.com/external_files/pm/doc/tds/tl/live/web_enabled/P13520_610051.pdf, accessed on 22.10.2011

⁸ Purified Mouse Anti-FAK Technical Data Sheet, BD Transduction Laboratories, http://www.bdbiosciences.com/external_files/pm/doc/tds/tl/live/web_enabled/F15020_610088.pdf accessed on 22.10.2011

1/1,000; anti-talin WB: 1/1,000, IF: 1/1,000; anti-GFP WB: 1/2,500; anti-paxillin WB: 1/3,000; anti-FAK WB: 1/1,000.

The following horseradish peroxidase (HRP) conjugated secondary antibodies were used for WB: anti-mouse HRP-conjugate produced in horse (Vector Laboratories Inc., Burlingame, CA, USA, Cat. No. PI-2000); anti-rabbit HRP-conjugate produced in goat (Vector Laboratories Inc., Cat. No. PI-1000). Both secondary antibodies were diluted 1/10,000 in the same buffer as indicated for the primary antibodies. For IF staining of fixed cells, the following secondary antibodies were used: ZyMaxTM anti-mouse FITC-conjugate produced in goat (Zymed, San Francisco, CA, USA, Cat. No. 81-5611; IF: 1/200), anti-mouse Alexa Fluor 568-conjugate (Molecular probes, Eugene, OR, USA, Cat. No. A11004; IF: 1/1,000).

3.4 Immunofluorescence staining of cells

The protocol for fixing and staining adherent MEF cells for immunofluorescence (IF) imaging was modified from (Marg et al. 2010). Approximately 2×10^5 cells were plated per coverslip (glass or gel-coated) in the well of a 6-well plate for immunofluorescence microscopy. Cells were generally left for 24 h in a cell culture incubator to adhere to their substrates, before aspirating medium, rinsing with PBS and fixing cells with 1.25 ml 4% paraformaldehyde in 100 mM phosphate buffer. The fixing solution was incubated for 10 min at 37 °C to ensure complete cross-linking of cellular structures. Fixed coverslips were washed once with PBS + 20 mM Glycine, permeabilised in PBS + 0.01% Tween 20, for 5 min, and blocked for 15 min with blocking solution containing 1% BSA, 5% FCS, and 0.05% Triton X-100, at room temperature. Antibody incubations were done in drops of ~25 µl of antibody solution (diluted in blocking solution) onto which the cell coverslip was laid, and incubated for 1 h at room temperature. Alexa Fluor 546-labeled phalloidin (Invitrogen, Cat. No. A22283) was used at a dilution of 1/40 in the secondary antibody solution for actin staining, where desired. Coverslips were washed 3 times for 5–10 min with PBS after each antibody incubation. Coverslips were briefly washed with dH₂O before mounting them onto microscope slides using 10-15 µl of HardSet mounting reagent (Vectashield, Cat. No. H-1400) with 1/50 of the DNA-stain 4',6-diamidino-2-phenylindole (DAPI). Ready-made samples were stored shielded from light at +4 °C.

3.5 Purification of FA proteins

FA protein purification was tested with both affinity chromatography-based methods and using previously reported methods for physical extraction of FA proteins. All lysis and PBS solutions used after or during cell lysis contained protease inhibitors from Complete Protease Inhibitor Cocktail tablets (Roche, Cat. No. 04693159001). The cross-linker dimethyl-3,3'-dithiobispropionimidate (DTBP, Thermo Scientific Cat. No. 20665) was used as a homobifunctional, amine-reactive cross-linker. The cross-linker is cleavable as it has a disulfide linkage in its structure enabling separation of cross-linked molecules using reducing conditions. The effective cross-linking distance (N–N) of DTBP has been estimated to be ~0.8 nm (Green, Reisler & Houk 2001).

3.5.1 Unspecific FA protein purification

Multiple unspecific FA protein purification protocols (protocols 1 through 4) were tested and the most promising one chosen for further optimisation. Throughout the different purification protocols, cell lysis and extent of purification was assessed by imaging the cells with an inverted phase contrast microscope (Labovert 090-122.012, Ernst Leitz Wetzlar GmbH., Germany) equipped with a digital camera (OptixCam Summit series, Omano, PRC) using a 10x objective (Leitz EF, N.A. = 0.25). Protocols 1.1, 2, 3, and 4 were tested simultaneously and all protein samples from these purifications were acetone precipitated (described in 3.5.3 below) and the precipitates resuspended in a constant volume to normalise the protein concentration and make the samples comparable to each other in the following silver stained SDS-PAGE gel and western blots.

3.5.1.1 Protocol 1: (3 mM DTBP, 30 min) + RIPA + (wash) – testing the effects of DTBP cross-linking and acetone precipitation

Protocol 1 was modified from the FA protein extraction protocol used in (Schiller et al. 2011). Proteins were extracted from untransfected MEFwt cells cultured on round 10 cm cell culture dishes. The dishes were coated by adsorbing 1 mg/ml FN in PBS onto the dishes for 1 h at 37 °C before seeding 4×10^5 MEFwt cells onto each plate 24 h before protein extraction. Medium was aspirated from all dishes, and dishes were washed twice with PBS to ensure removal of medium and serum proteins. 3 mM DTBP dissolved in serum-free DMEM was added onto plates for cross-linking and incubated for 30 min at 37 °C (Humphries et al. 2009). The pH of the cross-linking solution was corrected through dropwise addition of cell culture-grade 7.5%

NaH₂CO₃ (Sigma, Cat. No. S8761) until the medium could be seen to turn back to red. Cross-linking was quenched by adding Tris-HCl, pH 8 to a final concentration of 20 mM. All steps after cross-linking were done on ice to minimise protein degradation during purification. Cells were lysed by adding 2 ml of RIPA-buffer (25 mM Tris-HCl, pH 7.5, 150 mM NaCl, 1% Triton-X 100, 0.2% SDS, 0.5% sodium deoxycholic acid) onto the plates and incubated for 30 min. Lysed cells were washed with a strong stream of RIPA-buffer using a pipette after lysis. The resulting solution was stored (sample 'RIPA lysate' in Figure 6). Proteins were then removed from the plates by adding 750 µl of Elution Buffer (25 mM Tris-HCl, pH 7.5, 10 mM NaCl, 0.1% SDS) onto each plate and scraping remaining proteins from the plate using a cell scraper ('Scraped' in Figure 6). For cross-linked samples, the Elution buffer was supplemented with 100 mM dithiotreitol (DTT), dishes were incubated for 1 h at 56 °C, and the resulting solution was aspirated ('DTT-eluted' in Figure 6) before scraping of residual proteins. To assess the effects of acetone precipitation on protein samples, a subset of samples were acetone precipitated as described in 3.5.3 below.

3.5.1.2 Protocol 1.1: DTBP + RIPA + high-pressure water wash

Protocol 1.1 was refined from Protocol 1 (see 3.5.1.1 above). Cells were seeded on FN-coated 6-well plate wells or FN-coated glass coverslips in 6-well plate wells with a cell density of $\sim 5 \times 10^4$ cells per well, incubated for 24 h, and washed as previously described for Protocol 1. Cellular proteins were cross-linked with 0.5 mM DTBP in PBS for 5 min before quenching the cross-linking reaction as described above. Cells were lysed by adding 2 ml of RIPA buffer into each well and incubating 30 min on ice. Lysis buffer was removed (sample 'RIPA Lysate' in Figure 8), after which cells were washed by subjecting them to a high-pressure water stream from a tap. Proteins covalently cross-linked to the well bottom were then eluted in 750 µl Elution Buffer (augmented with 100 mM DTT) for 1 h at 56 °C and scraped off using a cell scraper ('DTT-scraped' in Figure 8).

Glass coverslips were fixed and immunostained (see 3.4 above) for vinculin, talin, and/or filamentous actin after certain purification steps to assess the extent of cell lysis and purification of FA core proteins.

3.5.1.3 Optimised Protocol 1.1: DTBP + RIPA + PBS wash

Protocol 1.1 (see 3.5.1.2 above) was optimised with respect to the cross-linking and lysis times. Cells were again seeded, incubated and washed as previously described

(see 3.5.1.2 above). Cellular proteins were then cross-linked with 0.5 mM DTBP in PBS for 5 or 10 min at RT, quenched with Tris-HCl (pH 8) to a final concentration of 20 mM, and lysed with RIPA buffer for 5, 15, or 30 min on ice. After removing the lysis solution (sample 'RIPA lysate' in Figure 7), wells were washed with a pressured stream of PBS from a pipette, and the wash solution was aspirated. Proteins cross-linked to the surface were then eluted with Elution Buffer + DTT as described in section 3.5.1.2 above ('DTT-scraped' in Figure 7).

3.5.1.4 Protocol 2: Hypotonic shock + wash + scraping + sonication in solution

Protocol 2 was modified from (Kuo et al. 2011). Cells were seeded, incubated and washed as described for Protocol 1.1 in section 3.5.1.2 above. Cells were gently lysed by subjecting them to a hypotonic shock in 2.5 mM triethanolamine (pH 7.0) for 3 min at RT. The hypotonic solution was removed (sample 'Hypotonic' in Figure 8), cells were washed with streaming PBS with a pipette ('PBS Wash' in Figure 8), and all remaining proteins scraped off in RIPA buffer ('Scraped' in Figure 8). The obtained protein solution was then sonicated in a bath sonicator (Diagenode Bioruptor UCD-200TM-EX, Tosho Denki Co., Ltd, Japan) with high intensity (200 W), 20 s on 30 s off cycles, for 5 min on ice.

3.5.1.5 Protocol 3: Detergent lysis with CSK buffer + sonication on plate

Protocol 3 was modified from (Humphries et al. 2009). Cells were seeded, incubated and washed as described for Protocol 1.1 in section 3.5.1.2 above, after which cell membranes were lysed with cytoskeleton (CSK) buffer (10 mM piperazine-N,N'-bis(2-ethanesulfonic acid) (PIPES) (pH 6.8), 50 mM NaCl, 150 mM sucrose, 3 mM MgCl₂, 1 mM MnCl₂, 20 mM Tris-HCl (added from 1 M stock solution with pH 8.5), 0.5% (w/v) Triton X-100) for 30 min on ice. After lysis, all wells were filled up with PBS (~4 ml) and sonicated using a VibraCell tip sonicator (Sonics & Materials Inc. Newtown, CT, USA) equipped with a 3 mm tip with 1 s on, 2 s off cycles for 15 s (A = 30%). The resulting lysate was removed (sample 'CSK lysate, tip sonicated' in Figure 8) and all remaining proteins were removed by scraping in RIPA buffer ('Scraped' in Figure 8).

3.5.1.6 Protocol 4: cleaving cells with a nitrocellulose sheet

Protocol 4 was modified from (Plopper, Ingber 1993). Cells were again seeded, incubated and washed as described for Protocol 1.1 in section 3.5.1.2 above. A small

piece of nitrocellulose sheet was then laid on the cells, left to adhere for exactly 1 min, after which the membrane was rapidly removed using tweezers with the intent of removing most of the apical parts of the membrane and cell structure thus leaving only the basal membrane with FAs adhered onto the surface. Lysed cells were then washed by streaming PBS from a pipette, after which PBS was removed ('PBS wash' in Figure 8), and all remaining proteins scraped off in RIPA buffer ('Scraped' in Figure 8).

3.5.2 Affinity chromatography purification of vinculin-associated complexes using the Strep-Tag®/Strep-Tactin® system

ST-tagged proteins were purified from cells cultured on either one or two 10 cm cell culture dishes. Dishes were FN-coated by incubating in 15 µg/ml FN-solution for 1 h at 37 °C. Cells were seeded at a density of $\sim 3 \times 10^5$ cells/dish. Cells were transfected 24 h after seeding with TurboFect using 10 µl transfection reagent and 5.0 µg EGFP-VinWT-ST plasmid per dish. Cells were cultured for 24 h after transfection to enable adequate protein expression. Transfection efficiency was estimated either from adherent cells or trypsinised cells as described in 3.6.1 below. Before purification, medium was aspirated and cells were washed twice with PBS. After washing, cellular proteins were cross-linked by adding 5 ml 0.5 mM cross-linking solution to each dish, incubated for 5 min at RT, and quenched by adding Tris-HCl to a final concentration of 20 mM. After cross-linking, dishes were kept on ice for the rest of the purification.

Prepurified FA-lysate was prepared by lysing adherent cells with RIPA buffer (25 mM Tris-HCl, pH 7.5, 150 mM NaCl, 1% Triton-X 100, 0.2% SDS, 0.5% Sodium deoxycholic acid) for 5 min, washing the plate by streaming PBS from a pipette, and scraping any proteins left on the dish with a cell scraper in a small amount of the same buffer. Whole-cell lysate was obtained by trypsinising cells off of the dish after cross-linking, washing the resulting cell suspension with PBS, and lysing cells with RIPA buffer for 30 min, while gently vortexing every 10 min. Both lysates (prepurified FAs or whole-cell lysate) were cleared by centrifugation (5 min at 14 000 g at +4 °C) before loading the supernatant into the Strep-Tactin resin. The pellet was resuspended in PBS for analysis with SDS-PAGE and immunoblotting (sample 'Pellet' in Figure 9 and Figure 10)

3.5.2.1 Purification with prepacked Strep-Tactin Superflow cartridges

Purification was done following the manufacturer's instructions. In summary, an unused 1 ml Superflow Strep-Tactin H-PR cartridge (IBA GmbH, Göttingen, Germany, Cat. No. 2-1106-000), was first equilibrated with 5 ml washing buffer (100 mM Tris-HCl, 150 mM NaCl, 1 mM EDTA, pH 8). The cleared lysate was applied to the column using a syringe at a flow-rate of approximately 0.5 drops/s. The first ~800 µl were discarded, before collecting the flow-through (sample 'Flow-Through' in Figure 9). Next the resin was washed with 5 ml of washing buffer, and the flow-through collected in four fractions (samples 'W1' through 'W4' in Figure 9). Bound proteins were eluted with ~3 ml elution buffer (100 mM Tris-HCl, 150 mM NaCl, 1 mM EDTA, 2.5 mM desthiobiotin, pH 8), which was collected in 6 fractions of ~0.5 ml each (samples 'E1' through 'E6' in Figure 9). The resin was regenerated by washing it with ~15 ml of regeneration buffer (100 mM Tris-HCl, 150 mM NaCl, 1 mM EDTA, 1 mM HABA (hydroxy-azophenyl-benzoic acid, pH 8), and then with ~8 ml of washing buffer.

3.5.2.2 Purification with loose Strep-Tactin resin from Superflow cartridges

Once-used and regenerated Strep-Tactin resin was taken from a Superflow cartridge by cutting the column open and transferring the resin in washing buffer into a 15 ml tube. The resin was washed with ~10 ml washing buffer and pelleted by centrifuging for 1–2 min at 500 g. 200 µl of pure resin was taken for purification of whole-cell lysate from two 10 cm cell culture dishes. Cleared whole-cell lysate was added onto the resin and incubated on a rolling shaker for 1 h at 4 °C. After binding the resin was pelleted and the supernatant collected ('Unbound' sample in Figure 10). The resin was then washed 4 times with 250 µl washing buffer. Each wash fraction was collected (samples 'W1' through 'W4' in Figure 10). The resin divided into two during the last wash step, and the resulting two samples were eluted either with (i) elution buffer, or (ii) by boiling in SDS-PAGE sample buffer. For (i) the resin was transferred into a cleaned purification column and eluted with 3×100 µl of elution buffer (samples 'E1' through 'E3' in Figure 10). For (ii) the resin (~100 µl) was suspended to an end concentration of 1× SDS-PAGE sample buffer (see 3.5.4 below) and heated to ~95 °C for ~10 min (sample 'Elution by boiling' in Figure 10).

3.5.3 Acetone precipitation of protein samples

Protein samples were concentrated using acetone precipitation as described in Acetone precipitation of proteins (Pierce)⁹. All samples were divided into batches of ≤ 400 μ l into 2 ml eppendorf tubes. Proteins were precipitated by adding 4 \times volume of pre-cooled (-20 °C) acetone to each sample, vortexing rigorously, and leaving tubes at -20 °C for 1–18 h. Formed precipitates were pelleted by centrifuging samples for 10 min at 15,000 g. The supernatant was carefully removed, and any residual acetone evaporated by leaving the tubes open at RT for 30–90 min until no more liquid was visible. Pellets were resuspended in (1 \times) SDS-PAGE sample buffer (see 3.5.4 below) by vortexing thoroughly to dissolve the pellet.

3.5.4 SDS-PAGE and Western blotting

Protein separation according to size was done using sodium dodecyl sulphate polyacrylamide gel electrophoresis (SDS-PAGE) in Mini-PROTEAN (Biorad) electrophoretic cells with a gel thickness of 0.75 mm. Acrylamide gels with 1% SDS were prepared using standard protocols with 4% or 5% stacking gels in 125 mM Tris (pH 6.8), and 6%, 8%, or 10% separating gels in 375 mM Tris (pH 8.8). Samples were boiled in Laemmli sample buffer (50 mM Tris-HCl (pH 6.8), 2% SDS, 6% glycerol, 1% β -mercaptoethanol, 0.002% bromophenol blue) for 5–10 min at 95 °C before loading into sample wells. PageRuler™ Prestained Protein Ladder (Fermentas, Cat. No. SM1811) was used as a protein size marker by adding 1 μ l of ladder to gels dedicated for silver staining and 7 μ l to gels for WB. Electrophoretic gels were run in SDS-PAGE running buffer (25 mM Tris-HCl, 192 mM Glycine, 0.1% SDS) first at 80 V for 15 min to allow concentration of samples into a single running front in the stacking gel, followed by a separation run at 180 V until the running front could be seen to approach or pass the lower end of the gel (approximately 45–60 min).

Proteins were transferred onto nitrocellulose transfer membranes (Whatman) using wet blotting in Mini Trans-Blot electrophoretic transfer cells (Biorad) running at 100 V for 1 h or 15 V overnight in transfer buffer (25 mM Tris, 192 mM Glycine, 20% Methanol). Transfer was done using cooled solutions at +4 °C. The resulting nitrocellulose blots were blocked with bovine serum albumin (1% BSA (Sigma, Cat. No. A7906-50G) in TBS-Tween (0.05%)) and incubated for 1 h at room temperature, or overnight at +4 °C, with antibody solutions prepared in 1% BSA in TBS-Tween.

⁹ Technical resource, PIERCE Biotechnologies 4/2004.

<http://sites.bio.indiana.edu/~ybelab/procedures/AcetonePrecipitation.pdf>, accessed on 21.1.2012

Blots were washed 3 times for 5–10 min with TBS-Tween after each antibody incubation. All antibody incubations and washes with blots were done in 50 ml tubes on a rolling-shaker. HRP-conjugated secondary antibodies were detected using the SuperSignal West Pico Chemiluminescence Substrate (Thermo Scientific, Cat. No. 34080) using the manufacturers protocol. In summary, blots were incubated for 1 min with HRP-substrate mix, transferred into a film cassette covered with plastic transparency film, and exposed to Super RX X-ray films (FUJIFILM, Cat. No. 47410) for 5 to 40 min. Ready-made films were scanned using a standard document scanner.

3.5.4.1 Silver staining

Silver staining was done using the PageSilver™ Silver Staining Kit (Fermentas, Cat. No. K0681) following the manufacturer's instructions for obtaining maximum sensitivity. In summary, PAA gels were briefly rinsed with dH₂O and fixed in 50% EtOH and 10% acetic acid for 60 min after running the gel. Gels were rehydrated by incubating them 3×20 min in 30% EtOH. Fixed and rehydrated gels were briefly washed twice in dH₂O (~20 s), before sensitising them for 1 min in Sensitising solution, and, again, washing them twice with dH₂O. Gels were then stained in Staining solution for 20 min and washed twice with dH₂O. Bands were developed in Developing solution until the desired band intensity was reached (1-5 min). The reaction was stopped with Stop solution, in which gels were incubated for 10 min. Ready-made gels were stored in dH₂O and scanned between two plastic transparency films using a standard document scanner.

3.6 Image processing and analysis

All image analysis was done using ImageJ (Rasband, W.S., ImageJ, U. S. National Institutes of Health, Bethesda, MD, USA, <http://imagej.nih.gov/ij/>, 1997-2011) version 1.44 or newer.

3.6.1 Estimation of transfection efficiency

Transfection efficiency was estimated from either 9 image mosaic images (3×3) taken with Surveyor of live adherent cells (see also 3.2.1.1 above), or multiple single images of trypsinised cells transferred on glass microscope slides.

3.6.1.1 Adherent cells

Due to high confluencies in samples, cells could often not be calculated separately from phase contrast images. Thus estimation of transfection efficiency was based on comparing total cell area with the total green fluorescing area from fluorescence

microscopy images. Total cell area was estimated from phase contrast images using a self-written sequence of ImageJ analysis tools (see Figure S1 in Appendix 1). In summary, the images were first slightly blurred using the Smooth filter multiple times to reduce noise, then cell area edges were detected with the Find Edges filter. Noise was reduced from the resulting image by using a medium-sized median filter to ease the following thresholding and create a rough estimation of cell area. The total area was then estimated from the resulting thresholded image mask.

For fluorescence images, cell area was estimated using a slightly modified approach (see Figure S2), in which fluorescent area was estimated from background-reduced and median-filtered images based on intensity differences using direct thresholding. The thresholded mask was then processed with the Fill holes tool to fill out hole in the mask created e.g. by dark nuclei in fluorescent cells. The Analyse Particles tool was then used to remove any major linear artefacts created by the image boundaries in the mosaic image by using the tool's 'Circularity' option.

Due to inconsistencies in sample and imaging quality, thresholding boundaries were set in all cases using a trial-and-error approach by eye individually for each image.

3.6.1.2 Trypsinised cells

To estimate transfection efficiency from trypsinised cells, a small sample of cell suspension was transferred onto a microscope slide, covered with a coverslip, and photographed with a fluorescence microscope (Olympus BX40F4, Olympus Optical Co., Ltd, Japan, equipped with a ColorView Soft Imaging System (Olympus) digital camera using a 40x oil immersion objective (Olympus UPlanApo, N.A. = 1.00). The number of cells was estimated from fluorescence and phase contrast images from 9 randomly chosen locations from the sample by manually counting the cells using the Cell Counter tool in ImageJ.

3.6.2 Estimation of cell area

Cell area estimation was done from 9 image mosaic images (3×3) taken with Surveyor on the inverted Olympus IX71 fluorescence microscope (mentioned in 3.2.1.1 above) using a 10x objective (N.A. = 0.30). Estimation was done using self-written scripts mainly utilising ImageJ's common operations Analyse Particles and Threshold combined with various background reductions and contrast enhancements, where necessary. Cell boundaries were estimated using images of cells stained for

vinculin with immunofluorescence labels, except where noted otherwise. In order to avoid any measuring artefacts caused by clustering of cells especially on pliable substrates, information from DAPI-stained images were used to only include mononucleate cells in the analysis of cell area. This was done using the ImageJ ROI manager tool combined with Analyse Particles and a simple for-loop to compare cell images with the DAPI-stained nuclei images to determine the amount of nuclei in each given cell-particle/cluster. The script used for this is given in Appendix 1, Figure S3.

3.6.3 Measuring focal adhesion size and number

Focal adhesion count and area were estimated from images of fixed cells using EGFP-Vinculin-ST fusion constructs as FA markers. Images were taken with an Axio Apotome (Zeiss) equipped with an AxioCam MRm camera using a 40x oil immersion objective (Zeiss Plan-NEOFLUAR, N.A. = 1.3). Cells for imaging were manually chosen based solely on the presence of visible EGFP-positive FA-like subcellular structures. Each cell was imaged as z-stacks of 10 to 30 slices with a slice distance of 0.275 μm . During image analysis the slice with the most clearly visible FAs was chosen manually for each cell analysed. In some samples cultured on very soft substrates (5% / 0.025% acrylamide / bis-acrylamide ratio) slices from several vertical positions were chosen for counting while taking care that no individual FA was counted multiple times.

Estimation was done using self-written scripts again mainly based on ImageJ's operations Analyse Particles and Threshold combined with background reductions and contrast enhancements, where necessary. Two different background-reduction / contrast-enhancement schemes had to be used for images from cells on very soft substrates and images from rigid substrate-grown cells due to the large difference in background fluorescence caused by differing amounts of cytoplasmic EGFP-Vinculin-ST. Scripts used for this are shown in Appendix 1 (Figure S4 and Figure S5).

In order to estimate FA density (FA number / cell area) the area of the cells used for FA counting was estimated by manually outlining the cells from EGFP-images and measuring the outlined area. In the case of cells with focal adhesions counted from multiple z-stack images, only the largest stack image with the largest visible cell area was used for area estimation.

4 Results

4.1 Optimisation of transfection

Out of the six tested transfection reagents and methods, the cationic polymer-based TurboFect and the lipid-based Lipofectamine2000 showed significantly higher transfection efficiencies compared to the other reagents, which all showed negligible amounts of EGFP-expression at both cell densities and post transfection (PT) incubation times tested (Figure 4). Initial results from image analysis of fluorescence microscope images (Figure 4: A) were verified by immunoblotting whole-cell lysates against vinculin (Figure 4: B). Although Lipofectamine2000 could be seen to induce less cell death than TurboFect at similar transfection efficiencies (data not shown), the latter was deemed to be significantly more cost-efficient, and thus chosen for further use.

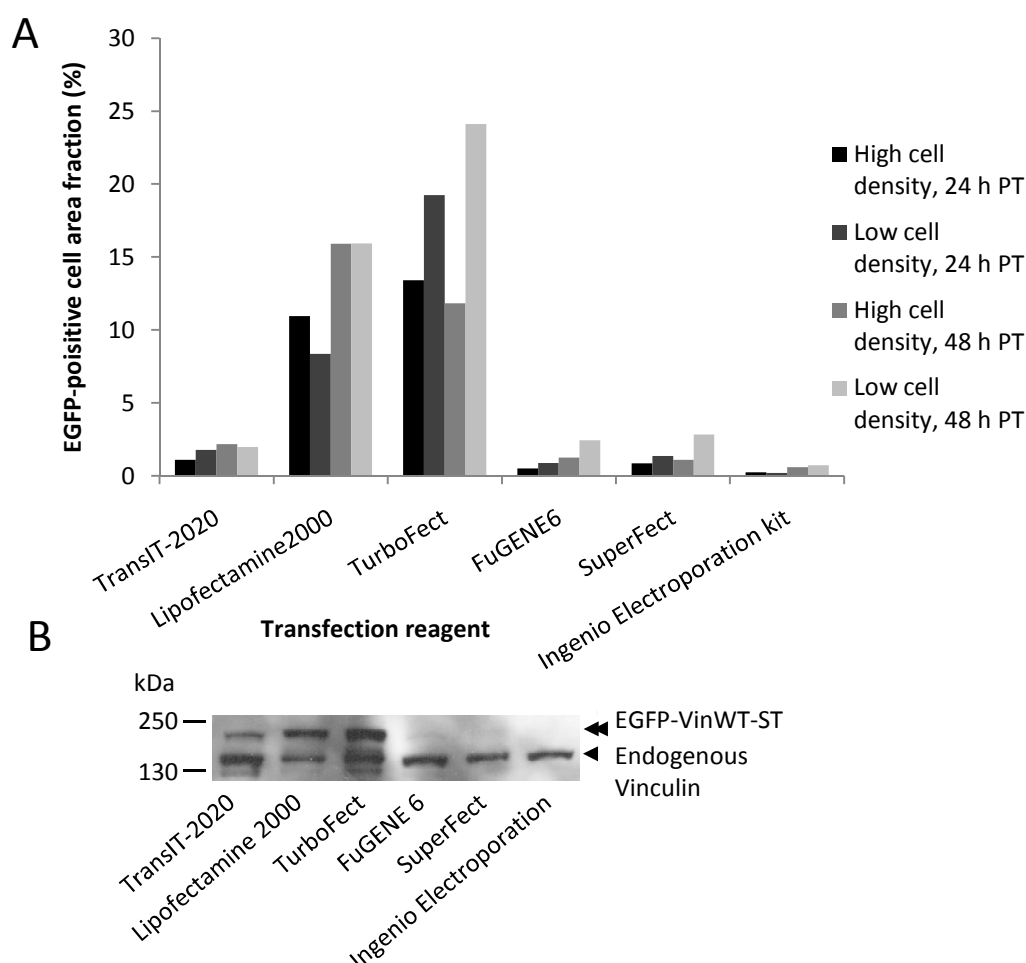


Figure 4: TurboFect and Lipofectamine2000 are most suitable for transfecting MEFwt cells. A: transfection efficiencies as estimated as the EGFP-positive cell area fraction of the whole cell area from fluorescence microscope images. B: anti-vinculin stained whole-cell lysates immunoblots showing the same trend. Whole-cell lysates were produced from high cell density samples 48 h PT. Cells used in chemical-based transfection were seeded at densities of 4×10^4 and 10^4 cells per 24-well plate well. Electroporated cells were seeded onto 24-well plate wells at densities of 1.5×10^5 and 7.5×10^4 cells per well directly after electroporation in suspension.

Optimising transfection further by assessing the effect of different plasmid DNA:transfection reagent ratios with TurboFect showed that the initial ratio of 1.0 μ g:2.0 μ l yielded the best reagent-to-efficacy ratio for transfection of both MEFwt and MEF^{Vin-/-} cells (Figure 5). Immunoblotting of whole-cell lysates against vinculin produced again similar results (Figure 5: B).

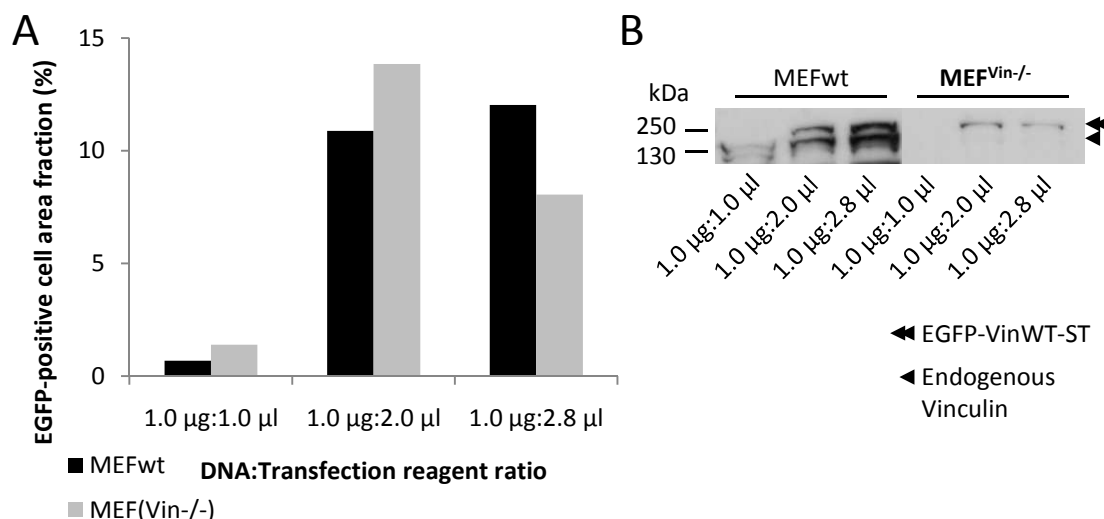


Figure 5: The DNA:transfection reagent ratio of 1.0 μ g:2.0 μ l yields the highest reagent-to-efficacy ratio for MEFwt and MEF^{Vin-/-} cells. A shows result from image analysis analysing the EGFP-fluorescing area to the total cell area. B displays anti-vinculin stained immunoblots made from whole-cell lysates 24 h PT. Protein amounts in samples were not explicitly normalised, but rather represent cell lysate from an identical amount of cell material, thus enabling comparison between MEF^{Vin-/-} and MEFwt samples internally.

4.2 Purification of the talin–vinculin complex from cytoplasmic parts of FAs

Purification of FA complex proteins was initially assessed using untransfected MEFwt cells with the intent of purifying endogenous FA protein complexes with various non-specific methods mostly based on utilising the physical location of FA complexes in the basal membrane of proteins. As a second means of purification affinity purification of protein complexes was assessed using overexpressed Strep-Tagged vinculin as a bait protein for purification of FA protein complexes.

4.2.1 Physical FA protein purification

4.2.1.1 DTBP cross-linking (3 mM, 30 min) effectively prevents RIPA buffer-induced cell lysis

Using Protocol 1 (see 3.5.1.1 above) modified from (Schiller et al. 2011) it could be shown that heavy cross-linking with DTBP (3 mM, 30 min incubation) intended to cross-link FA proteins complexes for purification was, in fact, too strong as it almost completely prevented cell lysis with RIPA buffer (Figure 6: B, 3. RIPA lysis). Washing cells with RIPA buffer during lysis did not have any visible effect on cell

lysis in phase-contrast microscope images (Figure 6: B). However, a slight effect could be seen in protein amounts in cross-linked cells – mechanically disturbing the buffer during lysis caused a slight increase in proteins ending up in the ‘RIPA lysate’ fraction, while simultaneously decreasing the total amount of protein in the ‘Scraped’ fractions (Figure 6: A, silver stained gel). Although quantitative estimates made from silver stained gels should not be considered very significant, a similar trend is visible in immunoblots made from the lysates. These show several bands of very high molecular weight in the undisturbed ‘Scraped’ samples (Figure 6: A, western blots, bands marked with arrowheads).

As is evident from phase contrast images taken during the purification protocol, uncross-linked cells are mostly lysed already during the 30 min incubation period, which leads to a situation where the FA proteins talin and vinculin can be found in the ‘RIPA lysates’ fractions in uncross-linked samples (Figure 6: A, immunoblots). In contrast, cross-linked cells could only be effectively lysed by treating cells with a strong reducing agent, thus cleaving cross-links (Figure 6: B, 5. DTT-elution).

4.2.1.2 Acetone precipitation does not reduce FA protein yield greatly

Silver stained gels (Figure 6: A) suggested that acetone precipitation could be used as a means to concentrate FA protein samples, as not many protein bands seem to vanish in the process. Those that were lost are expected to be mostly proteins with large hydrophobic parts, which do not precipitate in acetone. Interestingly, however, immunoblots did give ambiguous results about the usability of acetone precipitation with FA proteins like vinculin, as vinculin bands are not visible in acetone precipitated, cross-linked ‘Scraped’ samples, whereas uncross-linked ‘Scraped’ samples show a talin band only in the acetone precipitated lane (see Figure 6: A, immunoblots).

4.2.1.3 Short cross-linking combined with short lysis enables purification of small amounts of cellular vinculin adherent to the substrate

Use of multiple cross-linking and detergent lysis times with a lower concentration of DTBP cross-linker (0.5 mM) showed that short times in both resulted in the most vinculin remaining deposited on the surface and thus being retrieved in the ‘Scraped’ fraction (Figure 7). Silver staining indicated strong bands at around ~70 kDa along with some weaker bands at for example ~80 kDa and ~240 kDa in the scraped sample.

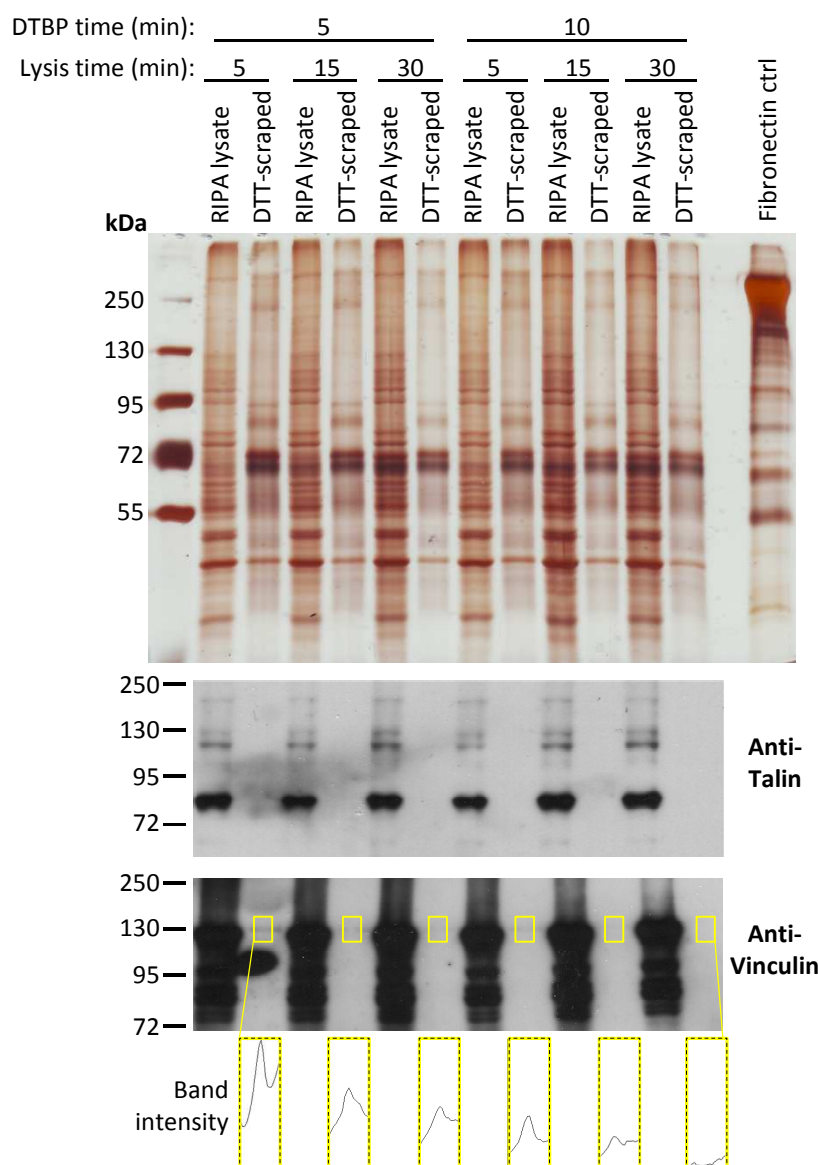


Figure 7: A short cross-linking time (5 min) combined with short detergent lysis (5 min) leaves most vinculin adherent to the substrate after lysis. From top to bottom: a silver stained gel, anti-talin and anti-vinculin immunoblots. The fibronectin control is included to facilitate estimation of composition of adherent protein mixture. Relative band intensities shown below the anti-vinculin blot were generated using ImageJ's gel analyser tool. Sample amount was normalised in acetone precipitation, and thus every lane contains the same relative amount of sample compared to the initial amount of cells. The large dark spot in the 5 min / 5 min 'DTT-scraped' lane in the Anti-Vinculin blot is most likely due to unspecific staining.

4.2.2 None of the other previously published methods tested proved to be useful in purifying FAs from untransfected MEFwt cells

Three other physical methods beyond protocol 1.1 were tested for purifying FAs from basal membranes of adherent cells. Immunofluorescence images taken from samples made at various time points during the purification procedures show that the most promising stages (i.e. showing most anti-vinculin staining, but no actin or chromosomal staining) were generated with protocols involving gentle lysing of cells using a hypotonic lysis buffer followed by a wash with PBS; and a slight modification

of the protocol using DTBP cross-linking and detergent lysis discussed above (Figure 8: A, Protocol 2, ‘3 PBS Wash’; and Protocol 1.1, ‘2 DTBP + RIPA lysis’, respectively). All other intermediates analysed showed either insufficient removal of cellular structures indicated by the presence of DAPI-staining nuclei and/or phalloidin-staining actin fibres, or too stringent washing conditions resulting in removal of all visible cellular structures – including adhesions as detected by anti-vinculin staining (Figure 8: A).

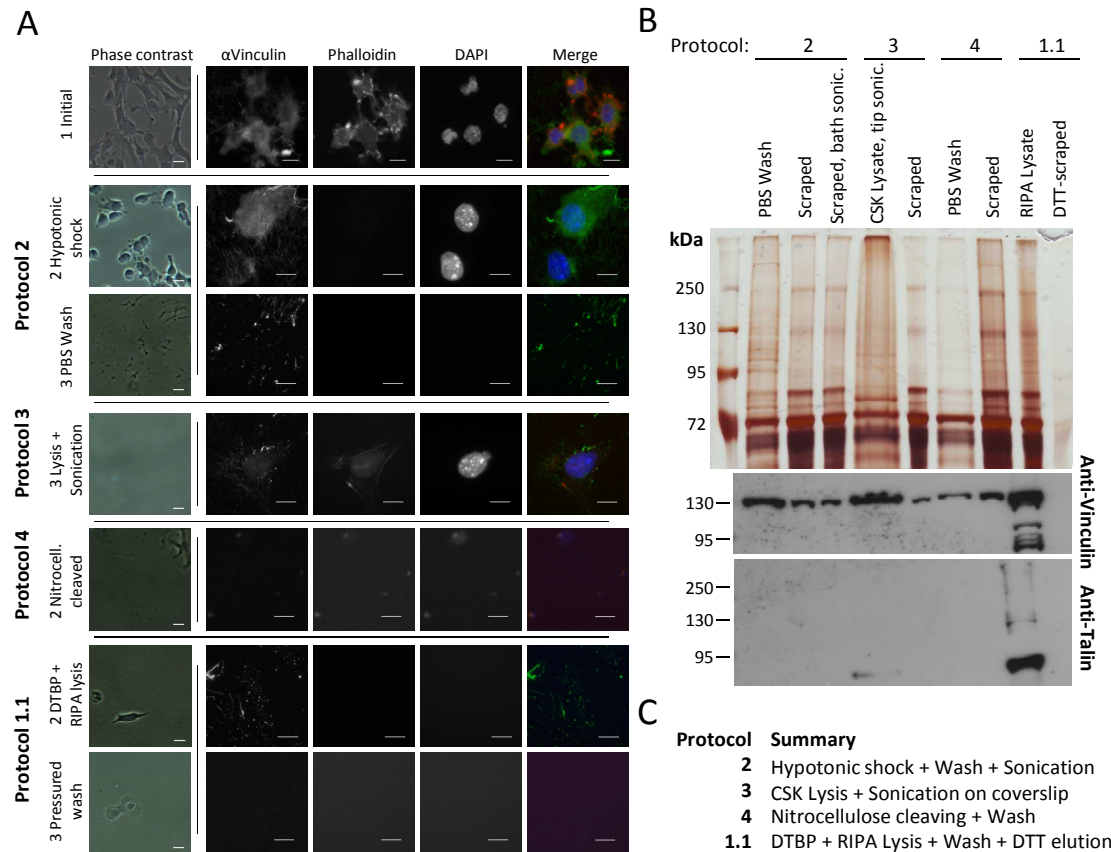


Figure 8: Immunofluorescence staining and western blot analysis shows that protocols 2 and 1.1 are the most promising ones for purification of FA proteins from MEFwt cells. A: Immunofluorescence stained coverslips showing various intermediates from the protein purification experiments. FA proteins are represented by anti-vinculin staining (green), cytoskeletal structures are shown using phalloidin-mediated staining of fibrous actin (red), and nuclei are shown using DAPI (blue). Scale bars are 25 μ m for phase contrast images and 10 μ m for fluorescence images. B: Silver stained gel and immunoblots showing some protein samples taken during the purifications. C: Table showing summaries of the steps taken during each of the different purification protocols.

Immunoblot analysis of various samples taken during the purification protocols show that talin is somehow lost in most purification methods. For protocols 2 and 4 most of talin might have been lost in the initial lysate containing most cellular proteins (not shown). The only clear talin signal is retrieved from the initial lysate from the cross-linked sample (Figure 8: B, Protocol 1.1 RIPA Lysate), although some talin-staining is also visible in an initial lysate produced with CSK buffer and

sonication with a tip sonicator (Figure 8: B, Protocol 3 CSK Lysate tip sonic.). The absence of talin and vinculin altogether in the end sample of protocol 1.1 (DTT-Scraped in Figure 8: B) was likely caused by too strong shear stress created during washing before elution, which might have led to all protein being removed from the surface.

4.2.3 Strep-Tag-based affinity chromatography enables purification of ST-tagged vinculin

Affinity chromatography purification from transfected MEFwt cell whole-cell lysates with Strep-Tactin-resin showed that ST-tagged EGFP-Vinculin fusion protein could be seen to reside in the resin longer than the endogenous vinculin present in MEFwt cells. Figure 9 shows immunoblots from various samples collected during the purification process. A GFP-positive band likely representing the EGFP-VinWT-ST fusion protein (expected molecular weight (MW) ~144 kDa) can be seen in all lanes bar the last elution fractions (E5 and E6 in Figure 9: Anti-GFP blot). Encouragingly, a slight increase in band intensity is visible going from sample 'E1' to 'E2', possibly indicating successful elution of Strep-Tagged fusion protein with desthiobiotin. Similar bands can be seen in the anti-vinculin blot, which also shows the diminution of endogenous vinculin (expected MW ~116 kDa) in the wash steps. Binding of Strep-Tagged vinculin to the Strep-Tactin resin is far from ideal, however, as strong vinculin and GFP-positive bands can be seen also in the wash fractions.

Despite DTBP cross-linking of cells prior to trypsinisation and lysis, the FA proteins talin, paxillin, and FAK could not be copurified in sufficient quantities to be detected by immunoblotting. Paxillin could be seen to diminish quicker than endogenous vinculin, while FAK and talin only showed weak bands in 'W2', and 'Flow-through' and 'W1' respectively (Figure 9).

Transfection efficiency in MEFwt cells transfected with EGFP-VinWT-ST and used for the purification was estimated from adherent cells as EGFP-positive area against total cell area (see 3.6.1.1 above), and was measured to be 7%.

4.2.3.1 Elution of ST-tagged EGFP-Vinculin by boiling shows that desthiobiotin elution is not sufficient to elute EGFP-VinWT-ST from Strep-Tactin resin

To estimate whether elution by boiling in SDS-PAGE sample buffer could enhance retrieval of ST-tagged EGFP-Vinculin purification was done with loose Strep-Tactin resin and proteins were eluted both by boiling and by conventional desthiobiotin

elution. Silver stained SDS-PAGE gels and immunoblots confirmed that stronger bands could be seen both in anti-vinculin and anti-GFP blots in the boiled sample compared to desthiobiotin elution fractions (Figure 10: B). Silver staining of the PAA gel showed that many different proteins could be eluted effectively by boiling (Figure 10: A) with some unique bands emerging compared to desthiobiotin eluted samples.

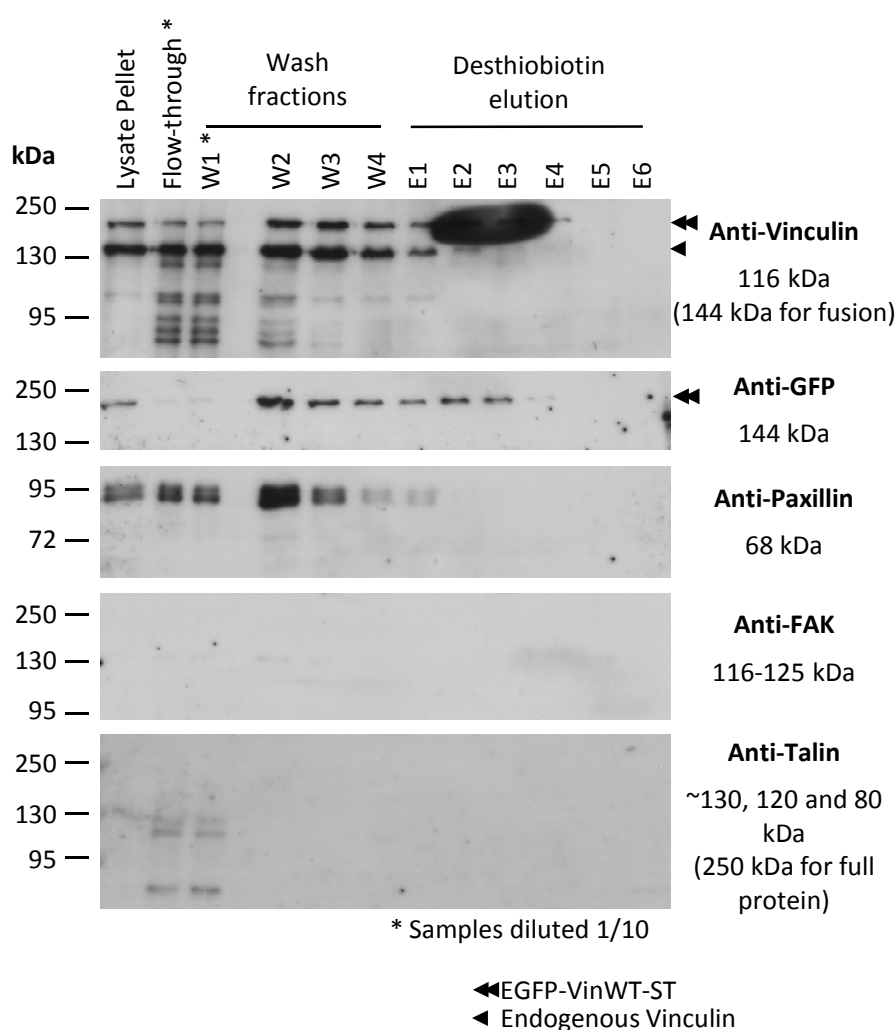


Figure 9: The EGFP-VinWT-ST construct can be partially enriched into elution fractions while other FA proteins are not copurified in detectable amounts. Presumed endogenous and EGFP-fusion vinculin bands are marked with arrowheads as indicated. The large oval stain in lanes E2 and E3 is unfortunate unspecific staining of the film. Sample amounts are normalised individually within samples W2–4 and samples E1 through E6. Thus band intensities can be compared from one wash or elution sample to another, but should not be directly compared between samples from wash and elution series.

The marked enrichment of EGFP-tagged vinculin in the elution samples seen in Figure 9 could not be repeated in the second affinity purification experiment done with loose resin as opposed to cartridge-based purification. Encouragingly, however, a faint talin band could be seen in the boiled sample in the anti-talin blot (Figure 10: B,

Anti-Talin blot, faint band marked with an arrow at ~80 kDa) indicating the possibility that some talin fragment could possibly be copurified in minute amounts.

General protein staining in the silver stained gel showed that minimal amounts of protein eluted from the resin in the later elution fractions (Figure 10: A, samples E2 and E3).

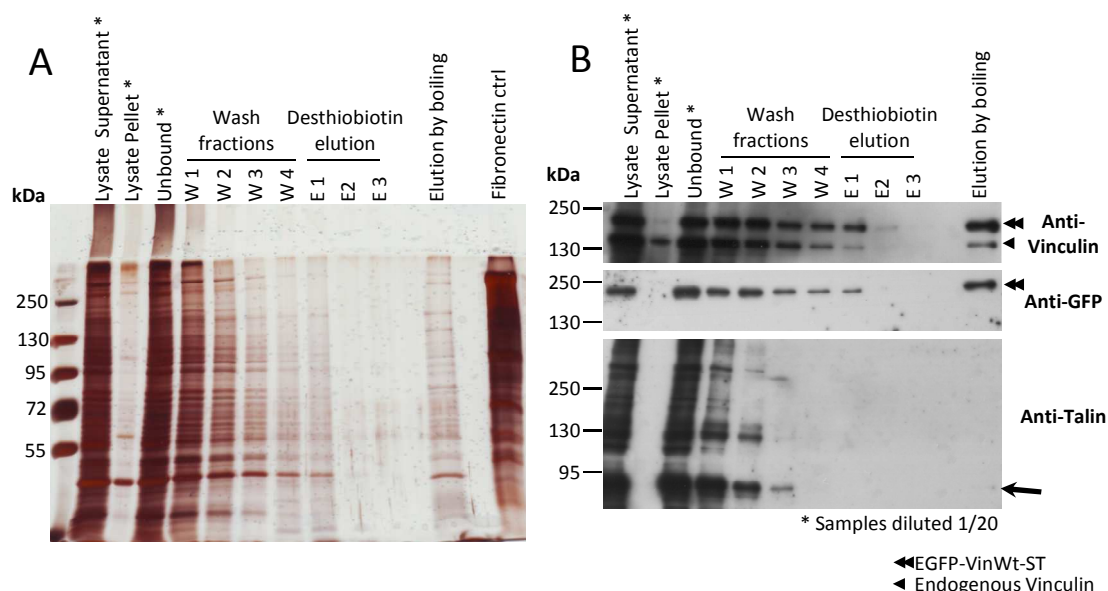


Figure 10: Elution by boiling releases higher amounts of both EGFP-VinWT-ST and endogenous vinculin than desthiobiotin elution. Arrowheads mark presumed different forms of vinculin as previously indicated. Faint talin-positive band in boiled sample is marked with an arrow. Sample amounts are normalised between all samples with regard to the original amount of cell lysate, except where noted.

4.3 EGFP-Vinculin-ST fusion proteins localise correctly into focal adhesions along with talin

The functionality of the EGFP-Vinculin-ST fusion constructs was assessed by transiently transfecting the constructs into MEF^{Vin^{-/-}} cells plated on glass coverslips covalently coated with FN. Fixing and staining against talin showed that both vinculin constructs localised correctly to FAs (Figure 11: A, EGFP-Vinculin). Similar structures could be seen also with anti-talin staining, although many of them were partly obscured by the strong cytoplasmic background (Figure 11: A, α Talin) which most likely represents a diffuse cytoplasmic pool of talin not bound to FAs.

Colocalisation of EGFP-Vinculin-ST constructs and talin was assessed also by analysing plot profiles (example shown in Figure 11: B), which showed reasonably good colocalisation of talin and the vinculin constructs not only at the cell periphery, where focal adhesions and focal complexes are expected, but also in more central areas of the cell, where other kinds of integrin–talin–vinculin-mediated adhesion structures like fibrillar adhesions form (see also Table 1).

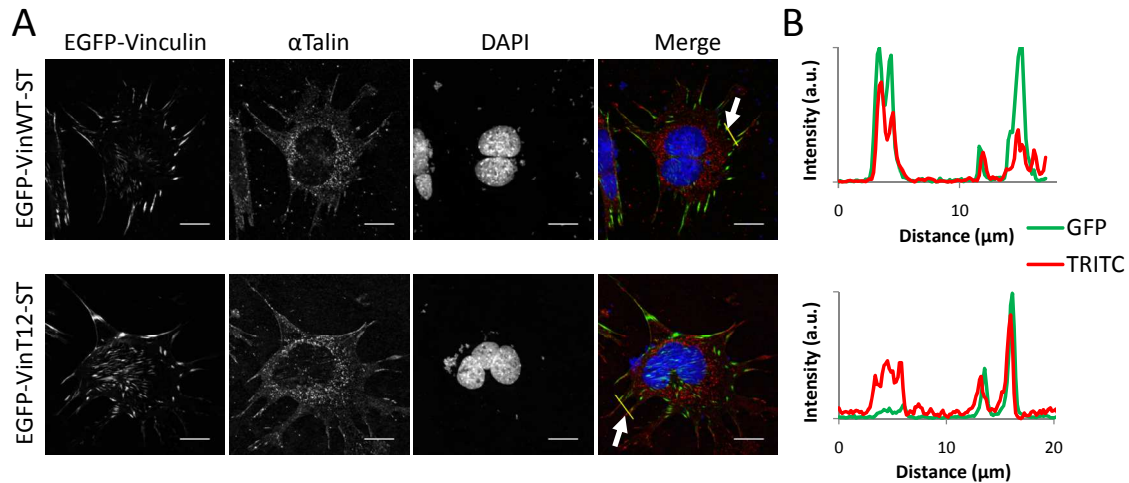


Figure 11: Both EGFP-Vinculin-ST constructs localise correctly to focal adhesions showing colocalisation with talin. A: Immunofluorescence images showing fixed MEF^{Vin-/-} cells transiently transfected with the vinculin construct shown. Vinculin localisation is shown using the EGFP tag (green), talin was detected with anti-talin immunofluorescence labelling (red), and nuclei are shown using DAPI (blue). Cells were cultured on glass functionalised with covalently linked FN. Scale bars are 20 μm. B: Plot profiles showing intensities (in arbitrary units) of EGFP-Vinculin and talin along the lines shown in the merged image (yellow lines marked with white arrows).

4.4 Effects of substrate stiffness on MEF cells

4.4.1 Both transfected MEF^{Vin-/-} and untransfected MEFwt cells show increased spreading on substrates of increasing stiffness

Effects of substrate stiffness on MEF cells were analysed by immunofluorescence staining of fixed cells grown on substrates of different stiffness on coverslips. Representative images of untransfected MEFwt cells, and MEF^{Vin-/-} cells transfected with EGFP-VinWT-ST and EGFP-VinT12-ST constructs are shown in Figure 12, A, B, and C, respectively. All cells could be seen to display similar characteristics on the different substrates: increasing substrate stiffness leads to an increase in cell spreading and larger cell areas. Cell spreading is also expected to lead to flattening of the nucleus, which can be seen as an increase in nucleus area in DAPI-stained images (Figure 12).

F-actin staining with Alexa Fluor 546-labelled phalloidin in untreated MEFwt cells shows an increase in presence of polymerised actin and the formation of distinct actin bundles in cells on totally rigid substrates (Figure 12: A, Glass). No visible actin bundles can be seen in cells on compliant substrates.

To further analyse the effects of substrate stiffness on the cells, cell areas were quantified from low-magnification fluorescence micrographs (see 3.6.2 above). Results of the quantification are summarised in Figure 13. Cell area distributions verify the trend observed in immunofluorescence staining (Figure 12), as a clear shift of the distribution to larger areas can be seen in cells on stiffer substrates

(Figure 13: A). This increase is most clearly visible in untransfected MEFwt cells, while MEF^{Vin-/-} cells that were transfection-reagent treated, but did not show EGFP-fluorescence (MEF^{Vin-/-} in Figure 13), seem to show a similar increase, albeit on a much smaller scale. The increase in cell area especially in MEFwt cells is also seen in the average cell areas portrayed in Figure 13: B, while hardly any increase in area can be seen in the transfected MEF^{Vin-/-} cells.

4.4.2 Expression of the EGFP-Vinculin-Strep-Tag-constructs cannot entirely rescue the MEF^{Vin-/-} phenotype

Figure 13: B also shows that expression of neither of the EGFP-Vinculin-ST fusion constructs (VinWT or VinT12) could bring back the MEFwt phenotype when measured as cell area. In fact, expression of the fusion constructs could not be seen to show practically any difference in cell area when compared to MEF^{Vin-/-} without EGFP-protein expression ($p = 0.708$ and 0.784 for EGFP-VinWT-ST and EGFP-VinT12-ST on glass, respectively; p -values are two-tailed values for Mann-Whitney U test; p -values for the other substrates were similarly not significant).

All analyses of cell area were done using only mononucleate cells. The presence of multiple nuclei visible in the representative images of single cells in Figure 11 and Figure 12 seemed to be characteristic for spontaneously immortalised MEF cells as they could be seen in both MEFwt and MEF^{Vin-/-} cells on all substrates used (data not shown). Since multinucleate cells could not be readily distinguished from clusters of multiple cells, in which dependency on substrate stiffness is known to be lost (Yeung et al. 2005), only cells with a single nucleus were chosen for analysis to ensure that the area measured was representative for single cells and comparable over all methods tested.

4.5 The HTI-deficient T12 vinculin mutant in EGFP-Vinculin-ST causes an increase in adhesion site density, but no difference in adhesion size compared to EGFP-VinWT-ST

To assess the effects of different substrates and the introduction of the T12 mutation into EGFP-Vinculin-ST constructs on cells further, vinculin-positive adhesions were measured and quantified from high-magnification microscope images of transfected MEF^{Vin-/-} cells on different substrates (see 3.6.3 above). The results of the quantification are summarised in Figure 14. The average area of adhesions could be seen to be almost constant in cells on PAA gel substrates – larger adhesions formed only on totally rigid substrates (see Figure 14: A and B). No difference could be seen

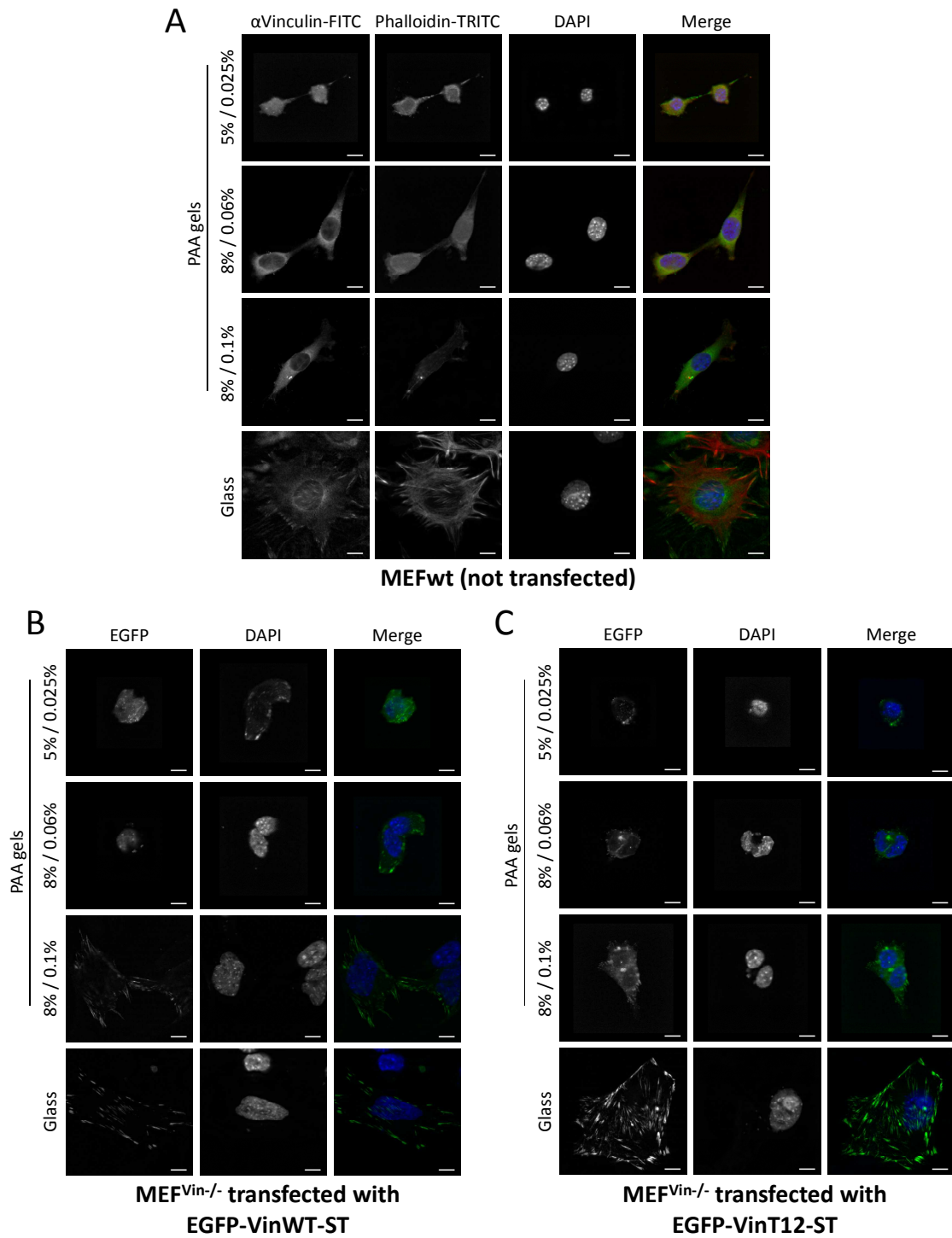


Figure 12: Representative images of immunofluorescence stained MEF cells cultured on different PAA substrates and glass. Cell spreading and area increases with increasing substrate stiffness in all analysed cells. Additionally, cells transfected with VinT12 show higher FA density than those transfected with VinWT constructs. **A:** Untransfected MEFwt cells grown on PAA gels of three different rigidities. Images are in increasing order of stiffness from top to bottom (5% / 0.025% being the softest gel, while glass is totally rigid). **B and C:** MEF^{Vin-/-} cells transfected with either EGFP-VinWT-ST or EGFP-VinT12-ST. All cells were cultured for 24 h on the substrates prior to imaging. Transfected cells were transfected on regular cell culture dishes, incubated for 24 h and then transferred onto the substrates shown. Scale bars are 10 μ m.

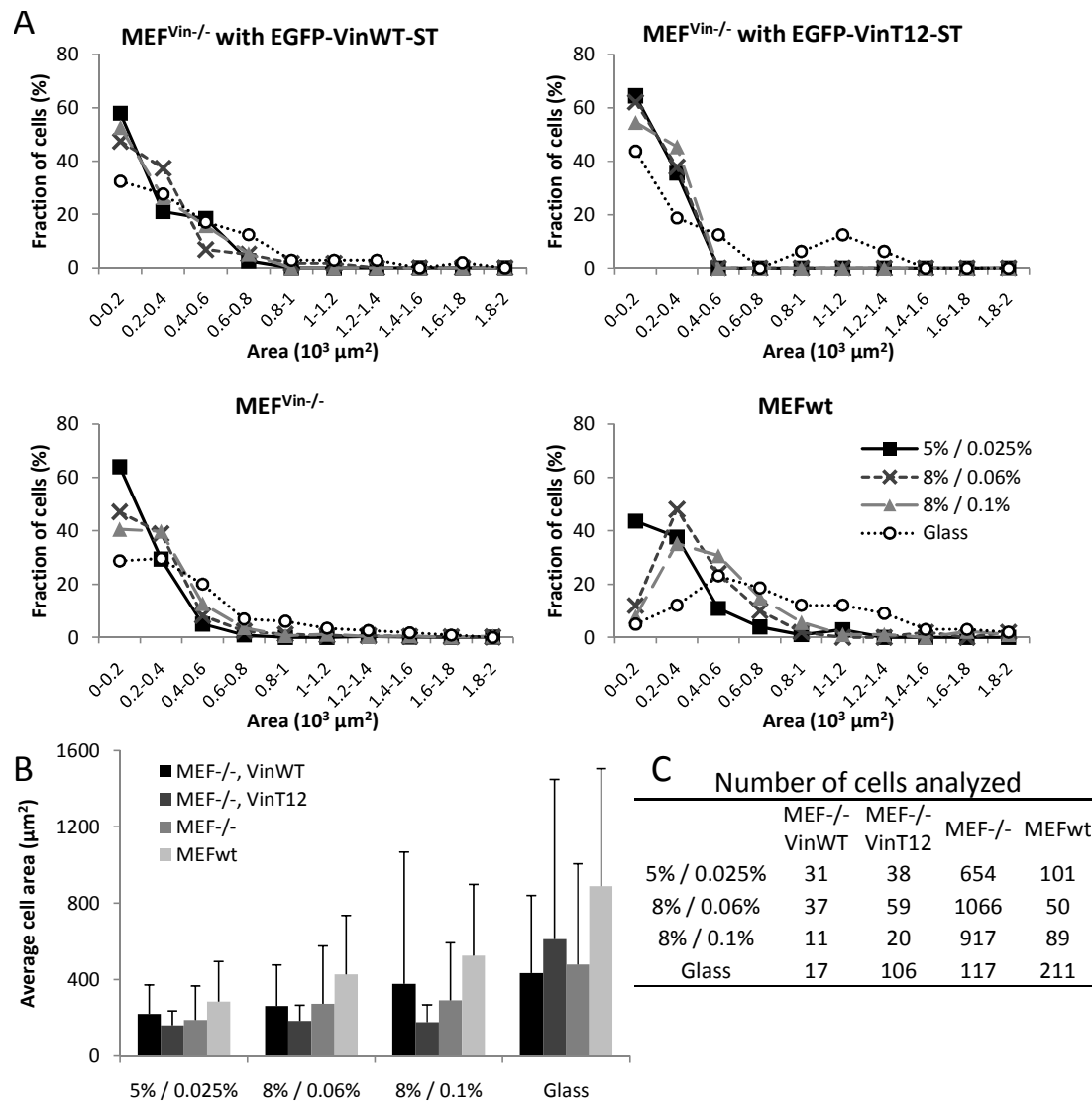


Figure 13: Comparison of cell area on different substrates shows increasing cell areas on substrates of increasing stiffness. Transfection with neither of the two analysed EGFP-Vinculin-ST constructs could rescue the MEF^{Vin-/-} phenotype as measured by cell area. A: Cell area distributions from the different EGFP-Vinculin-ST-expressing and non-expressing MEF^{Vin-/-} cells and MEF^{wt} cells. MEF^{wt} cells were not mock-transfected. B: Average cell areas on different substrates. Error bars shown are standard deviation values and highlight the non-gaussian distribution of cell areas. C: Table showing the numbers of individual cells analysed from different samples. Only mononucleate cells were chosen for analysis from microscope images.

in mean adhesion area between the two different EGFP-Vinculin-ST constructs (VinWT and VinT12) analysed ($p = 0.311$ for 5% / 0.025%; $p = 0.157$ for 8% / 0.06%; $p = 0.536$ for 8% / 0.1%; $p = 0.809$ for glass; two-tailed p -value of Mann-Whitney U test).

Looking at the number of adhesions in transfected MEF^{Vin-/-} cells compared to the total area of the cells analysed showed that the HTI-deficient EGFP-VinT12-ST construct caused a significant ($p < 0.05$) increase in adhesion density over cells transfected with EGFP-VinWT-ST on both stiffer gels ($p = 0.010$ for 8% / 0.06%; and

p = 0.042 for 8% / 0.1%) whereas no significant difference was observed on glass (p = 0.277). No statistical analyses were conducted for the 5% / 0.025% gel due to low cell numbers (Figure 14: C and D).

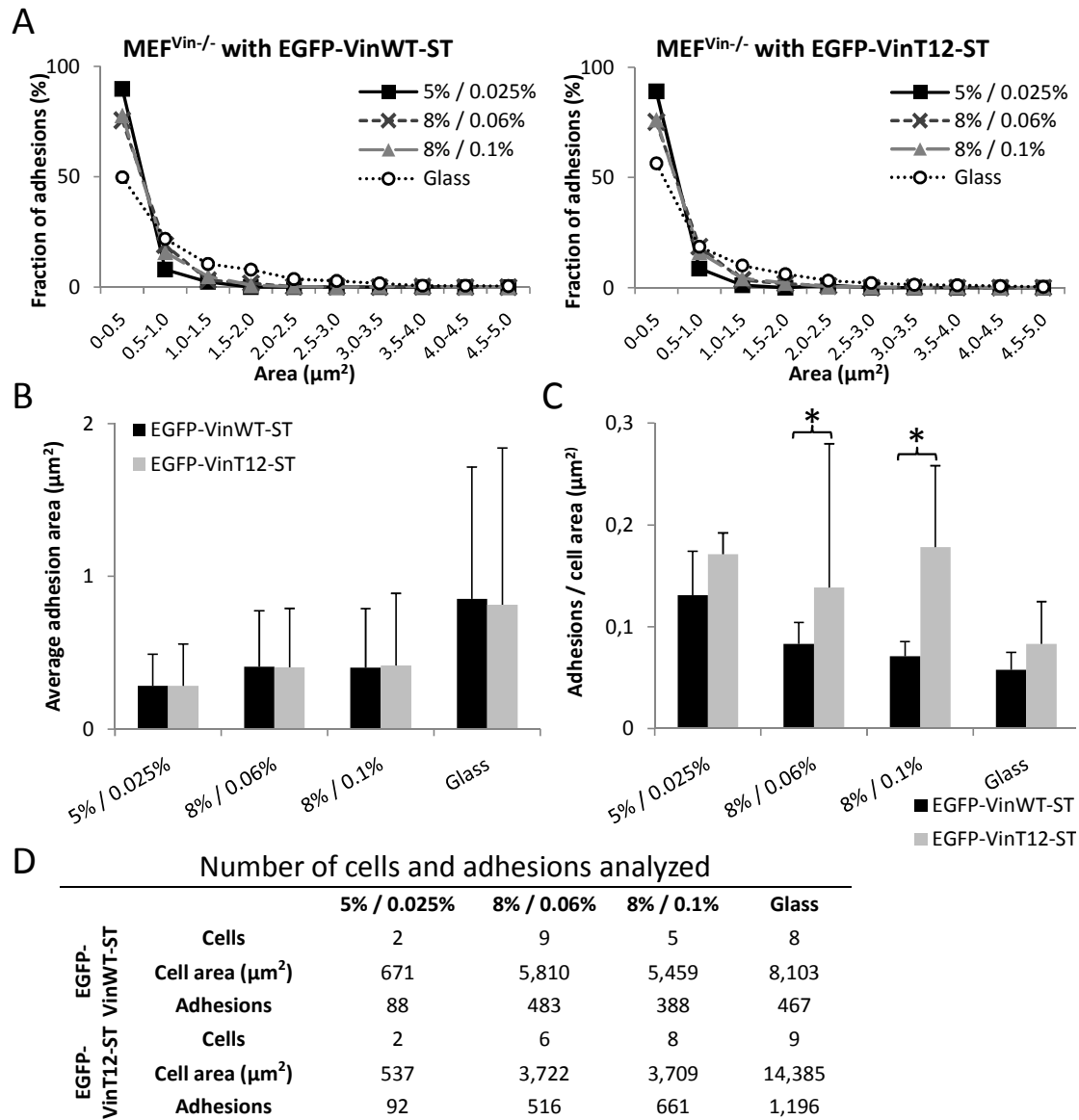


Figure 14: Area of adhesions increases with increasing substrate stiffness. Introducing the T12 mutation into EGFP-Vinculin-ST fusion constructs causes an increase in adhesion density, but does not affect their size. A: Area distribution of adhesions in transfected MEF^{Vin-/-} cells as estimated from fluorescence microscopy images using EGFP-Vinculin-ST as an adhesion marker. B: Average adhesion areas. C: Average adhesion numbers per total cell area analysed. D: Numbers of cells and adhesions analysed in the quantitation. Significant differences (two-tailed p-values on Mann-Whitney U test < 0.05) are marked with asterisks. Error bars are standard deviation.

5 Discussion

In natural environments cells grow on substrates with varying, and sometimes constantly changing, mechanical properties. Cells probe and feel the mechanical properties of these substrates and alter their behaviour accordingly (Eyckmans et al. 2011). The molecular mechanisms governing these mechanosensitive responses are still largely unknown. The work presented here aims to bring us one step closer to the elucidation of these mechanisms on the level of individual protein–protein interactions.

Although most cellular processes *in vivo* are set in a three-dimensional environment, two-dimensional substrates and most planar experimental setups should still be deemed a valid choice for assessing the processes of cell mechanotransduction and motility, which are very likely to be the same mechanisms and processes in use in 3D-situations *in vivo* (Eyckmans et al. 2011, Dubin-Thaler, Sheetz 2010). Furthermore, while 3D cell substrates would present a more natural environment, research on mechanosensing and mechanotransduction of cells in such matrices is still in its infancy (Doyle, Yamada 2010) and methodology is just emerging. Thus the more convenient two-dimensional substrates made of PAA were chosen for the purposes of this study.

Efficient transfection is a crucial factor for the viability of practically any approach involving rational mutagenesis or the use of tagged bait proteins for purification. Therefore, we assessed the efficiencies of several different transient transfection approaches to find a suitable option for future studies. We managed to find a reagent and conditions that will enable routine transfection with reasonably high transfection efficiency in a reproducible manner. It should be noted that the numerical values displayed in Figure 4 and Figure 5 are not transfection efficiencies *per se*, but rather rough estimates of the fluorescent cell area portion to the total cell area, and should thus not be directly compared with transfection efficiencies from most other sources. The ratios given are designed mainly for in-house comparison of samples.

When studying protein complex composition and interactions on the molecular level, extraction of the proteins in question is often inevitable. If interactions are to be studied, the complex should, furthermore, be retrieved in a relatively intact state. In previous studies looking into the composition of FAs, physical methods based on extraction of substrate-bound complexes have been used most widely since they

present an easy way of generating analysable material from relatively untreated cells (Kuo et al. 2011, Humphries et al. 2009, Schiller et al. 2011).

Our results from physical purification methods to extract FA protein complexes using protocols previously published in the literature suggest that these means of purification are not quite straightforward to implement and probably need extensive optimisation when applied to new systems. While there are several possible reasons for us not being able to reproduce the promising purification results from e.g. Plopper et al. (1993), Humphries et al. (2009), or Schiller et al. (2011), one primary reason might be the different cell lines used in our study compared to the aforementioned pieces of research. The stability of FAs and the expression levels of for example talin and vinculin can be expected to differ quite substantially from cell line to cell line. Therefore, purification characteristics of MEF cells used in our approach might differ from, for example, the bovine capillary endothelial cells used by Plopper et al. (1993).

Another, possibly more important factor is the application of a membrane permeable cross-linker that covalently fixes the inherently transient FA protein complexes. Staying faithful to the original protocols of Plopper et al. (1993) and Kuo et al. (2011) we did not apply cross-linkers in all different purification methods. In their 2009 study on the FA proteome, Humphries et al. could demonstrate that a membrane-permeable cross-linker was required to get talin to copurify using FN-coated beads and a mild detergent-based cell lysis protocol coupled with sonication of cells. No detectable amounts of talin could be retrieved without cross-linking as the talin–integrin linkage was presumably too fragile in the environment given (Humphries et al. 2009).

Even though we could not extract any detectable amounts of talin into the expected FA protein fraction even in our optimisation experiments of our best-performing protocol (Protocol 1.1: ‘Scraped’ samples in Figure 7), the most promising results – as estimated from the amount of vinculin detected – were obtained using short DTBP cross-linking together with short detergent lysis. This seemed to enable lysing cells sufficiently gently to leave some of the basal membrane proteins on the substrate (Figure 8: A, Protocol 1.1; and Figure 7). Stronger cross-linking with a longer incubation time and a higher cross-linker concentration (Protocol 1, Figure 6) seemed to fix cells completely, and was therefore not continued.

Stronger cross-linking did, however, create an interesting situation where high molecular weight bands positive to both vinculin and talin could be seen in the right

protein fractions (Figure 6: DTBP Cross-linked: 'Scraped'). Although these bands were at first disregarded, they could, in fact, represent promising purification of protein complexes, and should be discussed. The bands would at first seem to fit the criteria for FA protein clusters – yet finding intact complexes would be highly unexpected in the sort of gel presented. The boiling of the protein samples in reducing, SDS-containing sample buffer before loading into the gel is expected to not only denature proteins but also to reduce all possible DTBP cross-links, and thus cause any protein complexes to dissolve into their respective constituents. On a similar note, getting distinct bands like those seen in the immunoblots in Figure 6 are unexpected in protein complexes like FAs, since they are normally not expected to be well defined complexes with a set stoichiometry of components. In fact, cytoplasmic FA protein complexes could be expected to present a large variety of different proteins in variable amounts, with the exact composition depending on the subcellular localisation of each given adhesion complex in, for example, protruding or retracting parts of the cell (Zaidel-Bar, Geiger 2010, Doyle, Yamada 2010, Grashoff et al. 2010). To make matters even more complicated, numerous FA proteins are known to undergo frequent protease cleavage during their life-cycle, which would decrease the probability of finding exact complexes even further. Given this inherent heterogeneity, a biochemical extraction method of intact complexes could be expected to most likely show up as ill-defined smear-like bands in immunoblots due to the large variety of molecular weights present. Although the high-MW bands in Figure 6 should thus not be expected to contain any intact complexes *per se*, they do present an interesting observation. Their apparent disappearing during acetone precipitation further enhances the peculiar nature of the bands, while simultaneously casting doubt on the suitability of acetone precipitation in studies like this. The bands were not observed in later experiments of our study using weaker DTBP cross-linking, which leaves further investigation and characterisation of them to future studies.

Another means of purifying protein complexes is using affinity tagged 'bait' proteins to enable retrieving 'prey' proteins that are presumed to be interacting (directly or indirectly) with the bait used. In our set-up, using the Strep-tagged vinculin as bait in affinity chromatography yielded more encouraging results than the unspecific purification methods. Using EGFP-Vinculin-ST fusion constructs we could show that while much of the tagged vinculin did purify, some endogenous vinculin could be seen to partially copurify with the tagged vinculin as well (Figure 9 and

Figure 10). This copurification could be caused simply by unspecific binding of proteins onto the ST-tagged vinculin or the Strep-Tactin resin. This possibility should be investigated using one or more antibodies against generic cytoplasmic proteins as controls to assess the ability of the purification to specifically purify FA-associated proteins.

The presence of endogenous vinculin also in the elution fractions might, however, also indicate successful purification of more-or-less intact FA complexes, which would be expected to contain multiple vinculin molecules – some of which could easily be endogenous. Additionally, vinculin has been known to form dimers in FAs, especially after binding to F-actin (Saunders et al. 2006). Thus purifying these sorts of dimers from transfected MEFwt cells seems likely.

In order for the purification method to be used for studying the talin–vinculin interaction, however, purification of intact talin–vinculin complexes is of paramount importance. As can be seen from Figure 10 we could observe a talin band only after using very harsh elution conditions. While the low amounts of especially talin retrieved could be caused by simply a too low starting amount of cells (see also discussion on protein purification from mammalian cells below), it could also be due to the fact that only a small fraction of the total amount of cellular talin is probably active and present in FAs, and thus accessible for our vinculin-based purification. This distribution of talin into cytoplasmic and FA populations is evident from immunofluorescence staining of cells using an anti-talin antibody (Figure 11). Adding to this, that the stoichiometry of the talin–vinculin interaction would suggest talin-to-vinculin ratios from 1:5 to 1:10 even in ideal FA protein complexes (Critchley 2009), it is probably not surprising that the retrieved amounts of talin are small (Figure 9 and Figure 10) even if whole complexes could be efficiently retrieved intact.

Furthermore, the talin band observed in Figure 10 and other figures is not the size of a full-length protein, but possibly rather indicates presence of a proteolytic cleavage product of talin, as talin is known to be frequently cleaved by specific proteases during its life-cycle in adhesions (Critchley 2009). Whether this fragment would contain the necessary rod-domain components to assess the binding of vinculin to talin VBSs remains to be seen.

One defining factor of both of the tested protein purification methods is the extremely small total amount of protein as a monolayer of cells effectively produces very limited amounts of cell mass for analysis. This challenge was also acknowledged

by Kuo and co-workers (2011) who mentioned having to use rather large cell culture areas to analyse FA proteins. Culture areas mentioned included, for example, 460 cm² (the equivalent of eight 10 cm dishes) needed for mass spectrometrical analysis, and 3,000 cm² (corresponding to around 55 dishes) for one two-dimensional differential gel electrophoresis (2D-DIGE) experiment. With cell culture areas this big, transfection reagent expenditure quickly becomes a significant factor when using transient transfection with traditional lipid or polymer-based reagents.

One way to circumvent the issue of having to use large culture areas was presented by Humphries et al. (2009). They used non-adherent leukaemia-derived K562 cells transfected with integrins. This enabled culturing cells in suspension, which naturally increases protein yield per volume of medium substantially. They used FN-coated paramagnetic microbeads in the suspension to effect FA formation in the suspension cells, while simultaneously using the beads as a means to purify presumed FA proteins after covalent cross-linking and lysing of cells. While this approach certainly does increase the productivity and the amounts of proteins purified, using cells naturally growing in suspension to study the exact molecular make-up of adhesion complexes seems somewhat questionable.

In cases where exogenous proteins are used as affinity bait, the amount of extractable protein can naturally also be enhanced by raising the ratio of transfected to untransfected cells. This can be achieved by higher transfection efficiencies, which we did aspire to by thoroughly optimising transfection reagents and conditions. Alternatively, transfection could also be made more cost-effective using alternative methods like virus-mediated transduction. A complementary means is also enriching the cell population by sorting for EGFP-positive cells as demonstrated by, for example, Kuo et al. (2011), or the creation of cell lines stably expressing the protein construct of interest. The last mentioned means of creating stable cell lines was in this case, however, chosen to be avoided due to large fluctuations in transgenic protein expression levels usual to cell lines with externally introduced protein genes randomly integrated in their genome (Ungureanu D. 2011, *Personal communication*).

In the work with pliable substrates the protocol used for making PAA gels was found to be feasible, albeit somewhat laborious. The protocol should also be readily scalable for substrates of larger areas, although some of the steps, like removing the upper glass after gel polymerisation, can be expected to turn out to be a non-trivial task requiring steady hands and patience with larger glass slips.

In previous studies, the effects of altering the mechanical environment on FA proteins have been studied among other systems, using Triton cytoskeletons (reviewed in Hytönen, Smith & Vogel 2010) in which the cell membrane is removed using a mild detergent treatment and only the cytoskeletal proteins remain (Sawada, Sheetz 2002). While Triton cytoskeletons undoubtedly provide an efficient means to study primary protein interactors, it is not entirely clear what the consequences from removing the cell membrane are with regard to the mechanical integrity of the cytoskeleton and, simultaneously, what possible soluble FA-associated proteins might be lost once the cell membrane is ruptured. Thus in the work covered here, whole untreated cells were chosen to serve as an experimental platform. The cells were initially analysed for effects of substrate rigidity and mutant constructs by looking at cell and adhesion size with image analysis tools.

Analysis of MEFwt cell size on different substrates showed a constant increase in average cell size when increasing substrate stiffness (Figure 13). This result is perfectly in line with previous results from studies on myoblasts on PAA gels of different stiffness. In a series of publications Engler et al. (2004c, 2004b, 2004a) managed to quantify the cell spreading response with regard to substrate stiffness by using atomic force microscopy (AFM) to measure substrate stiffness and image analysis to estimate cell area. They also introduced a simple equation describing the correlation between cell area and the substrate's Young's modulus (Engler et al. 2004a). The gel substrates used by Engler et al. (2004b) spanned a range of Young's moduli of 1 to 8 kPa corresponding to PAA gels of acrylamide / bis-acrylamide ratios of 5% / 0.03% to 10% / 0.3%. Seeing that the gel compositions producing our results with MEF cells lie along the same range of ratios, the Young's moduli of our substrates presented above can be similarly expected to cover a range of around 1 to 6 or 7 kPa, which spans rigidities expected in, for example, smooth muscle tissue (Engler et al. 2004c) or fibroblast cells (Engler et al. 2004b). Since stiffness of the PAA substrates was not explicitly quantified in our initial experiments presented here, however, assessment of the equation of Engler et al. (2004a) and its usability for MEF cells will not be quantitatively evaluated here.

One especially striking result of our studies was the apparent inability of our EGFP-Vinculin-ST constructs to rescue the MEF^{Vin^{-/-}} phenotype (see Figure 13). Previous studies on vinculin-deficient MEF cells (Saunders et al. 2006) and parental F9 embryonic carcinoma cells (γ228 strain) (Xu, Coll & Adamson 1998) have shown

that the mutant phenotype caused by lack of vinculin could be rescued practically completely by reintroducing wild type vinculin into the cells by transfection (Xu, Coll & Adamson 1998, Saunders et al. 2006). The parameters analysed for example by Xu et al. (1998) included cell morphology and area, cell migration, and cell adhesion, all of which could be seen to be restored to wild type levels following vinculin reexpression. Looking at cell area only, we could not observe total rescue of the MEF^{Vin^{-/-}} phenotype as a result of transiently expressing EGFP-ST-fusion constructs of either wild-type vinculin or the HTI-deficient T12 mutant form.

One aspect that could possibly explain the stark difference observed in the cell sizes of transfected MEF^{Vin^{-/-}} and untreated wild-type cells in our study, could be caused by the transfection reagent itself, as chemical transfection reagents might have deleterious effects on cell growth and morphology in general. This, however, cannot explain why there is no visible difference between transfection reagent-treated MEF^{Vin^{-/-}} cells that do visibly express EGFP-Vinculin-ST-fusion constructs and those that do not (Figure 13).

Another possible cause of the observed discrepancy is that the mode of microscopy image acquisition and the image analysis techniques used here suffer from unequal lighting conditions and poor resolution in low-magnification fluorescence images used for the estimation of cell area. Although these shortcomings affect all samples similarly, they do lower the amount of cells that can be reliably analysed and thus lower the reliability of the mode of analysis. To avert these kinds of sources of error in future analyses, usage of large numbers of high-magnification images should be preferred. This could enhance homogeneity and reproducibility of the imaging and analysis process, while simultaneously increasing sensitivity of imaging and thus enabling identification of cells with lower EGFP-Vinculin-ST expression levels. Such cells, with low overall fluorescence, could still have sufficient expression of functional vinculin fusion proteins to cause changes in cell size, while only showing weak or highly localised EGFP-fluorescence, which might go unnoticed in lower-resolution low-magnification images. Failure of identification of these kinds of cells as vinculin-expressing cells could thus easily cause diminution of possible differences between non-expressing MEF^{Vin^{-/-}} cells and cells identified as successfully EGFP-protein expressing.

The third, and possibly largest single cause of error in our rescue results, is the question about the functionality of the fusion protein construct itself. Interference of

vinculin function caused by fusion of EGFP and ST onto the protein structure is naturally a primary cause of suspicion in this respect. In order to avoid these kinds of speculations, both Saunders et al. (Saunders et al. 2006) and Xu et al. (Xu, Coll & Adamson 1998) got their rescue results using non-fusion vinculin constructs along with an antibiotic-based selection system to distinguish transfected from non-transfected cells. In the case of the N-terminally fused EGFP our results showing colocalisation of EGFP-Vinculin with talin (Figure 11), along with previous results by Cohen et al. (2006, 2005), do not speak for any reduction in biological functionality of vinculin with N-terminally added EGFP. More recent results using wild-type vinculin with N-terminal EGFP fusions from Diez et al. (2011, 2009) could furthermore display successful rescue of MEF^{Vin-/-} cells' mechanical properties – i.e. the stiffness of the cells and the strain energy exerted by the cells on their substrate (Diez et al. 2011, Diez et al. 2009) – as well as the number of FAs per cell (Diez et al. 2009). These results do not suggest any impairment to vinculin function caused by EGFP.

The addition of the C-terminal Strep-Tag, on the other hand, could in fact influence the biological function of the vinculin construct significantly. Previous studies have implicated that the C-terminal residues are important for vinculin activity by regulating the interaction of vinculin with PIP₂, a known inhibitor of the autoinhibitory HTI-interaction in vinculin (Saunders et al. 2006). Furthermore, multiple C-terminal residues with presumed lipid-binding functions have been shown to affect mechanical properties of whole cells (Diez et al. 2009). Although the portion of vinculin interacting with PIP₂ has later been narrowed down to not contain the C-terminal hairpin in vinculin (residues 1061–1066) (Palmer et al. 2009), the importance of the C-terminus for proper vinculin function has remained unquestionable.

An important, very recent study by Shen and co-workers (2011) shed light on the subject by identifying the vinculin C-terminus as important for regulating the vinculin–actin interaction. They used recombinant Vt constructs (residues 879–1066) to show that while deleting C-terminal residues did not influence actin binding of vinculin, the deletion of even a single C-terminal amino acid (Q1066) significantly lowered the ability of vinculin to create actin bundles, with the reduction becoming more drastic as more residues were deleted. Assessing the effects the deletions had on the formation of “native” and actin-induced Vt-dimers led them to the conclusion that the reduction in actin-bundling capability of the hairpin-less mutant (residues 879-1061) might be caused by the formation of too tight actin-induced dimers (Shen

et al. 2011). They, furthermore, assessed the effects of loss of C-terminal amino acids also in full-length vinculin N-terminally fused to GFP and transfected into MEF^{Vin-/-} cells. Removal of five C-terminal amino acids led to (i) a decrease in cell area, (ii) a decrease in FA number per cell, (iii) slight increase in average FA size (albeit not statistically significant), and (iv) to a loss of force-induced stiffening of cells, while not influencing the basal stiffness of the cell (Shen et al. 2011).

While some of the effects could be explained by the loss of tyrosine 1065, the phosphorylation of which is known to be rather important for the correct function of vinculin in FAs (Diez et al. 2009, Küpper et al. 2010), it seems that weakening of vinculin's actin-bundling capabilities reduces the capacity of force-transmission in FAs. Interestingly, most of the effects (i, iii, and iv) observed by Shen et al. (2011) could directly be explained with the model of a mechanosensitive talin with cryptic vinculin binding sites opened by the mechanical stretching of the talin rod (Critchley 2009, Hytönen, Vogel 2008). In the model, stretching of talin is expected to be caused by force applied in an end-to-end manner, with the N-terminal head being bound to cytoplasmic parts of integrin and the C-terminal tail being bound to actin through its own actin-binding site (Critchley 2009). Since this mode of actin binding is not compromised in cells with C-terminally truncated vinculin, talin could be expected to be stretched, thus recruiting more vinculin to the complex. If, however, the force transmission of the vinculin-to-actin linkage is compromised due to insufficient bundling of actin, the recruitment of vinculin to talin would not lead to any actual strengthening of the integrin-to-cytoskeleton linkage. This could explain the inability of cells transfected with actin-bundling deficient vinculin to strengthen their cytoskeleton-to-ECM linkages, while also explaining the slight increase in adhesion size observed by Shen et al. (2011).

Since the important amino acids for actin bundling are the few very last amino acids in vinculin, a C-terminal fusion of, for example, a Strep-Tag as used in our study could be expected to also interfere with both the phosphorylation of Y1065 and actin-bundling and thus lead to a weakening of force-transmission in FAs. This could then lead to the inability of EGFP-Vinculin-ST constructs to rescue the MEF^{Vin-/-} phenotype as measured by cell size. The effects of the Strep-Tag addition on FA size can unfortunately not be assessed with the present data, since comparison to MEF^{wt} FAs would require FA quantitation from immunofluorescence-stained wildtype cells, which is not possible using our immunofluorescence staining protocol and antibodies

because of too high cytoplasmic background fluorescence (see Figure 12: A). Similarly, the same reason also prevents analysis of adhesions in untransfected MEF^{Vin-/-} cells (which could be visualised using anti-talin antibodies) from our present data, which prevents comparison of adhesions in MEF^{Vin-/-} cells to MEF^{Vin-/-} cells expressing vinculin constructs. To counteract these shortcomings, usage of a different adhesion marker, like for example paxillin, should be considered as a secondary means of verification in future studies. Furthermore, future experiments using other EGFP-Vinculin constructs without Strep-Tags (or with N-terminal tags) should be conducted to assess the effect of C-terminal additions on vinculin's behaviour.

Despite the previously-discussed possible compromising effects the Strep-Tag might have on vinculin's actin-regulatory (and thus mechanotransmissive) functions, introduction of the T12 mutations into the vinculin structure in EGFP-Vinculin-ST constructs seems to still cause expected results in MEF cells. Already while characterising the mutant for the first time, Cohen et al. (2005) suggested that cells with VinT12 could be seen to have increased FA numbers per cell. This has later also been observed by Humphries et al. (2007) who used EGFP fusion vinculin constructs and reported VinT12-positive FAs to cover over twice the area in NIH3T3 mouse fibroblast cells compared to regular vinculin. They did, however, also mention observing larger FA sizes with VinT12 and other HTI-deficient constructs like C-terminally truncated forms, although they did not explicitly compare VinT12 with tail-less vinculin and thus did not state whether the FA enlargement was special to tail-less constructs or also present in VinT12 (Humphries et al. 2007). While the increase in FA size could be expected to happen in C-terminally modified forms (see discussion above), we could not observe any increase in FA size caused by weakening of the HTI using VinT12 (Figure 14: B).

On a more general level, our data does nicely show an increase in average adhesion area with increasing stiffness of the substrate. This trend, seen with both EGFP-Vinculin-ST constructs used, is also clearly visible in representative images of transfected MEF^{Vin-/-} cells, which show small dot-like adhesions on the softer substrates, while large, elongated adhesions are visible mainly on totally rigid glass. These results are in perfect accord with previously published findings, according to which adhesion sites, as observed by vinculin localisation, appear as poorly defined spots in cells cultured on compliant substrates, whereas adhesions form distinct,

elongated regions on rigid substrates (Bershadsky, Balaban & Geiger 2003, Saez et al. 2005, Pelham, Wang 1997).

As previously mentioned, the magnitude of force transmitted through an adhesion is proportional to the rigidity of the substrate (Saez et al. 2005). Our results regarding increased average adhesion size with increasing substrate stiffness would thus seem to suggest some relationship between FA size and force transmitted through them also when measured adhesion area is averaged over all vinculin-positive adhesions in all cell regions. This would somewhat contradict the notion of Stricker et al. (Stricker et al. 2011) according to which no clear correlation exists between force and FA size when looking at all adhesions in a cell. Due to limitations in the amount of analysed cells and adhesions, and the lack of exact quantitation of substrate rigidity, our data does, however, not permit rigorous analysis of the exact nature of the relationship between average adhesion area and substrate stiffness.

Looking at the actual area of adhesions observed in our experiments shows that most of the adhesions are under $1 \mu\text{m}^2$ in area, which was the lower size limit of mechanosensitive adhesions interpreted as FAs by Tan et al. (2003). While it is possible that the large number of small adhesions seen in all of our cells could represent nascent FXs, which fail to mature into FAs in cells on soft substrates (Figure 14), broader inspection of the literature shows, that in addition to there not being a general standard agreed upon for a minimum size for adhesions to be classified as mechanosensitive FAs, FA size might be highly dependent on the cell and experiment type used. Thus, for example, Berginski et al. (2011) analysed 3T3 cells with fluorescently labelled FAK and paxillin using quantitative image analysis tools applied on movies of single cells and reported FA size distributions looking much alike the ones extracted from our MEF cell models. Small adhesions of $0\text{--}0.5 \mu\text{m}^2$ were overwhelmingly the most abundant type (Berginski et al. 2011), which might, however, also be caused by the used image analysis method, as it used similar thresholding as our method to create binary images for area measurements. Similarly small adhesions ($0\text{--}0.5 \mu\text{m}^2$) seem to be highly represented in results from Stricker et al. (Stricker et al. 2010), when looking at U2OS osteosarcoma cells stained with anti-vinculin antibodies.

Interestingly, results from Stricker et al. (2011, 2010) also clearly show that the size distribution and frequency of emergence of adhesions are very much influenced by not only the rigidity of the substrate, but also by the distribution of ECM proteins

on the surface. As micropatterning of substrates with integrin ligands is quite often used when analysing traction forces and adhesions on continuous substrates (Stricker et al. 2011, Stricker et al. 2010, Chen et al. 2003) the notion that adhesion size distribution, presumably along with other aspects of adhesions, can vary considerably depending on the distribution of ECM proteins on the surface should be taken into account when analysing results. Moreover, similar effects should also be expected when using non-continuous surfaces like the micropillars used by Tan et al. (2003) and others (e.g. Saez et al. 2005, Saez et al. 2010). In these sorts of setups not only the ECM proteins are distributed discontinuously in a patterned manner, but also the rigidity of the substrate is discontinuous as the “softness” of the substrate comes on a larger scale from the bending of individual PDMS pillars, each of which still presents a rather stiff contact surface on a microscale. Thus results from studies using these rather differing methodologies should be compared only with the utmost care.

Importantly, our results do, however, seem to corroborate the functionality of our PAA-made substrates in their ability to alter FA assembly, and thus pave the way for future studies aimed at assessing the mechanosensitivity of the talin–vinculin interaction using methods described here.

Studying focal adhesions using transiently transfected MEF cells initially brought up the, at first unexpected, observation that cells could not be transfected with the EGFP-Vinculin constructs directly on soft substrates as the transfection efficiency fell to negligible levels. This was rather quickly explained by the finding that the MEF^{Vin-/-} cells used seemed to practically cease to grow and divide on the gel substrates and confluency remained low even when culturing cells for extended amounts of time (data not shown). This was most evident on the softest substrates used (5% / 0.025% acrylamide / bis-acrylamide ratio), although significantly impeded cell proliferation could be seen also on the stiffer gels. Since most modes of chemical transfection rely at least partly on introducing the plasmid DNA into the nucleus during cell division (Tros de Ilarduya, Sun & Düzgüneş 2010), it is no surprise that transfection efficiency was low in these cells.

The observation that the MEF cells used do not grow readily on a substrate other than totally rigid glass or polystyrene, however, also raises another important question about mechanobiological studies done in cellular models using cell lines. Most well-established cell lines are derived from primary tissue homogenised and plated on a rigid substrate, like clear polystyrene, for example. This approach essentially creates a

powerful selection pressure that favours cells able to grow and divide efficiently on unyielding surfaces. This, combined with routinely culturing cells on stiff substrates, would be expected to bring forth and maintain cells that are “specialised” on growing (only) on these kinds of substrates. With this in mind, it might even be expected that especially high-passage number cell lines do not grow well on mechanically different substrates like the ones used in this study. There are, however, also exceptions to this, as shown, for example, by Yeung et al. (2005) with NIH3T3 and bovine aorta epithelial cells.

Similarly, the question arises whether such cell lines actually represent biologically relevant situations in mechanobiology. Having a totally rigid substrate to grow on is rare indeed for cells in *in vivo* surroundings, with the sole exception probably being some cell types in bone tissue. Many tissues, like muscle or arterial blood vessels, are comparably soft and can be mechanically mimicked by PAA gels with compositions close to the ones used in this study (Engler et al. 2004c, Engler et al. 2004b).

With these considerations in mind, using primary cells, as exemplified by Case et al. (2011), should probably be stressed in mechanobiological studies. Furthermore, these primary cells might have to be extracted and routinely cultured on pliable substrates to avoid inducing unnecessary selection pressures and thus keep the cells closer to real *in vivo* conditions.

Finally, with the basic methodology set up for manipulating the talin–vinculin system in a cell model both by reintroducing mutant protein constructs and by altering the mechanical environment, some consideration should be given to the next logical step – i.e. means to investigate the interaction between talin VBSs and the vinculin head. Recent developments in the field of protein interaction methodologies have brought forth some interesting options for detecting protein–protein interactions in or from cellular contexts. Examples of these include the proximity-ligation assay (PLA) (Gullberg, Andersson 2010) and a single-molecule pull-down (SiMPull) method recently published by Jain et al. (2011).

The first-mentioned PLA uses a double-antibody labelling system to detect interaction partners together with an ingenious *in situ* PCR system to detect proximity of the oligo-DNA-labelled antibodies, and simultaneously amplify the signal so that even single molecule interactions can be detected (Gullberg, Andersson 2010). Although this method is undoubtedly powerful and presumably quite sensitive, it is

probably somewhat ill-suited for detecting (and quantifying!) interactions in crowded and complex systems like adhesion complexes where the interaction partners are likely to be present in high amounts in any case. The PLA method put forward by Gullberg and Andersson (2010) might however be an interesting alternative when combined with the extraction of intact, cross-linked protein complexes described in this work. In that case, the extraordinary sensitivity of the PLA could partly negate the problems generated by the low total protein amounts discussed earlier.

The second, maybe more directly suitable, method SiMPull (Jain et al. 2011), involves incubating cell lysate on an antibody-coated surface and then detecting target proteins using e.g. immunofluorescence or previously added fluorescence tags, like EGFP in our vinculin constructs. Cross-linking of cellular proteins before lysis would probably be advised also in this method to ensure extraction of transient protein complexes as close to their native state as possible. Probably the most interesting aspect of this technique would be that the immobilised complexes could be analysed using single molecule fluorescence microscopy, in which the exact number of bound fluorophores in an individual complex can be assessed by observing successive bleaching steps (see also del Rio et al. 2009, Jain et al. 2011).

Furthermore, interaction studies on pliable substrates could in the future also be combined with the use of novel single-molecule force sensors, like the one described by Grashoff et al. (2010). Their sensor is based on intramolecular Förster resonance energy transfer (FRET) between two fluorophores separated by an entropic spring and flanked by vinculin N and C-terminal domains on each side. This setup enables gauging the force transmitted across vinculin inside cells, and could be used for example to assess the effects of substrate stiffness on the force transmitted through vinculin in adhesions. Additionally, using the sensors in conjunction with substrates like the ones used in this study, measurement of the force transmitted through a vinculin molecule in FAs of different sizes in cells on different substrates would be possible. This information could be used to assess whether the force along a single vinculin molecule in different adhesions is, in fact, constant, and the force transmitted by an adhesion would be determined simply by the number of molecules (seen as FA size), as has been so often proposed (Critchley 2009, Bershadsky, Balaban & Geiger 2003, Tan et al. 2003, Choquet, Felsenfeld & Sheetz 1997).

Lastly, any of these methods for analysing the interaction between talin and vinculin or the force transmitted through single molecules will have to be

accompanied by rational mutagenesis. Use of one of the frequently used vinculin mutants (VinT12) (Cohen et al. 2006, see e.g. Cohen et al. 2005, Humphries et al. 2007) has been demonstrated in this work, but in order to completely elucidate the talin–vinculin interaction mutations should probably be introduced into both interaction partners. Ideally – although challenging to say the least – complementing mutations in both talin and vinculin should be used in conjunction to pinpoint residues important for the interaction and activation of the interacting portions. This, together with the interaction and force-sensing methodologies discussed, could be used to completely understand the nature and potential mechanosensory abilities of the talin–vinculin interaction.

6 Conclusions

In conclusion, the results presented here represent the first steps taken on the way towards the experimental elucidation of the intracellular mechanotransduction machinery in focal adhesions. Optimisation experiments were described of various aspects of the experimental workflow. Suitable reagents and conditions were found for the transient transfection of mouse embryonic fibroblasts with EGFP- and Strep-Tag-coupled vinculin fusion constructs. Multiple protein purification protocols for the extraction of FA proteins were assessed, and none of the previously published physical extraction methods proved directly suitable when using relatively small amounts of adherent MEF cells as the starting material. Strep-Tag-based affinity purification, on the other hand, showed promising results as copurification of endogenous vinculin molecules and minor amounts of talin alongside Strep-Tagged EGFP-vinculin fusion proteins implied successful isolation of protein complexes. Additionally, biofunctionalised polyacrylamide was successfully used as a cell culture substrate with modifiable rigidity. These substrates could be shown to have expected effects on cell and adhesion morphology, and thus were deemed to be suitable for future experiments. Simultaneously, multiple interesting new questions arose especially concerning the specific role of the C-terminal parts of vinculin and the possible impairment of vinculin function due to addition of tags to the vinculin C-terminus.

As it stands these experiments open the door for future studies using modifiable substrates to alter the mechanobiological environment of mammalian cell models. Together with transient transfection of various fusion constructs of FA proteins, the methodology presented also enables a rational mutagenesis approach to the study of the mechanosensory protein complexes in focal adhesions, while simultaneously providing tools for the analysis of cell and adhesion area and morphology.

References

- Balaban, N.Q., Schwarz, U.S., Riveline, D., Goichberg, P., Tzur, G., Sabanay, I., Mahalu, D., Safran, S., Bershadsky, A. & Addadi, L. 2001, "Force and focal adhesion assembly: a close relationship studied using elastic micropatterned substrates", *Nature cell biology*, vol. 3, no. 5, pp. 466–472.
- Berginski, M.E., Vitriol, E.A., Hahn, K.M. & Gomez, S.M. 2011, "High-Resolution Quantification of Focal Adhesion Spatiotemporal Dynamics in Living Cells", *PloS one*, vol. 6, no. 7, e22025.
- Bershadsky, A.D., Balaban, N.Q. & Geiger, B. 2003, "Adhesion-dependent cell mechanosensitivity", *Annual Review of Cell and Developmental Biology*, vol. 19, no. 1, pp. 677–695.
- Block, M.R., Badowski, C., Millon-Fremillon, A., Bouvard, D., Bouin, A.P., Faurobert, E., Gerber-Scokaert, D., Planus, E. & Albiges-Rizo, C. 2008, "Podosome-type adhesions and focal adhesions, so alike yet so different", *European journal of cell biology*, vol. 87, no. 8–9, pp. 491–506.
- Bois, P.R.J., O'Hara, B.P., Nietlispach, D., Kirkpatrick, J. & Izard, T. 2006, "The vinculin binding sites of talin and α -actinin are sufficient to activate vinculin", *Journal of Biological Chemistry*, vol. 281, no. 11, pp. 7228–7236.
- Butler, P.J. & Chien, S. 2010, "Role of the Plasma Membrane in Endothelial Cell Mechanosensation of Shear Stress" in *Cellular Mechanotransduction*, eds. M.R.K. Mofrad & R.D. Kamm, Cambridge University Press, pp. 61–88.
- Buxboim, A., Rajagopal, K., Brown, A.E.X. & Discher, D.E. 2010, "How deeply cells feel: methods for thin gels", *Journal of Physics: Condensed Matter*, vol. 22, p. 194116 (10 pp.).
- Case, L.B. & Waterman, C.M. 2011, "Adhesive F-actin Waves: A Novel Integrin-Mediated Adhesion Complex Coupled to Ventral Actin Polymerization", *PLoS ONE*, vol. 6, no. 11, pp. e26631.
- Chen, C.S., Alonso, J.L., Ostuni, E., Whitesides, G.M. & Ingber, D.E. 2003, "Cell shape provides global control of focal adhesion assembly", *Biochemical and biophysical research communications*, vol. 307, no. 2, pp. 355–361.
- Chicurel, M.E., Chen, C.S. & Ingber, D.E. 1998, "Cellular control lies in the balance of forces", *Current opinion in cell biology*, vol. 10, no. 2, pp. 232–239.
- Choi, C.K., Vicente-Manzanares, M., Zareno, J., Whitmore, L.A., Mogilner, A. & Horwitz, A.R. 2008, "Actin and α -actinin orchestrate the assembly and maturation of nascent adhesions in a myosin II motor-independent manner", *Nature cell biology*, vol. 10, no. 9, pp. 1039–1050.
- Choquet, D., Felsenfeld, D.P. & Sheetz, M.P. 1997, "Extracellular matrix rigidity causes strengthening of integrin-cytoskeleton linkages", *Cell*, vol. 88, no. 1, pp. 39–48.
- Cohen, D.M., Chen, H., Johnson, R.P., Choudhury, B. & Craig, S.W. 2005, "Two distinct head-tail interfaces cooperate to suppress activation of vinculin by talin", *Journal of Biological Chemistry*, vol. 280, no. 17, pp. 17109–17117.
- Cohen, D.M., Kutscher, B., Chen, H., Murphy, D.B. & Craig, S.W. 2006, "A conformational switch in vinculin drives formation and dynamics of a talin-vinculin complex at focal adhesions", *Journal of Biological Chemistry*, vol. 281, no. 23, pp. 16006–16015.
- Critchley, D.R. 2009, "Biochemical and structural properties of the integrin-associated cytoskeletal protein talin", *Annual review of biophysics*, vol. 38, pp. 235–254.

- Davies, P.F. & Helmke, B.P. 2010, "Endothelial Mechanotransduction" in *Cellular Mechanotransduction*, eds. M.R.K. Mofrad & R.D. Kamm, Cambridge University Press, pp. 20–60.
- del Rio, A., Perez-Jimenez, R., Liu, R., Roca-Cusachs, P., Fernandez, J.M. & Sheetz, M.P. 2009, "Stretching single talin rod molecules activates vinculin binding", *Science*, vol. 323, no. 5914, pp. 638–648.
- Diez, G., Kollmannsberger, P., Mierke, C.T., Koch, T.M., Vali, H., Fabry, B. & Goldmann, W.H. 2009, "Anchorage of vinculin to lipid membranes influences cell mechanical properties", *Biophysical journal*, vol. 97, no. 12, pp. 3105–3112.
- Diez, G., Auernheimer, V., Fabry, B. & Goldmann, W.H. 2011, "Head/tail interaction of vinculin influences cell mechanical behavior", *Biochemical and biophysical research communications*, vol. 406, no. 1, pp. 85–88.
- Doyle, A.D. & Yamada, K.M. 2010, "Cellular Mechanotransduction: Interactions with the Extracellular Matrix" in *Cellular Mechanotransduction*, eds. M.R.K. Mofrad & R.D. Kamm, Cambridge University Press, pp. 120–160.
- Dubin-Thaler, B.J. & Sheetz, M.P. 2010, "Toward a Modular Analysis of Cell Mechanosensing and Mechanotransduction: A Manual for Cell Mechanics" in *Cellular Mechanotransduction*, eds. M.R.K. Mofrad & R.D. Kamm, Cambridge University Press, pp. 181–195.
- Engler, A.J., Bacakova, L., Newman, C., Hategan, A., Griffin, M. & Discher, D. 2004a, "Substrate compliance versus ligand density in cell on gel responses", *Biophysical journal*, vol. 86, no. 1, pp. 617–628.
- Engler, A.J., Griffin, M.A., Sen, S., Bönnemann, C.G., Sweeney, H.L. & Discher, D.E. 2004b, "Myotubes differentiate optimally on substrates with tissue-like stiffness", *The Journal of cell biology*, vol. 166, no. 6, pp. 877–887.
- Engler, A.J., Richert, L., Wong, J.Y., Picart, C. & Discher, D.E. 2004c, "Surface probe measurements of the elasticity of sectioned tissue, thin gels and polyelectrolyte multilayer films: correlations between substrate stiffness and cell adhesion", *Surface Science*, vol. 570, no. 1–2, pp. 142–154.
- Eyckmans, J., Boudou, T., Yu, X. & Chen, C.S. 2011, "A Hitchhiker's Guide to Mechanobiology", *Developmental cell*, vol. 21, no. 1, pp. 35–47.
- Geiger, B. & Yamada, K.M. 2011, "Molecular architecture and function of matrix adhesions", *Cold Spring Harbor Perspectives in Biology*, vol. 3, no. 5.
- Golji, J., Lam, J. & Mofrad, M.R.K. 2011, "Vinculin Activation Is Necessary for Complete Talin Binding", *Biophysical journal*, vol. 100, no. 2, pp. 332–340.
- Grashoff, C., Hoffman, B.D., Brenner, M.D., Zhou, R., Parsons, M., Yang, M.T., McLean, M.A., Sligar, S.G., Chen, C.S., Ha, T. & Schwartz, M.A. 2010, "Measuring mechanical tension across vinculin reveals regulation of focal adhesion dynamics", *Nature*, vol. 466, no. 7303, pp. 263–267.
- Green, N.S., Reisler, E. & Houk, K. 2001, "Quantitative evaluation of the lengths of homobifunctional protein cross-linking reagents used as molecular rulers", *Protein Science*, vol. 10, no. 7, pp. 1293–1304.
- Gullberg, M. & Andersson, A.C. 2010, "Visualization and quantification of protein-protein interactions in cells and tissues", *Nature Methods*, vol. 7, no. 6.
- Humphries, J.D., Byron, A., Bass, M.D., Craig, S.E., Pinney, J.W., Knight, D. & Humphries, M.J. 2009, "Proteomic analysis of integrin-associated complexes identifies RCC2 as a dual regulator of Rac1 and Arf6", *Science signaling*, vol. 2, no. 87, ra51.

- Humphries, J.D., Wang, P., Streuli, C., Geiger, B., Humphries, M.J. & Ballestrem, C. 2007, "Vinculin controls focal adhesion formation by direct interactions with talin and actin", *Journal of Cell Biology*, vol. 179, no. 5, pp. 1043–1057.
- Hytönen, V.P., Smith, M.L. & Vogel, V. 2010, "Translating Mechanical Force into Discrete Biochemical Signal Changes: Multimodularity Imposes Unique Properties to Mechanotransductive Proteins" in *Cellular Mechanotransduction*, eds. M.R.K. Mofrad & R.D. Kamm, Cambridge University Press, pp. 286–338.
- Hytönen, V.P. & Vogel, V. 2008, "How force might activate talin's vinculin binding sites: SMD reveals a structural mechanism", *PLoS Computational Biology*, vol. 4, no. 2, e24.
- Ingber, E. 2003, "Mechanobiology and diseases of mechanotransduction", *Annals of Medicine*, vol. 35, no. 8, pp. 564–577.
- Jain, A., Liu, R., Ramani, B., Arauz, E., Ishitsuka, Y., Ragunathan, K., Park, J., Chen, J., Xiang, Y.K. & Ha, T. 2011, "Probing cellular protein complexes using single-molecule pull-down", *Nature*, vol. 473, no. 7348, pp. 484–488.
- Kamm, R.D. & Mofrad, M.R.K. 2010, "Introduction" in *Cellular Mechanotransduction*, eds. M.R.K. Mofrad & R.D. Kamm, Cambridge University Press, pp. 1–19.
- Kanchanawong, P., Shtengel, G., Pasapera, A.M., Ramko, E.B., Davidson, M.W., Hess, H.F. & Waterman, C.M. 2010, "Nanoscale architecture of integrin-based cell adhesions", *Nature*, vol. 468, no. 7323, pp. 580–584.
- Kojic, N. & Tschumperlin, D.J. 2010, "Mechanotransduction through Local Autocrine Signalling" in *Cellular Mechanotransduction*, eds. M.R.K. Mofrad & R.D. Kamm, Cambridge University Press, pp. 339–359.
- Kuo, J.C., Han, X., Hsiao, C.T., Yates III, J.R. & Waterman, C.M. 2011, "Analysis of the myosin-II-responsive focal adhesion proteome reveals a role for [beta]-Pix in negative regulation of focal adhesion maturation", *Nature cell biology*, vol. 13, no. 4, pp. 383–393.
- Küpper, K., Lang, N., Möhl, C., Kirchgeßner, N., Born, S., Goldmann, W.H., Hoffmann, B. & Merkel, R. 2010, "Tyrosine phosphorylation of vinculin at position 1065 modifies focal adhesion dynamics and cell tractions", *Biochemical and biophysical research communications*, vol. 399, no. 4, pp. 560–564.
- Lee, S.E., Kamm, R.D. & Mofrad, M.R.K. 2010, "A Molecular Perspective on Mechanotransduction in Focal Adhesions" in *Cellular Mechanotransduction*, eds. M.R.K. Mofrad & R.D. Kamm, Cambridge University Press, pp. 250–268.
- Marg, S., Winkler, U., Sestu, M., Himmel, M., Schönherr, M., Bär, J., Mann, A., Moser, M., Mierke, C.T. & Rottner, K. 2010, "The Vinculin-ΔIn20/21 Mouse: Characteristics of a Constitutive, Actin-Binding Deficient Splice Variant of Vinculin", *PLoS one*, vol. 5, no. 7, e11530.
- Margadant, F., Chew, L.L., Hu, X., Yu, H., Bate, N., Zhang, X. & Sheetz, M. 2011, "Mechanotransduction In Vivo by Repeated Talin Stretch-Relaxation Events Depends upon Vinculin", *PLoS biology*, vol. 9, no. 12, e1001223.
- Palmer, S.M., Playford, M.P., Craig, S.W., Schaller, M.D. & Campbell, S.L. 2009, "Lipid binding to the tail domain of vinculin", *Journal of Biological Chemistry*, vol. 284, no. 11, pp. 7223–7231.
- Pelham, R.J. & Wang, Y. 1997, "Cell locomotion and focal adhesions are regulated by substrate flexibility", *Proceedings of the National Academy of Sciences of the United States of America*, vol. 94, no. 25, pp. 13661–13665.

- Plopper, G. & Ingber, D.E. 1993, "Rapid induction and isolation of focal adhesion complexes", *Biochemical and biophysical research communications*, vol. 193, pp. 571–571.
- Saez, A., Anon, E., Ghibaudo, M., du Roure, O., Di Meglio, J., Hersen, P., Silberzan, P., Buguin, A. & Ladoux, B. 2010, "Traction forces exerted by epithelial cell sheets", *Journal of Physics: Condensed Matter*, vol. 22, pp. 194119 (9 pp.).
- Saez, A., Buguin, A., Silberzan, P. & Ladoux, B. 2005, "Is the mechanical activity of epithelial cells controlled by deformations or forces?", *Biophysical journal*, vol. 89, no. 6, pp. L52–L54.
- Saunders, R.M., Holt, M.R., Jennings, L., Sutton, D.H., Barsukov, I.L., Bobkov, A., Liddington, R.C., Adamson, E.A., Dunn, G.A. & Critchley, D.R. 2006, "Role of vinculin in regulating focal adhesion turnover", *European journal of cell biology*, vol. 85, no. 6, pp. 487–500.
- Sawada, Y. & Sheetz, M.P. 2002, "Force transduction by Triton cytoskeletons", *The Journal of cell biology*, vol. 156, no. 4, pp. 609–615.
- Sawada, Y., Tamada, M., Dubin-Thaler, B.J., Cherniavskaya, O., Sakai, R., Tanaka, S. & Sheetz, M.P. 2006, "Force sensing by mechanical extension of the Src family kinase substrate p130Cas", *Cell*, vol. 127, no. 5, pp. 1015–1026.
- Schiller, H.B., Friedel, C.C., Boulegue, C. & Fässler, R. 2011, "Quantitative proteomics of the integrin adhesome show a myosin II-dependent recruitment of LIM domain proteins", *EMBO reports*, vol. 12, no. 3, pp. 259–266.
- Shen, K., Tolbert, C.E., Guilluy, C., Swaminathan, V.S., Berginski, M.E., Burridge, K., Superfine, R. & Campbell, S.L. 2011, "The Vinculin C-Terminal Hairpin Mediates F-Actin Bundle Formation, Focal Adhesion and Cell Mechanical Properties", *Journal of Biological Chemistry*, vol. 286, no. 52, pp. 45103–45115.
- Smith, M. *Personal communication*, June and July 2010.
- Stricker, J., Aratyn-Schaus, Y., Oakes, P.W. & Gardel, M.L. 2011, "Spatiotemporal constraints on the force-dependent growth of focal adhesions", *Biophysical Journal*, vol. 100, pp. 2883–2893.
- Stricker, J., Sabass, B., Schwarz, U.S. & Gardel, M.L. 2010, "Optimization of traction force microscopy for micron-sized focal adhesions", *Journal of Physics: Condensed Matter*, vol. 22, pp. 194104 (10 pp.).
- Tan, J.L., Tien, J., Pirone, D.M., Gray, D.S., Bhadriraju, K. & Chen, C.S. 2003, "Cells lying on a bed of microneedles: an approach to isolate mechanical force", *Proceedings of the National Academy of Sciences of the United States of America*, vol. 100, no. 4, pp. 1484–1489.
- Tros de Ilarduya, C., Sun, Y. & Düzgüneş, N. 2010, "Gene delivery by lipoplexes and polyplexes", *European Journal of Pharmaceutical Sciences*, vol. 40, no. 3, pp. 159–170.
- Ungureanu, D. August 2011, *Personal communication*.
- Xu, W., Baribault, H. & Adamson, E.D. 1998, "Vinculin knockout results in heart and brain defects during embryonic development", *Development*, vol. 125, no. 2, pp. 327–337.
- Xu, W., Coll, J.L. & Adamson, E.D. 1998, "Rescue of the mutant phenotype by reexpression of full-length vinculin in null F9 cells; effects on cell locomotion by domain deleted vinculin", *Journal of cell science*, vol. 111, no. 11, pp. 1535–1544.
- Yeung, T., Georges, P.C., Flanagan, L.A., Marg, B., Ortiz, M., Funaki, M., Zahir, N., Ming, W., Weaver, V. & Janmey, P.A. 2005, "Effects of substrate stiffness on

- cell morphology, cytoskeletal structure, and adhesion", *Cell motility and the cytoskeleton*, vol. 60, no. 1, pp. 24–34.
- Zaidel-Bar, R. & Geiger, B. 2010, "The switchable integrin adhesome", *Journal of cell science*, vol. 123, no. 9, pp. 1385–1388.
- Zhang, Y., Frangos, J.A. & Chachisvilis, M. 2010, "Mechanotransduction by Membrane-Mediated Activation of G-Protein Coupled Receptors and G-Proteins" in *Cellular Mechanotransduction*, eds. M.R.K. Mofrad & R.D. Kamm, Cambridge University Press, pp. 89–119.
- Ziegler, W.H., Liddington, R.C. & Critchley, D.R. 2006, "The structure and regulation of vinculin", *Trends in cell biology*, vol. 16, no. 9, pp. 453–460.

Appendix 1

ImageJ macros used in image analysis

```
// Cell area estimator for analysing multiple phase contrast
// images with ImageJ

// Opening of a directory for analysis
dir1 = getDirectory("Choose Source Directory ");
list = getFileList(dir1);
for (i=0; i<list.length; i++) {
    showProgress(i+1, list.length);
    open(dir1+list[i]);
    filename = File.getName(dir1+list[i]);

    // Preparing image for thresholding by removing noise
    run("Smooth");
    run("Smooth");
    run("Smooth");
    run("Smooth");

    // Finding edges of cell populated area and again
    // removing noise by averaging
    run("Find Edges");
    run("Median...", "radius=10");

    // Thresholding image to obtain mask. NOTE: Thresholding
    // boundaries have to be adjusted and corrected on an image
    // by image basis, where necessary
    setThreshold(0, 4);
    run("Convert to Mask");

    // Removing image boundaries generated by mosaic imaging
    makeRectangle(0, 0, 4767, 16);
    run("Fill", "slice");
    makeRectangle(4751, 0, 4767, 3572);
    run("Fill", "slice");
    makeRectangle(0, 3556, 4767, 3572);
    run("Fill", "slice");
    makeRectangle(0, 0, 16, 3572);
    run("Fill", "slice");
    run("Select None");

    // Measuring area of mask
    run("Invert");
    run("Create Selection");
    run("Measure");

    // Creating overlay images of measured cell area for quality control
    selectWindow(filename);
    rename("Mask of "+filename);
    run("Green");
    open(dir1+list[i]);
    selectWindow(filename);
    run("Add Image...", "image=[Mask of "+filename+"] x=0 y=0 opacity=10");
    run("Flatten");
    selectWindow("Mask of "+filename);
    close();
    selectWindow(filename);
    close();
}
```

Figure S1: ImageJ script used for estimating total cell area from phase contrast images. Thresholding boundaries noted were adjusted as needed to correctly represent the cells in the image in question. This estimation was done by eye.

```

// Cell area estimator for analysing multiple fluorescence
// images with ImageJ

// Opening of a directory
for analysis
dir1 = getDirectory("Choose Source Directory ");
list = getFileList(dir1);
//setBatchMode(true);
for (i=0; i<list.length; i++) {
    showProgress(i+1, list.length);
    open(dir1+list[i]);
    filename = File.getName(dir1+list[i]);

    // Preparing image for thresholding by removing background and noise
    run("Subtract Background...", "rolling=100 dark");
    run("Median...", "radius=5");

    // Removing image boundaries generated by mosaic imaging
    makeRectangle(0, 0, 4767, 16);
    run("Fill", "slice");
    makeRectangle(4751, 0, 4767, 3572);
    run("Fill", "slice");
    makeRectangle(0, 3556, 4767, 3572);
    run("Fill", "slice");
    makeRectangle(0, 0, 16, 3572);
    run("Fill", "slice");
    run("Select None");

    // Contrast enhanced in case of too dark images
    run("Enhance Contrast", "saturated=0.001");

    // Thresholding image to obtain mask. NOTE: Thresholding
    // boundaries have to be adjusted and corrected on an image
    // by image basis, where necessary
    setThreshold(2,255);
    run("Convert to Mask");

    // Filling holes in thresholded mask created e.g. by dark nuclei
    run("Fill Holes");

    // Analyse particles is used to remove linear artefacts caused by
    // mosaic image boundaries
    run("Analyse Particles...", "size=100-30000 circularity=0.10-1.0 show=Masks");

    // Measuring area of mask
    run("Create Selection");
    run("Measure");

    // Creating overlay images of measured cell area for quality control
    selectWindow(filename);
    close();
    selectWindow("Mask of "+filename);
    run("Green");
    open(dir1+list[i]);
    selectWindow(filename);
    run("Add Image...", "image=[Mask of "+filename+"] x=0 y=0 opacity=35");
    run("Flatten");
    selectWindow("Mask of "+filename);
    close();
    selectWindow(filename);
    close();
}

```

Figure S2: ImageJ script used for fluorescent area estimation.

```

// Cell counter for counting GFP-positive cell numbers and areas from low-
// magnification images. Comparison to DAPI-stained images will be used to
// only select mononucleate cells for counting.

// GFP and DAPI images should be named "FITC.bmp" and "DAPI.bmp", respectively
FITC = "FITC.bmp"
DAPI = "DAPI.bmp"

// Choosing a directory for the result files
dir_FITC = getDirectory("Choose target directory ");

// Adjusting DAPI image
selectWindow(DAPI);

    // Removing image boundaries generated by mosaic imaging
    run("Properties...", "channels=1 slices=1 frames=1 unit=pixel pixel_width=1
pixel_height=1

voxel_depth=1.0000000 frame=[0 sec] origin=0,0");
    makeRectangle(0, 0, 4767, 16);
    run("Fill", "slice");
    makeRectangle(4751, 0, 4767, 3572);
    run("Fill", "slice");
    makeRectangle(0, 3556, 4767, 3572);
    run("Fill", "slice");
    makeRectangle(0, 0, 16, 3572);
    run("Fill", "slice");
    run("Select All");

    run("Duplicate...", "title=DAPI_Duplicate");

    // Preparing image for thresholding
    run("Subtract Background...", "rolling=40 dark");
    run("Enhance Contrast", "saturated=0.5 normalize");

    // Thresholding image to obtain mask. NOTE: Thresholding
    // boundaries have to be adjusted and corrected on an image
    // by image basis, where necessary

    setThreshold(71,255);
    run("Convert to Mask");
    run("Despeckle");
    run("Watershed");

    // Count nuclei. Exclude any double nuclei not divided by watershed with size
    limit.
    // Convert the single nuclei image into mask to be used for nuclei/cell countin
    later.

    run("Analyse Particles...", "size=10-600 circularity=0.05-1.00 show=Masks display
summarize");

    DAPI_MASK = "Mask of DAPI_Duplicate"

    // Save results of nuclei counting
    saveAs("Measurements", dir_FITC+"nucleus_count_results.txt");

    run("Clear Results");

// Adjusting FITC image

selectWindow(FITC);

    run("Properties...", "channels=1 slices=1 frames=1 unit=pixel pixel_width=1
pixel_height=1

voxel_depth=1.0000000 frame=[0 sec] origin=0,0");
    makeRectangle(0, 0, 4767, 16);
    run("Fill", "slice");
    makeRectangle(4751, 0, 4767, 3572);
    run("Fill", "slice");
    makeRectangle(0, 3556, 4767, 3572);
    run("Fill", "slice");
    makeRectangle(0, 0, 16, 3572);
    run("Fill", "slice");
    run("Select All");

```

```

run("Duplicate...", "title=FITC_Duplicate");
run("Enhance Contrast", "saturated=0.5 normalize");

// Thresholding image to obtain mask. NOTE: Thresholding
// boundaries have to be adjusted and corrected on an image
// by image basis, where necessary

setThreshold(120,255);
run("Convert to Mask");
run("Despeckle");

// Count GFP-positive cell areas. Exclude linear artefacts using circularity-
parameter
selectWindow("FITC_Duplicate");
run("Analyse Particles...", "size=50-10000 circularity=0.05-1.00 show=Masks
display summarize");

n_cells=nResults;

// Save results of GFP-positive cell counting
saveAs("Measurements", dir_FITC+"cell_count_results.txt");

CELL_MASK = "Mask of FITC_Duplicate"

print("Number of cells found: " + n_cells);

run("Clear Results");

// Create a region-of-interest (ROI) list of all GFP-positive areas

selectWindow(CELL_MASK)
run("ROI Manager...");
run("Create Selection");

roiManager("Add");
roiManager("Select", 0);
roiManager("Split");
roiManager("Select", 0);
roiManager("Delete");

// Go through all ROIs, and analyse each GFP-positive area one at a time for
the number of nuclei

j=0;

n_ROIs = roiManager("count");

print("ROI count is "+n_ROIs);

for (i=0; i<n_ROIs; i++) {

    print("i = " +i);
    print("j = " +j);
    selectWindow(CELL_MASK);
    roiManager("Select", j);
    selectWindow(DAPI_MASK);

    run("Restore Selection");
    run("Analyse Particles...", "size=20-600 circularity=0.05-1.00 show=Nothing
display
summarize");

    print("Nuclei count is " + nResults);
    n_nuclei=nResults;
    run("Clear Results");

    // Remove the ROI from the list, if it contains more or less than 1 nucleus
    if (n_nuclei!=1) {
        roiManager("Delete");
    } else {
        j++;
    }
    selectWindow(DAPI_MASK);
    run("Select None");
}

```

```

selectWindow(CELL_MASK);
run("Select None");
run("Duplicate...", "title=FITC_mononucleate");

selectWindow(CELL_MASK);

// Combine the new ROI-list into one selection and make a new image with only
the selected cells
roiManager("deselect");
roiManager("Combine");

selectWindow("FITC_mononucleate");
run("Restore Selection");
run("Make Inverse");
run("Fill", "slice");
run("Invert");
run("Select None");

// Threshold the new image for particle analysis
setAutoThreshold("Default");
run("Convert to Mask");

// Count mononucleate, GFP-positive cells and save results
run("Analyse Particles...", "size=10-10000 circularity=0.05-1.00 show=Nothing
display summarize");

saveAs("Measurements", dir_FITC+"mononucleate_FITC+_cells_results.txt");

// Makes an overlay of the counted cells + the counted nuclei for verification
of the counting

selectWindow("FITC_mononucleate");
run("Green");
selectWindow(DAPI_MASK);
run("Invert");
run("Add Image...", "image=FITC_mononucleate x=0 y=0 opacity=50");

// Closing unnecessary windows
selectWindow(CELL_MASK);
close();
selectWindow("FITC_Duplicate");
close();
selectWindow("DAPI_Duplicate");
close();
selectWindow("FITC_mononucleate");
close();

```

Figure S3: ImageJ script for counting mononucleate GFP-positive cells

```

// ImageJ script for counting of focal adhesions from high-magnification
// Apotome or confocal microscopy images with low cytoplasmic background
// fluorescence. Images to be analysed should be cropped to only contain
// a single cell / few cells per image.

dir1 = getDirectory("Choose Source Directory ");
list = getFileList(dir1);
for (i=0; i<list.length; i++) {

    showProgress(i+1, list.length);
    open(dir1+list[i]);

    run("Properties...", "channels=1 slices=1 frames=1 unit=pixel pixel_width=1
pixel_height=1 voxel_depth=1.0000000 frame=[0 sec] origin=0,0");

    // Preparing image for thresholding
    run("Subtract Background...", "rolling=15 dark");
    run("Subtract...", "value=10");
    run("Mean...", "radius=0.1");

    // Enhancing contrast with convolve
    run("Convolve...", "text1=[ -1 -1 -1 -1 -1\n -1 -1 -1 -1 -1\n -1 -1 24 -1 -1\n -1
-1 -1 -1 -1\n -1
-1 -1 -1 -1\n] normalize");

    setAutoThreshold();
    run("Convert to Mask");
    run("Despeckle");

    // Counting FAs
    run("Analyse Particles...", "size=4-1000 circularity=0.00-1.00 show=Outlines
display summarize");
    open(dir1+list[i]);
}

```

Figure S4: ImageJ script used for counting FAs from fluorescence microscopy images with low cytoplasmic background fluorescence.


```

// ImageJ script for counting of focal adhesions from high-magnification
// Apotome or confocal microscopy images with high cytoplasmic background
// fluorescence. Images to be analysed should be cropped to only contain
// a single cell per image.

dir1 = getDirectory("Choose Source Directory ");
list = getFileList(dir1);
for (i=0; i<list.length; i++) {
    showProgress(i+1, list.length);
    open(dir1+list[i]);

    run("Properties...", "channels=1 slices=1 frames=1 unit=pixel pixel_width=1
pixel_height=1 voxel_depth=1.0000000 frame=[0 sec] origin=0,0");

    // Preparing image for thresholding
    run("Subtract Background...", "rolling=15 dark");
    run("Subtract...", "value=20");
    run("Mean...", "radius=0.1");

    // Enhancing contrast with convolve
    run("Convolve...", "text1=[ -1 -1 -1 -1 -1\n -1 -1 -1 -1 -1\n -1 -1 24 -1 -1\n -1
-1 -1 -1\n -1 -1 -1 -1 -1\n] normalize");

    setAutoThreshold();
    run("Convert to Mask");
    run("Despeckle");

    // Counting FAs
    run("Analyse Particles...", "size=4-1000 circularity=0.00-1.00 show=Masks display
summarize");
    open(dir1+list[i]);
}

```

Figure S5: ImageJ script used for counting FAs from fluorescence microscopy images with high cytoplasmic background fluorescence.